SYNTHESIS, STRUCTURAL AND MAGNETIC PROPERTIES OF HIGH NUCLEARITY SELF-ASSEMBLED CLUSTER COMPLEXES

LIANG ZHAO

Synthesis, Structural and Magnetic Properties of High Nuclearity Self-assembled Cluster Complexes

by

Liang Zhao. B. Sc., M. Sc.

A thesis submitted to the

School of Graduate Studies

in partial fulfillment of the

requirement for the degree of

Master of Science

Department of Chemistry

Memorial University of Newfoundland

St. John's Newfoundland

Table of Contents

Abstract

This thesis describes synthesis, structural and magnetic properties of high nuclearity cluster complexes self assembled from polydentate alkoxo-diazine ligands. In Chapter 1, clusters and self-assembly have been briefly reviewed. In Chapter 2, synthesis, characterization, X-ray structures and the magnetic properties of three trinuclear copper(II) complexes are described. These compounds exhibit moderate to strong antiferromagnetic coupling as a result of superexchange via the N-N linkages. The magnetic properties are explained on the basis of large rotational angles of the copper magnetic planes about the diazine bridges. In Chapter 3, four predominantly square grid $M_4(\mu\text{-}O)_4$ (M = Cu(II), Ni(II) and Co(II)) complexes and a rectangular $Mn_4(N\text{-}N)_2O_2$ grid complex are synthesized and structurally characterized by X-ray techniques. The square [2×2] copper(II) cluster exhibits intramolecular ferromagnetic spin exchange, associated with the orthogonal alkoxide bridging arrangement and the close proximity of the copper centers. Both the $Ni_4(\mu\text{-}O)_4$ and $Co_4(\mu\text{-}O)_4$ clusters are antiferromagnetically coupled due to the large M-O-M angles and for the rectangular Mn_4 complex the exchange is dominated by antiferromagnetic coupling via the N-N bridge. Chapter 4 describes the ligand paoh, which has two widely separated tridentate (N_2O) terminal coordination pockets, and uncoupled square [2×2] $Fe(II)_4$ grid complex. Replacement of the NH_2 groups with 2-pyridyl residues gives the ligand dpkoh with the additional coordination capacity of an exo-N_4 coordination pocket, leading to an octanuclear metallacyclic cluster complex $[Ni_8(dpkoh\text{-}2H)_4(H_2O)_8](ClO_4)_8\cdot 4H_2O$, in which eight nickel(II) centers are

bridged just by the diazine N-N single bond. Substantial antiferromagnetic coupling exists between the nickel(II) ions throughout the metallacycle. In Chapter 5, the synthesis, structural characterization and magnetism studies of [3×3] Mn(II) and Cu(II) nanonuclear square grid complexes are described. The $Mn(II)_9$ systems exhibit intra-molecular antiferromagnetic coupling, while for the $Cu(II)_9$ complexes ferromagnetic exchange is observed with an S = 7/2 ground state. The aggregation of nine octahedral Mn(II) and Cu(II) centers (fifty four coordination positions) into an alkoxo-bridged, portcullis-like [3×3] grid by six heptadentate 2poap ligands (fifty four donor positions) is a unique example of a self assembly process.

List of Tables

List of Schemes

List of Figures

List of Abbreviations and Symbols

g	Landé splitting factor
H	Hamiltonian
J	magnetic interaction parameter
k	Boltzmann constant
N	Avogadro's number
R	residual factor
S	spin quantum number
T	temperature (K)
α	torsional angle
β	electronic Bohr magneton
ε	molar extinction coefficient
χ	magnetic susceptibility
μ_{eff}	effective magnetic moment
θ	Weiss-like temperature correction
ρ	fraction of paramagnetic impurity
IT	information technology

Acknowledgements

I would like to express my sincere gratitude to my supervisor Dr. L. K. Thompson for his advice, encouragement, patience and financial support during the course of my thesis research. I am also grateful to my supervisory committee members Dr. C. R. Lucas and Dr. H. J. Clase for their kind help and support.

Thanks go to Mr. D. O. Miller of Memorial University of Newfoundland, Claire Wilson, Michael Leech, and Prof. Judith A. K. Howard of University of Durham (U. K.), and Dr. Sarah L. Heath of University of York (U. K.) for the X-ray structure determinations. My thanks are due as well to Dr. B. Gregory and Ms. M. Baggs for mass spectrometry determination.

I am also grateful to the Department of Chemistry and the School of Graduate Studies, Memorial University of Newfoundland, for financial support during the course of this study. I would like to acknowledge all of my colleagues in Dr. L.K. Thompson's group, Dr. C. Matthews, Dr. Z. Q. Xu, Mr. S. Parsons, Mr. S. DeGrace, Ms. L. Dawe and Ms. V. Milway for their kindness, valuable suggestions and discussion. Thanks also are extended to all faculty, staff and students of the Chemistry Department for their help.

Finally, I would like to thank my wife, Xiaoying Jia, for her love, understanding, encouragement and care of our children, Charlie and Chenchen.

Chapter 1. General Introduction

1.1 Clusters in Proteins

It is well known that nature can use metal ions to perform a wide variety of specific functions associated with life processes, e.g. dioxygen transport, electron transfer, or structural roles, etc. [1] Many metal ions form mononuclear complexes when they coordinate to the binding sites in proteins, e.g. Fe(II) in hemoglobin, but sometimes, more complicated metal-containing units, inorganic metal clusters, are required to achieve certain specific functions in metalloproteins. A few examples have been found in proteins. Iron-sulfur clusters (e.g. Fe_4S_4 cluster, Figure 1-1), in which iron ions are bridged by simple sulfur atoms or sulfur from the side-chain thiolate of cysteine, are typical examples. Iron-sulfur cluster proteins have been found to facilitate electron transfer as well as dinitrogen reduction. Structural studies of the nitrogenase proteins have revealed that nitrogenase consists of two component proteins, the MoFe-protein and Fe-protein that together contain three distinct types of redox centers: two unusual Fe-S clusters, the FeMo-cofactor (Figure 1-2) and P-cluster pair, located within the MoFe-protein, and a single Fe_4S_4 cluster bound to the Fe-protein.[2] Nature has designed a cavity in the interior of the FeMo-cofactor that could be used to accommodate only N_2, which is potentially small enough to fit in the cavity unlike other substrates, and then is reduced to ammonia or other intermediates.

A more dramatic example of the occurrence of polynuclear clusters in biology is the iron-storage protein ferritin.[3] Ferritin is a protein that stores iron and releases it in a controlled fashion. Ferritin has the shape of a hollow sphere. Iron is stored in the Fe(III)

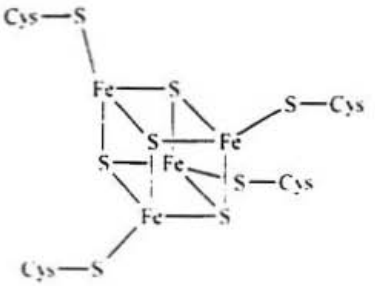

Figure 1-1. Schematic representation of Fe_4S_4 cluster.

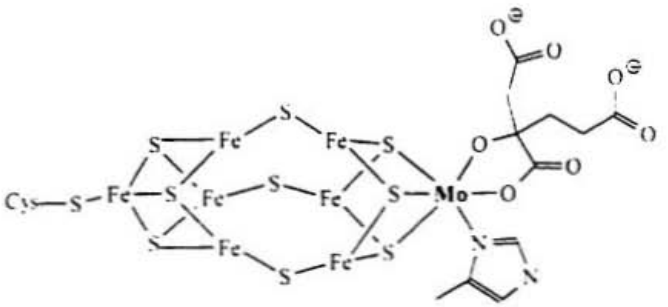

Figure 1-2. Schematic representation of FeMo-cofactor.

oxidation state, as ferrihydrite, $[FeO(OH)]_8[FeO(H_2PO_4)]$, which is attached to the inner wall of the sphere. To release iron when the body needs it, the iron must be changed from the Fe(III) to the Fe(II) oxidation state. The iron then leaves through channels in the spherical structure. Thus, the structure of ferritin is extremely important for the protein's ability to store and release iron in a controlled fashion. Structural studies on the ferritin core by a variety of spectroscopic techniques show that octahedrally coordinated iron(III) ions are bridged by oxide and /or hydroxide. The mechanism of the ferritin core assembly has been studied by examination of its model complexes. A series of high-nuclearity iron oxo cluster complexes, e.g., hexanuclear [4], octanuclear [5], decanuclear [6], undecanuclear [7], dodecanuclear [8], heptadecanuclear [9], and octadecanuclear [10a]

Fe(III) cluster complexes have been reported as ferritin models. The highly symmetrical $Fe(III)_{18}$ ring cluster (Figure 1-3a) is the largest cyclic ferric cluster reported so far, in which iron(III) ions are bridged by the alkoxide (from both the primary ligand XDK (where XDK is the dianion of *m*-xylylenediamine bis(Kemp's triacid imide) [10b] (Figure 1-3b) and acetate) and hydroxide.

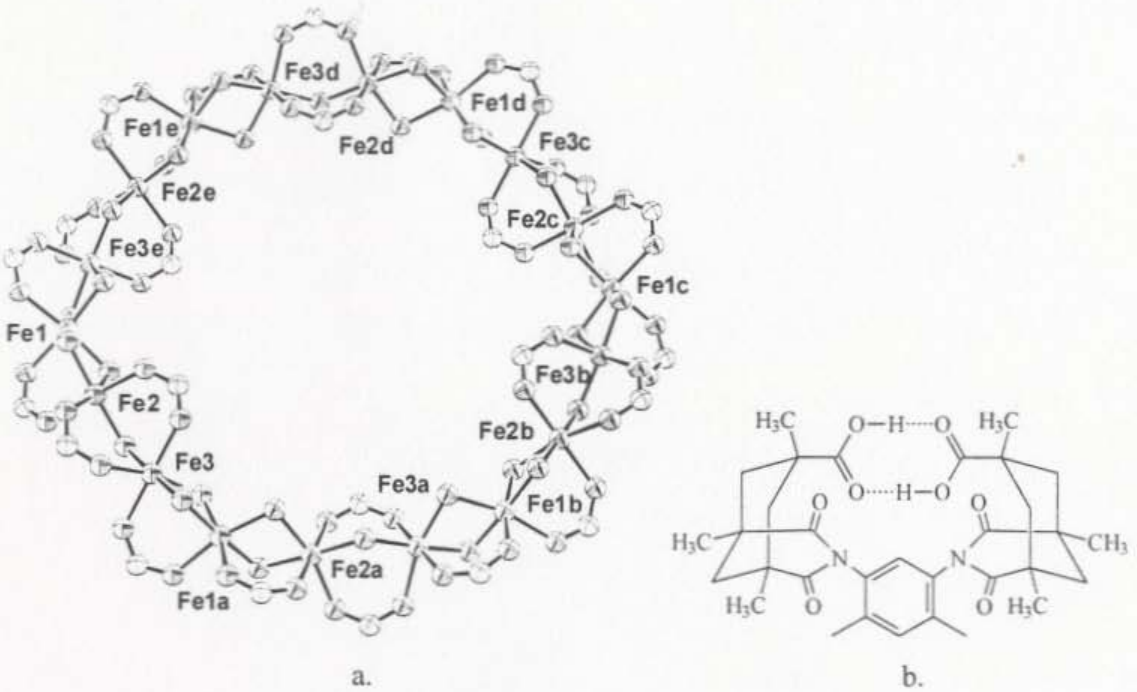

Figure 1-3. Structural representation of a Fe_{18} wheel cluster core (a) and its primary ligand XDK (b). (Phenyl groups are omitted for clarity.)

1.2 Clusters and Single-Molecular Magnets

The magnetic properties of large polynuclear complexes (clusters) have attracted much attention in the last decade after the discovery of the new magnetic phenomenon of "single-molecule magnetism". Single molecular magnets (SMM) are molecules that can act as small magnets themselves and have the properties of bulk magnets. The first

SMM, $[Mn_{12}O_{12}\cdot(CH_3COO)_{16}(H_2O)_4]\cdot 2CH_3COOH\cdot 4H_2O$ ($Mn_{12}Ac$) was reported one decade ago. [11, 12] $Mn_{12}Ac$ has been observed with an S = 10 ground-state split by zero-field splitting and slow relaxation of the magnetization, the so-called hysteresis effect, which is well-known in bulk magnets, but first found of molecular origin.[13a] Such molecule-based magnets do not have real applications at the present time, since very few of the known molecule-based systems possess the key characteristic: retaining their magnetism well above room temperature. However, a few recent reports of molecule-based magnets with magnetic ordering temperature (i.e. Curie temperature, T_c) above room temperature, even above 100°C, [13b] may make feasible the construction of the ultimate high-density information storage devices in the IT industry.

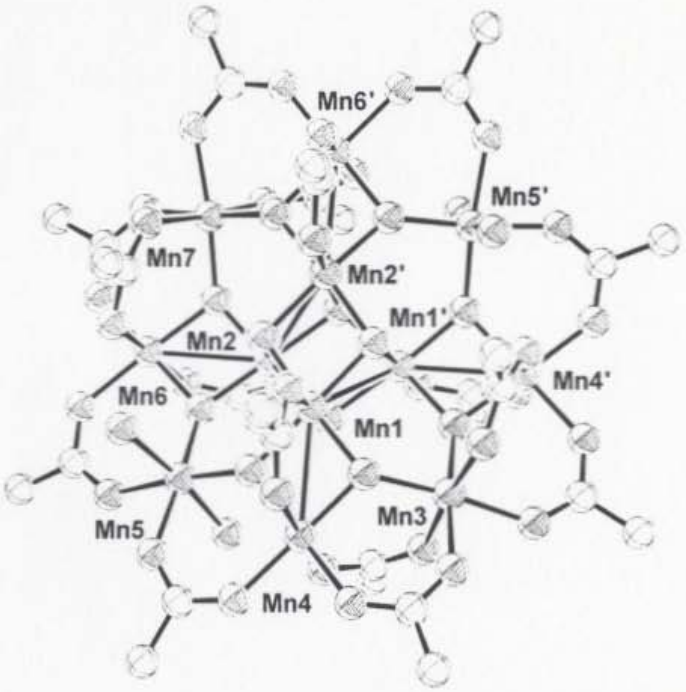

Figure 1-4. Structural representation of the core [$Mn_{12}Ac$] cluster.

There are two basic requirements in order for a molecule to function as a SMM. First, the ground state of the molecule should have a large spin S; and second, there needs to be considerable negative magnetic anisotropy present, which is derived from zero-field splitting in the ground state of a SMM. [14] In addition to $Mn_{12}Ac$, a number of structurally related dodecanuclear manganese cluster complexes showing SMM properties have been characterized with the composition $[Mn_{12}O_{12}(O_2CR)_{16}(H_2O)_4]$ (R = -Et, [15] $-C_6H_5$, [15] $-C_6H_5$-2-Cl, [16] $-C_6H_5$-2-Br, [16] etc. $[Mn_7(OH)_3Cl_3(hmp)_9]^{2+}$ (Hhmp=2-hydroxymethylpyridine; S≥10) [17] and $[Mn_4(O_2CMe)_2(Hpdm)_6][ClO_4]_2$ (H_2pdm=pyridine-2,6-dimethanol; S=8) [18] etc. have also been found to behave as single molecular magnets. Recently, a few vanadium [19], chromium [20 - 22] (Cr_{12} cluster[22], Figure 1-5) and iron [3, 23 - 25] clusters have also been found to exhibit similar properties, with one iron(III) cluster having 33 unpaired electrons. [23]

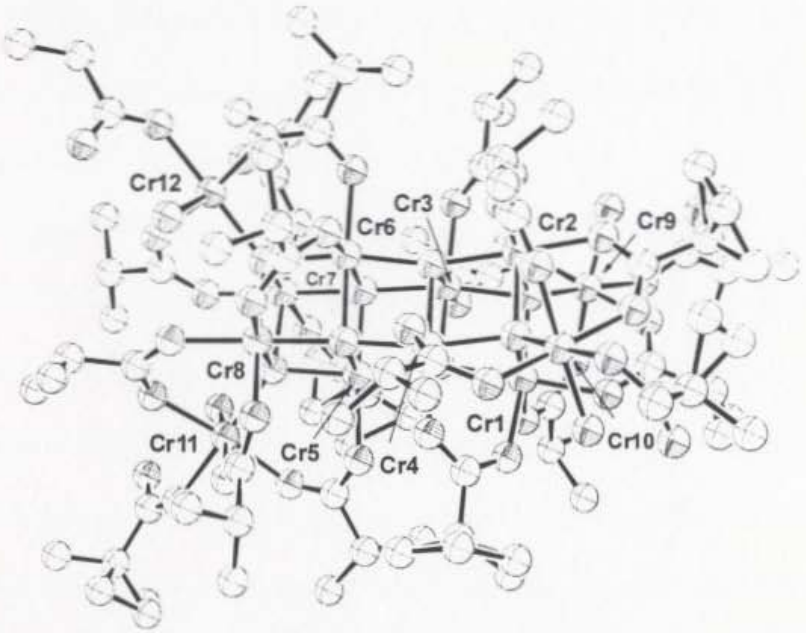

Figure 1-5. Structural representation of a Cr_{12} cluster.

Usually the yield of such cluster syntheses is low, and it is difficult to predict in advance the clusters' topologies and structures, and even more difficult to then achieve a deliberate synthesis of high-spin ground state clusters. [17] Can we predict the topologies and structures of clusters and synthesize them in high yield? Fortunately we can do it by self-assembly.

1.3 Self-Assembly and Clusters

Self-assembly and self-organization are well-known terms and have mainly been studied in physics and in biology. [26,27] Non-covalent interactions (hydrogen bonding and other weak reversible interactions with bond energies ca. 0.6 – 7 Kcal mol^{-1}) play a leading role in controlling the secondary and tertiary structures of natural macromolecules.

Lehn defined self-assembly in chemistry as: "Supramolecular self-assembly concerns the spontaneous association of either a few or many components resulting in the generation of either discrete oligomolecular supramolecules or of extended poly-molecular assemblies such as molecular layers, films, membranes, etc. The formation of supramolecules results from the recognition-directed spontaneous association of a well-defined and limited number of molecular components under the intermolecular control of the non-covalent interations that hold them together." [28] These non-covalent interactions, such as hydrogen bonds, aromatic-stacking, and polar and van der Waal's interactions, are the ones that bring molecules together into complex compounds. While coordinate bonds can be considered to have intermediate properties when compared to

covalent bonds (strong and kinetically inert) and the interactions of biology (weak and kinetically labile). Therefore, they offer unique opportunities to generate securely fastened compounds having distinctive and elaborate architectures using a self-assembly process. Indeed, many fascinating architectures, for example, helicates, grids, racks, ladders, triangles, squares, hexagons and other polygons, various polyhedra/boxes, cylinders, rods, metallo-dendrimers, rotaxanes, catenanes, knots, etc. have been documented in the past decade.[29] Among these different types of superstructures, entities in which metal ions are arranged in a grid-type fashion are of special interest, in particular in view of their possible incorporation into information storage devices.[30]

Self-assembly provides a new methodology for synthesizing predetermined topologies and cluster structures. Lehn et al. have reported a few [n×n] n^2 grid clusters self-assembled from rigid, linear polytopic ligands in very high yield, which include a [2×2] $Cu(II)_4$ square grid [31] (Figure 1-6) and a [3×3] $[Ag(I)_9L_6]^{9+}$ grid (Figure 1-7). [32]

1.4 Open-chain N-N Diazine Ligands and Self-assembled Clusters

The diazine (N-N) moiety in heterocyclic ring systems is rigidly fixed [33], while the N-N linkage in open-chain systems containing the N-N single bond is much more flexible. Ligands containing such groups have been found to form mononuclear, [34 - 37] dinuclear, [38 - 44] trinuclear, [45] and tetranuclear [46] copper(II) complexes. Recent studies on spiral dinuclear copper(II) complexes (e.g. Figure 1-8a) of a series of novel open-chain diazine ligands (e.g. pahap, Figure 1-8a) have found a linear relationship between the rotational angle of the metal magnetic planes about the N-N bond and the exchange

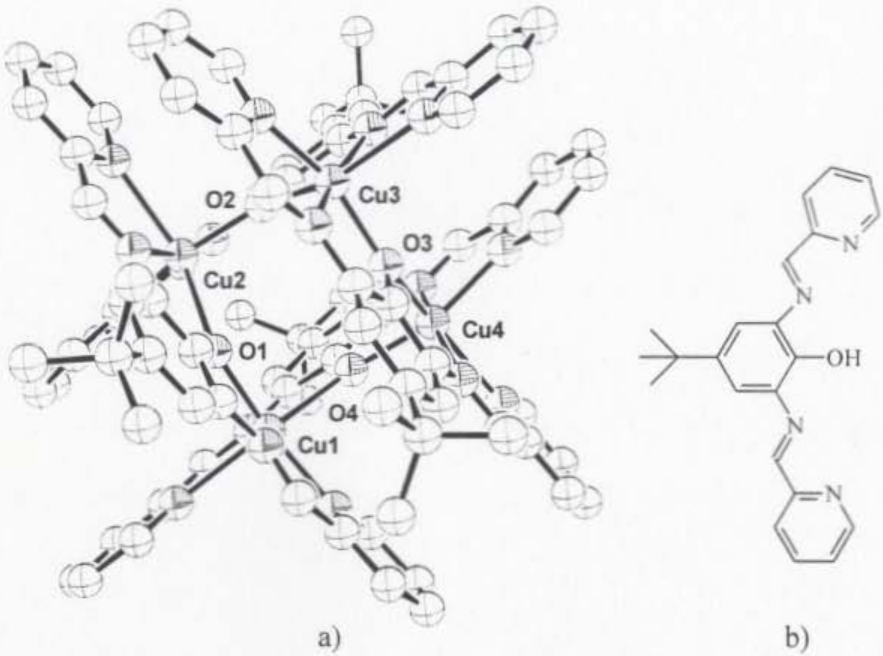

Figure 1-6. Structural representation of a [2×2] Cu_4 grid (b) and its ligand (a).

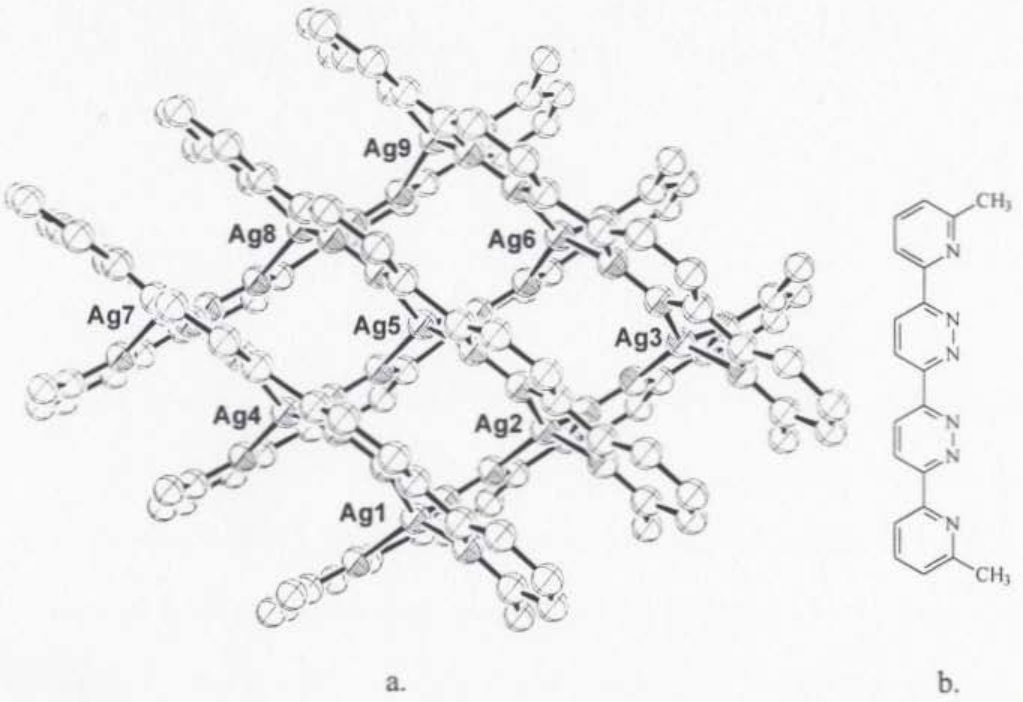

Figure 1-7. X-ray structures of [3×3] $[Ag_9L_6]^{9+}$ grid (a) and its ligand (b).

integral, with a change from ferromagnetic coupling at angles < 80° to antiferromagnetic coupling >80°.[47-9]

When one NH_2 group in the ligand pahap is substituted by an OH group, the resulting novel ligand poap (Figure 1-9a) can self-assemble four copper(II) centers into a [2×2] tetranuclear grid cluster $[Cu_4(POAP\text{-}H)_4(H_2O)_2](NO_3)_4 \cdot 4H_2O$ (Figure 1-9b).[50] In order to produce a [2×2] grid cluster with a predetermined structure, the alkoxide group in the ligand poap plays a key role, and acts as a bridge between metal centers.

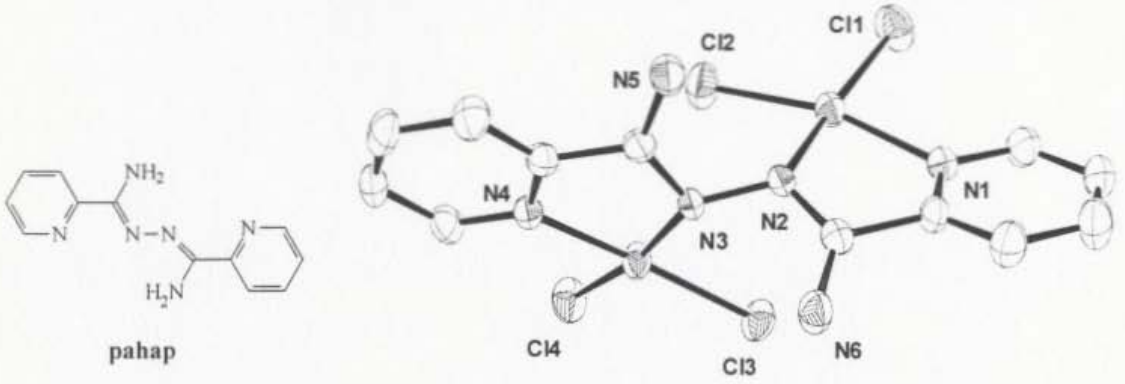

Figure 1-8. Structure of the ligand pahap (a) and its $[Cu_2(pahap)Cl_4] \cdot H_2O$ (b).

Recently, a new class of polynuclear clusters, metallacrowns, self assembled by reactions of salicylhydroxamic acid (H_3shi) and similar ligands with transition metal salts have been reported. [51] These metallacrowns, which may have potential applications as nano-scale magnetic materials, are analogous to crown ethers in both structure and functions. A few examples of this new kind of cluster are well documented, e.g.,

trinuclear [9]metallacrowns-3, [52, 53] tetranuclear [12]metallacrowns-4, [51, 54 - 58] and pentanuclear [15]metallacrowns-5, [59] which have a $[M\text{-}N\text{-}O]_n$ repeating unit that produce a macrocyclic structure. Lah reported a hexanuclear [18]metallacrown-6 $[Mn^{III}{}_6L_6(MeOH)_6)]$ with a $[M\text{-}N\text{-}N]_n$ repeating unit self-assembled with a simple N-N open-chain ligand N-formylsalicyl-hydrazide (H_3fshz).[60] More recently, Liu found a [30]metallacrown-10 compound $[Mn^{III}(bzshz)\text{-}(CH_3OH)]_{10}$ [61] (Figure 1-10) which is the second metallacrown with a $[M\text{-}N\text{-}N]_n$ repeating unit. This new type of metallacrown has a vacant cavity in the center of the ring cluster structure, which may have interesting host-guest recognition properties.

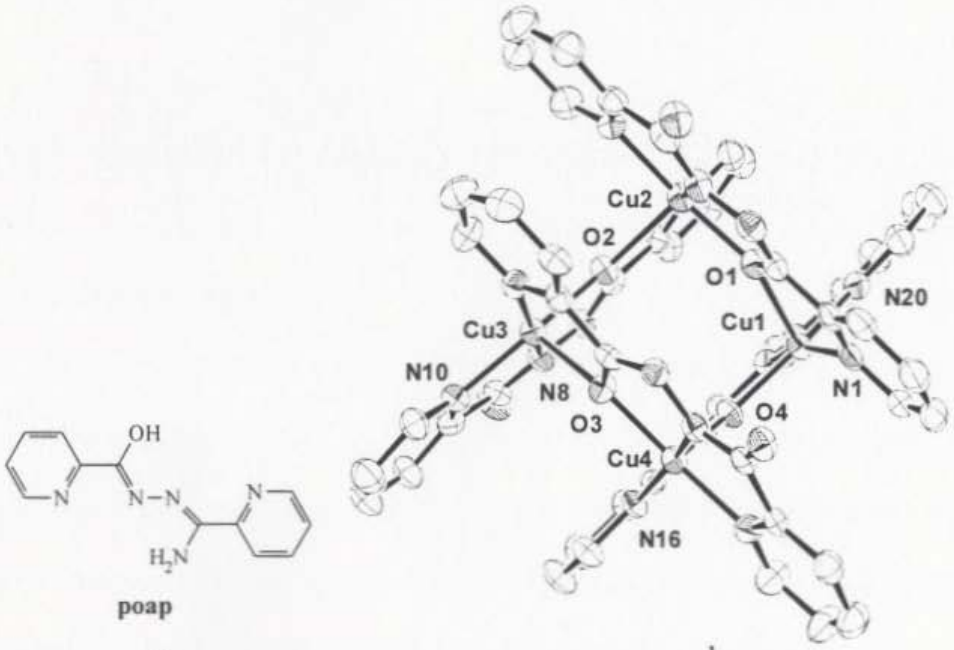

Figure 1-9. Structure representation of ligand poap (a) and the cation in $[Cu_4(poap\text{-}H)_4(H_2O)_2](ClO_4)_4 \cdot 4H_2O$ (b).

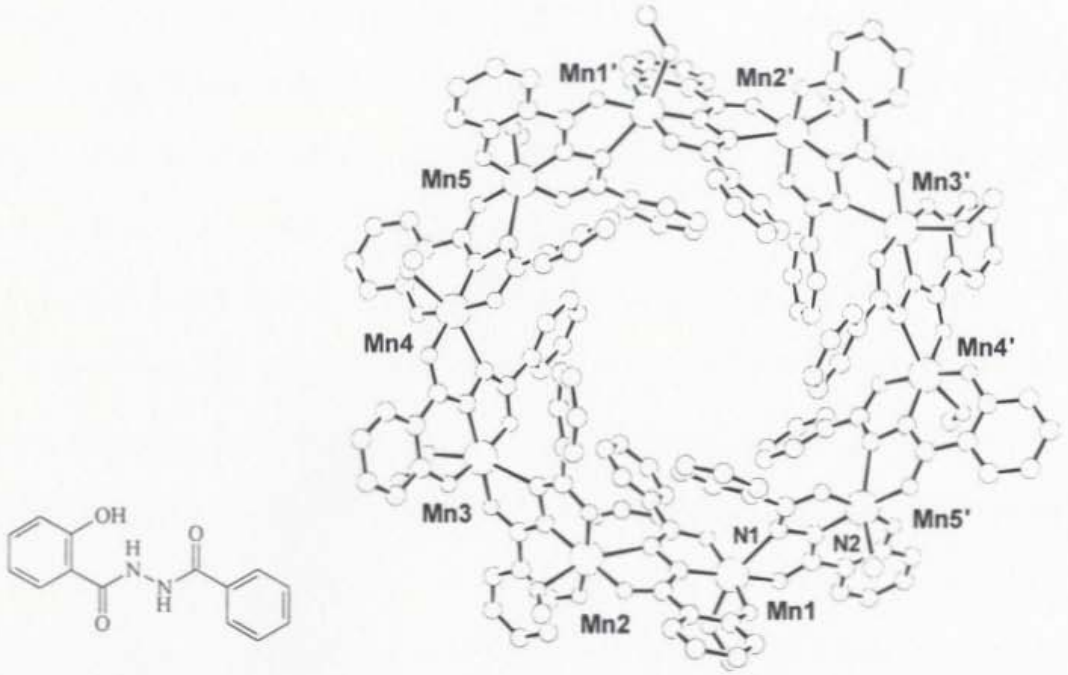

a. b.

Figure 1-10. Structure of H_3bzshz (a) and $[Mn^{III}(bzshz)(CH_3OH)]_{10}$ (b).

1.5 Significance of the Study

It is well known that molecule-based magnetic materials have potential applications in nano-technology, and may form the next generation of molecular information storage devices for the IT industry. It has been demonstrated in the last few years that information stored in molecular components can be read out by non-covalent interactions, e.g. hydrogen bonding, or metal-ligand interactions, and used to assemble the final well-ordered architectures. Recent studies by Lehn, etc. show that the excellent stability and reproducibility of controlled arrangements of metallo-supramolecular grids on surfaces makes it possible to provide practical information devices by spontaneous

self-assembly.[62] Nanometric sized magnetic materials have more advantages than traditional magnetic materials. For example, they can be formed by spontaneous assembly from solution chemistry, instead of microfabrication. The design of these high nuclearity clusters with novel magnetic properties is a major goal of current research in the area of nanoscale materials and supramolecular chemistry. In general, the size and geometry of large metal clusters are difficult to control, and these systems are invariably obtained serendipitously through self-assembly. Although self-assembly strategies have succeeded in a few cases for the formation of relatively low nuclearity molecular clusters ($<M_6$), high nuclearity predetermined grids and clusters are still rare (only one nonmagnetic [3×3] $Ag(I)_9$ and one [4×4] $Pb(II)_{16}$ (no X-ray structure) were reported so far). Recently our group reported [2×2] $Cu(II)_4$, $Ni(II)_4$, $Mn(II)_4$ and $Co(II)_4$ tetranuclear complexes self-assembled from simple tetradentate ligands, and in the case of the $Cu(II)_4$ systems ferromagnetic coupling prevails.[50] In order to extend these interesting systems, we have designed a series of more complicated polytopic ligands and succeeded in the preparation of a series of predetermined [3×3] $Cu(II)_9$ and $Mn(II)_9$ magnetic clusters.

The generation of these predetermined, large grid and cluster architectures by self-assembly processes, using preprogrammed ligands, provides a unique opportunity to produce complex nanostructures with the potential for information storage. Using the same methodology, a simple extension of this type of ligand may produce [4×4] and [5×5] grids, and even higher homologues.

1.6. Spectroscopic and Physical Measurements

Melting points were measured on a Fisher-Johns melting point apparatus. Electronic spectra were recorded as Nujol mulls and in solution using a Cary 5E spectrometer. Infrared spectra were recorded as Nujol mulls using a Mattson Polaris FTIR instrument. Mass spectra were obtained using a VG micromass 7070HS spectrometer. C, H, N analyses on vacuum dried samples (24 hr) were performed by the Canadian Microanalytical Service, Delta, B.C., Canada. ^{1}H NMR spectra were recorded on a GE 300-NB spectrometer, and chemical shifts are given in ppm relative to tetramethylsilane as an internal reference. Variable temperature magnetic data were obtained with a Quantum Design MPMS5S Squid magnetometer operating at 0.1-5.0 T (2-300K). Calibrations were carried out with a palladium standard cylinder, and temperature errors were determined with $[H_2TMEN][CuCl_4]$ ($H_2TMEN = (CH_3)_2N\text{-}CH_2CH_2NH(CH_3)_2^{2+}$). [63]

1.7 Safety Note

Perchlorate compounds are potentially explosive and should be treated with care and used only in small quantities.

Chapter 2. Trinuclear Complexes*

2.1 Introduction

In order for bioinorganic chemists to explain the relationship between functions and structures of the various copper proteins, a large number of mononuclear and dinuclear copper(II) complexes have been investigated as structural models in the last two decades.[64-68] Magneto-structural correlation's in many dinuclear copper(II) complexes have also been studied.[69 - 73] In comparison, there is little work on magnetic properties of trinuclear copper(II) complexes.[74 - 80] Trinuclear copper(II) clusters may also be of importance as models for a number of multicopper oxidases, for example, ascorbate oxidase.[1] Recently, a linear trinuclear copper(II) complex $[Cu_3L(dmso)_5(H_2O)](ClO_4)2{\cdot}H_2O$ (H_4L = 2,6-bis(salicylidene-hydrazinocarbonyl)pyridine, dmso = dimethyl sulfoxide) has been reported, in which single N-N bonds bridge adjacent copper(II) centers and moderate antiferromagnetic spin exchange among adjacent copper(II) ions was found [45]

Ligands combining the flexible N-N diazine fragment, and potentially bridging alkoxide groups (e.g. **poap**, Scheme 2-1) can bridge metal ions into a self-assembled square grid clusters (M = Cu(II), Co(II), Ni(II), Mn(II)) by the latter, or alternately into rectangle grids (M = Mn(II)).[50, 81] by both (see also Chapter 3) When extending **poap** to **2poap**, nonanuclear M_9 square grids (M= Mn, Cu) [82, 83] (see also Chapter 5) have been observed when **2poap** reacted with $Cu(NO_3)_2$, $Mn(ClO_4)_2$ and $Mn(NO_3)_2$. In all these cases intramolecular spin coupling is observed, with examples of ferromagnetic ($Cu(II)_9$)

* Zhao, L., Thompson, L.K., Xu, Z., Miller, D.O., Stirling, D.R., J. Chem. Soc. Dalton Trans., 2001, 1706.

and antiferromagnetic behavior ($Mn(II)_9$). But, if potential co-ligands are present, for example, acetate or DMF, trinuclear copper(II) complexes are formed from these tritopic ligands. When the ligand po2p, which has one more pyridyl group than **poap**, reacts with copper(II) perchlorate, a bent trinuclear copper(II) complex is formed.

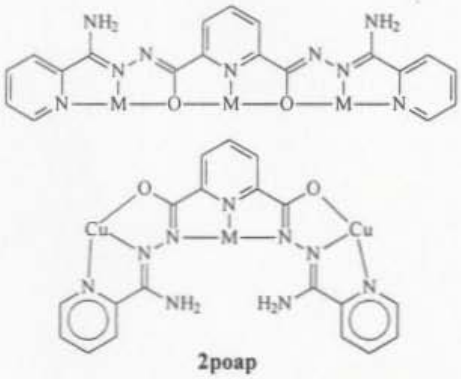

2poap

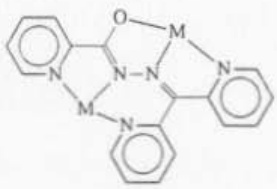

po2p

Scheme 2-1. Coordination modes of ligands for trinuclear complexes.

2.2 Experimental

2.2.1 Materials

Commercially available solvents and reagent chemicals were used without further purification.

2.2.2 Synthesis of Ligands

2poap: The methyl ester of iminopicolinic acid was prepared in situ by reaction of 2-cyanopyridine (5.2 g, 50 mmol) with sodium methoxide solution, produced by

dissolving sodium metal (0.050 g. 2.2 mmol) in dry methanol (50 mL). 2,6-pyridine dicarboxylic acid dihydrazide [45] (3.9 g. 20 mmol) was added to the above solution and the mixture was refluxed for 24 h. Yellow powder was obtained. which was filtered off. washed with water. methanol. and then diethyl ether and dried under vacuum. Yield: 6.84g. 85 %. M.P. >260°C (Dec.). Found: C. 56.23: H. 4.20: N. 30.99. Calcd. for $C_{19}H_{17}N_9O_2$: C. 56.57: H. 4.25: N. 31.35%. IR (cm^{-1}): 3475. 3328 (υ NH_2/H_2O): 1687. 1654. 1606 (υ CO/CN). . ^{1}HNMR (ppm. d_6-DMSO): 11.09 (s. 2H. OH). 8.65 (d. 2H. py). 8.23 (m. 5H. py). 7.96 (m. 2H. py). 7.54 (m. 2H. py). 7.07 (s. 4H. NH_2). MS: 403 (M^+). 386. 367 (M-2H_2O). 338. 310. 261. 223. 194. 169. 107. 78.

Po2p: 2-picolinic hydrazide (1.37 g. 0.010 mol) was dissolved in ethanol (40 mL) and a solution of dipyridyl ketone (1.84 g. 0.010 mol) in ethanol (10 mL) was added. The resulting clear solution was refluxed for 10 hr. and concentrated to a volume of 20 mL. A white crystalline product formed (Yield 2.5 g. 83 %). M.P. 162-63 °C (Found: C. 67.38: H. 4.34: N. 23.19. $C_{17}H_{13}N_5O$ requires C. 67.32: H. 4.32: N. 23.09 %): ν_{max} cm^{-1} (Nujol) 3368 (υ NH_2). 1687. 1583. 1564 (υ C=O. C=N) and 993 (py): m/z 304 (M+1). 197. 169. 168. 141. 115. 78.

2.2.3 Synthesis of Complexes

$[Cu_3(2poap\text{-}2H)(CH_3COO)_4]\cdot 3H_2O$ (1)

2poap (0.20 g. 0.50 mmol) was added with stirring to a warm solution of $[Cu(OAc)_2(H_2O)]_2$ (0.40 g. 2.0 mmol) dissolved in 20 mL deionized water. The clear

green solution was filtered and allowed to stand at room temperature for a few days. Dark yellow-green crystals suitable for structural analysis formed, which were filtered off, washed with ice water and dried in air (Yield: 0.20g, 46 %) (Found: C, 36.45; H, 3.71; N, 14.21. $[Cu_3(C_{19}H_{15}N_6O_2)(CH_3COO)_4]\cdot 3H_2O$: requires C, 36.76; H, 3.77; N, 14.29 %). λ_{max}/ nm (Nujol) 744 ; ν_{max}/cm^{-1}: 3500 (H_2O), 3320 (NH_2), 1667, 1641 (C=N), 1025 (py).

$[Cu_3(2poap\text{-}2H)(H_2O)(DMF)_3](BF_4)_4$ (2)

2poap(0.40g, 1.0 mmol was added to a solution of $Cu(BF_4)_2\cdot 6H_2O$ in MeOH /DMF and the mixture stirred at room temperature to give a greenish yellow solution. Green crystals suitable for structure determination were obtained by ether diffusion into the solution. However, the crystals were found to be unstable outside the mother liquor. Consequently a sample was stored under mother liquor prior to the structural determination. Yield: 0.48g, 42%. Found: C, 29.08; H, 2.87; N, 14.72. $[Cu_3(C_{19}H_{15}N_6O_2)\cdot(DMF)_3]\cdot(BF_4)_4$ requires C, 29.02; H, 3.13; N, 14.51 %). λ_{max}/nm (Nujol) 813; ν_{max}/cm^{-1} (crystalline sample, Nujol) 3514 (H_2O), 3440 (MeOH), 1697 (DMF), 1658, 1645 (C=N), 1072 (BF_4) and 1027 (py).

$[Cu_3(po2p\text{-}H)_2(H_2O)_2](ClO_4)_4\cdot 2H_2O$ (3)

po2p (0.15 g, 0.50 mmol) was added with stirring at room temperature to a solution of $Cu(ClO_4)_2\cdot 6H_2O$ (0.74g, 2.0 mmol) in water (20 mL) to give a greenish yellow solution. Dark green, almost black crystals were obtained on standing at room

temperature (Yield: 0.31g, 49 %) (Found: C, 32.02; H, 2.60; N, 11.01. $[Cu_3(C_{11}H_{12}N_5O)_2(H_2O)_2](ClO_4)_4 \cdot 2H_2O$ requires C, 32.29; H, 2.55; N, 11.07 %). λ_{max}/nm (Nujol) 768; ν_{max}/cm^{-1} 3600, 3450 (H_2O), 1628, 1603, 1591, 1576, 1563 (C=N) and 1096, 1051 (ClO_4).

2.2.4 Crystallography

The diffraction intensities of a dark green, irregular crystal of **1** were collected with graphite-monochromatized Cu-Kα X-radiation using a Rigaku AFC6S diffractometer at 299(1) K and the ω-2θ scan technique. The data were corrected for Lorentz and polarization effects. The structure was solved by direct methods.[84,85] All atoms except hydrogens were refined anisotropically. Hydrogen atoms were placed in calculated positions. Neutral atom scattering factors [86] and anomalous-dispersion terms [87,88] were taken from the usual sources. All calculations were performed with the teXsan [89] crystallographic software package using a PC computer. Crystal data collection and structure refinement for **3** were carried out in a similar manner using Mo-Kα radiation. Abbreviated crystal data for **1**, **3** are given in Table 2-1.

Diffraction data for single crystals of **2** were collected using a Bruker SMART CCD diffractometer, equipped with an Oxford Cryostream N_2 cooling device [90], with graphite monochromated Mo-Kα radiation. Cell parameters were determined and refined using the SMART software, [91a] raw frame data were integrated using the SAINT program,[91b] and the structure was solved using direct methods and refined by full-matrix least squares on F^2 using SHELXLT. [92] Disorder problems associated with the BF_4^-

anions have so far prevented a satisfactory refinement of this structure. Therefore only a preliminary account of the structure of the molecular cation, which is clearly defined, is presented at this time. Cell constants for **2**: Space group monoclinic C_2 m, a = 21.5552(19) Å, b = 21.1525(18) Å, c = 11.8600(10) Å, β = 120.8490(10)°, R1 = 0.0659, wR2 = 0.2122.

2.3 Results and discussion

2.3.1 X-ray Structures

Crystal structure of $[Cu_3(2poap\text{-}2H)(CH_3COO)_4]\cdot 3H_2O$ (1)

The X-ray crystal structure of **1** is illustrated in Figure 2-1, and selected bond distances and angles with their estimated standard deviations are listed in Table 2-2. The trinuclear unit consists of a single nona-dentate ligand **2poap** bound to three copper centers in an approximately linear array, with all ligand donor sites involved in coordination with the exception of the NH_2 groups. The large torsion angles Cu(2)-N(4)-N(3)-Cu(1) 168.4°, Cu(2)-N(6)-N(7)-Cu(3) 160.7° show that three coppers centers are bridged by two almost *trans* diazine (N-N) single bonds. Within the trinuclear complex the copper-copper distances exceed 4.8 Å (Cu(1)-Cu(2) 4.892(3) Å, Cu(2)-Cu(3) 4.962(3) Å).

The central copper (Cu(2)) adopts an approximately square pyramidal coordination environment, and coordinates to three nitrogen atoms from pyridine (N5) and two N-N diazine (N4, N6) and two oxygens from acetate (O5, O7). The Cu(2)-N(5) bond distance is quite short (1.933(5) Å), but the Cu(2)-N(4) and Cu(2)-N(6) distances

are much longer (2.080(5) Å and 2.141(5) Å respectively). The basal plane of the square-pyramid is defined by N(4), N(5), N(6) and O(5), with the long axial bond to mono-dentate acetate oxygen O(7). The terminal coppers are also square planar, coordinated by the terminal N_2O pocket of the ligand and a terminal acetate. However long contacts from Cu(1) and Cu(3) to acetate oxygen atoms on neighboring trinuclear subunits (Cu(1)-O(9) 2.45394) Å, Cu(3)-O(3) 2.335(4) Å) actually link the complex into a linear chain (Figure 2-2), which leads to a short inter-trinuclear metal-metal separation (Cu(1)-Cu(3) 3.371(2) Å). However despite the short distance, the connection between Cu(1) and Cu(3), which is bridged by oxygen of acetate, is strictly orthogonal (Figure 2-2), leading to the absence of any antiferromagnetic interaction between them.

The ligand **2poap** in complex **1** formally has two negative charges, which means that it loses two protons when it reacts with copper(II) ions. However, it is not easy to define the sites of deprotonation based on the bond distance assessment. Compared to C-N (1.294 – 1.341 Å) and N-N [N(3)-N(4) 1.388 Å and N(6)-N(7) 1.409 Å) distances, the short distances of C-O bonds (C(7)-O(1) 1.284(7) Å, C(13)-O(2) 1.281(7) Å) imply that C-O bonds have significant double bond character, while C-N and N-N bonds have single bond character. All this suggests that nitrogens N(3) and N(7) are the most likely sites of deprotonation, considering that the deprotonation sites should occur within the O-C-N-N fragments. The relatively short bonding distances of Cu(3)-N(7) (1.921(5) Å) and Cu(1)-N(3) (1.920(3) Å) support this inference, though some charge delocalization over the whole framework may occur at the same time.

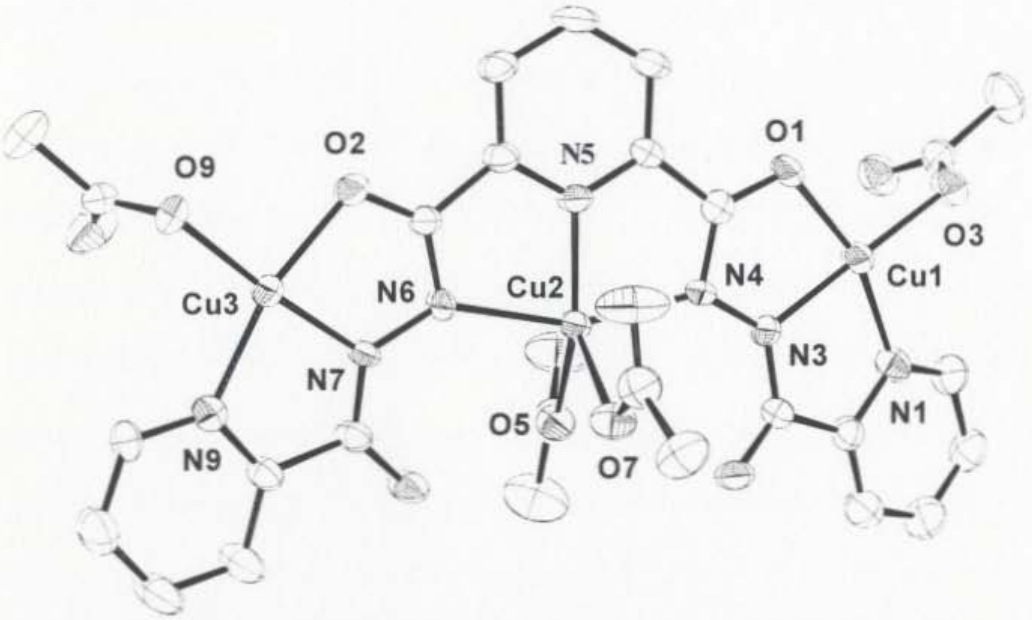

Figure 2-1. Structural representation of the trinuclear fragment in **1** (50% probability thermal ellipsoids).

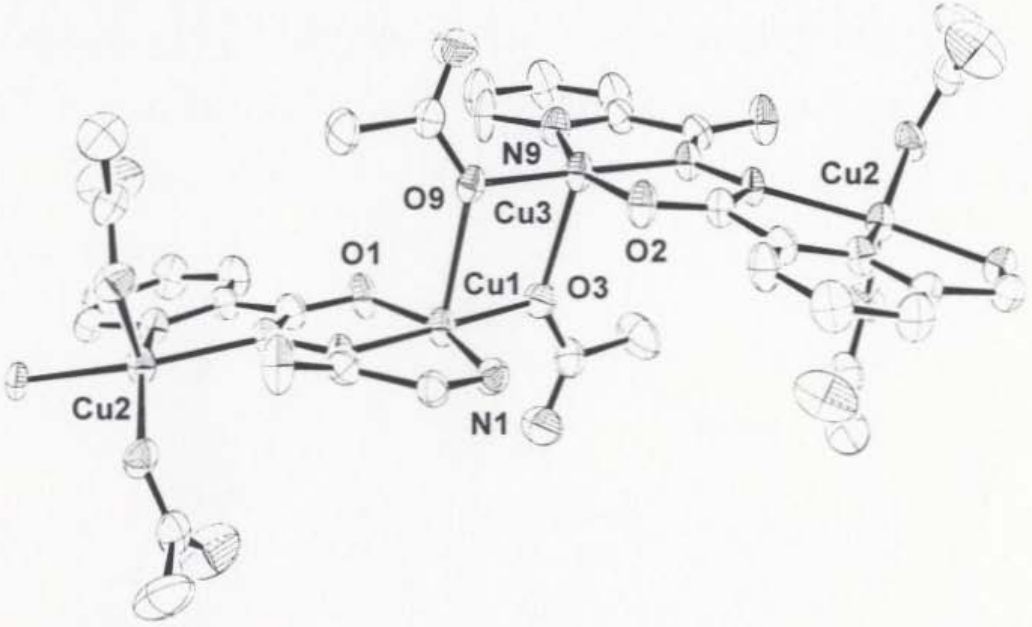

Figure 2-2. Structural representation of a chain fragment in **1** showing the orthogonal connection at Cu(1) and Cu(3) (40% probability thermal ellipsoids).

Crystal structure of $[Cu_3(2poap\text{-}2H)(H_2O)(DMF)_3(H_2O)(CH_3OH)_2](BF_4)_4$ (2)

The preliminary structural representation of the trinuclear copper(II) cation in **2** is shown in Figure 2-3. Like the structure of compound **1**, all three copper(II) centers are square pyramidal in the tricopper(II) cation and are coordinated by a single, essentially flat nano-dentate ligand **2poap**. One terminal DMF molecule is bound equatorially to Cu(1) and Cu(1)' and one DMF coordinates axially to Cu(2). In order to complete the square pyramidal coordination sphere, Cu(2) also has an equatorial coordinated water molecule, while oxygens from the solvent methanol coordinate axially to Cu(1) and Cu(1'). The neighboring copper centers separations are 4.94 Å and all copper centers are bridged only by single N-N diazine groups in almost *trans* configurations (Cu(1)-N(3)-N(4)-Cu(2) 164.6° and Cu(2)-N(4')-N(3')-Cu(1') 164.5°). No inter-trinuclear close contacts are found in **2**, but instead there is a mirror plane, which includes Cu(2), O(3), O(4), N(5) and one DMF molecule. The ligand **2poap** also loses two protons, as in **1**, and it appears that the site of negative charge is N(3). This is also supported by a short contact from Cu(1) to N(3) (1.93 Å).

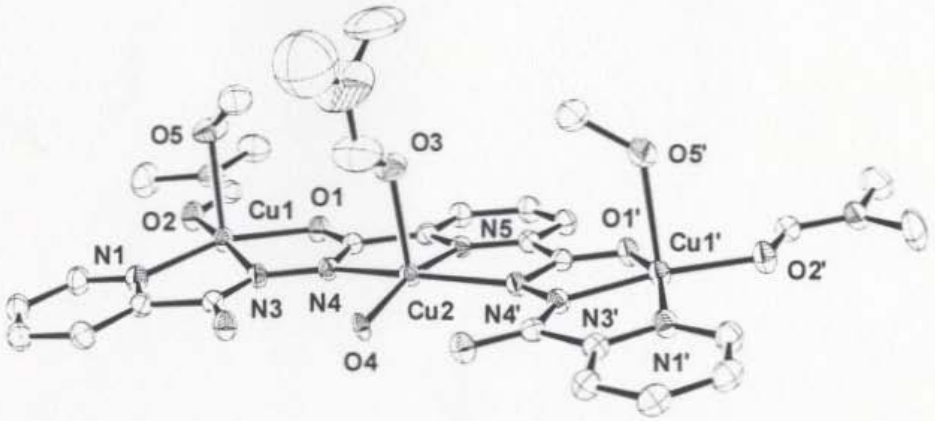

Figure 2-3. Preliminary structural representation of the cation in **2.**

Table 2-1. Summary of Crystallographic Data for **1** and **3**.

compd.	**1**	**3**
Empirical formula	$C_{27}H_{33}Cu_3N_9O_{13}$	$C_{34}H_{32}Cu_3N_{10}O_{22}Cl_4$
Formula Weight	882.25	1265.13
Crystal System	Monoclinic	Triclinic
Space group	$P2_1/n$	$P\bar{1}$
A (Å)	9.722(3)	14.751(2)
B (Å)	23.218(3)	17.692(2)
C (Å)	15.305(2)	9.773(1)
α(deg.)	90	93.269(9)
β(deg.)	93.62(2)	101.909(9)
γ(deg.)	90	110.253(7)
V ($Å^3$)	3448(1)	2318.2(5)
ρ_{calcd} (g cm^{-3})	1.696	1.807
Z	4	2
μ(mm^{-1})	1.911	4.563
λ(Å)	0.71073	0.71073
T (K)	299(1)	299(2)
R_1 (R)	0.055	0.067
wR_2 (R_w)	0.054	0.216

Table 2-2. Selected Bond Distances (Å) and Angles (°) for **1**.

Cu(1)-O(1)	1.975(4)	O(1)-Cu(1)-N(1)	161.2(2)
Cu(1)-O(3)	1.913(4)	O(1)-Cu(1)-N(3)	80.8(2)
Cu(1)-N(1)	2.006(5)	O(3)-Cu(1)-N(1)	98.8(2)
Cu(1)-N(3)	1.920(5)	O(3)-Cu(1)-N(3)	178.8(2)
Cu(1)-O(9)	2.435(4)	N(1)-Cu(1)-N(3)	80.7(2)
Cu(2)-O(5)	1.955(4)	O(5)-Cu(2)-O(7)	85.9(2)
Cu(2)-O(7)	2.129(4)	O(5)-Cu(2)-N(4)	100.1(2)
Cu(2)-N(4)	2.080(5)	O(5)-Cu(2)-N(5)	151.2(2)
Cu(2)-N(5)	1.933(5)	O(5)-Cu(2)-N(6)	98.1(2)
Cu(2)-N(6)	2.141(5)	O(7)-Cu(2)-N(4)	94.6(2)
Cu(3)-O(2)	1.971(4)	O(7)-Cu(2)-N(5)	122.9(2)
Cu(3)-O(9)	1.929(4)	O(7)-Cu(2)-N(6)	99.1(2)
Cu(3)-N(7)	1.921(5)	N(4)-Cu(2)-N(5)	79.1(2)
Cu(3)-N(9)	1.999(5)	N(4)-Cu(2)-N(6)	157.9(2)
Cu(3)-O(3)	2.335(4)	N(5)-Cu(2)-N(6)	78.9(2)
Cu(1)-Cu(2)	4.892(3)	O(2)-Cu(3)-O(9)	94.9(2)
Cu(2)-Cu(3)	4.962(3)	O(2)-Cu(3)-N(7)	80.0(2)
Cu(1)-Cu(3)	9.725(2)	O(2)-Cu(3)-N(9)	160.4(2)
N(3)-N(4)	1.388(6)	O(9)-Cu(3)-N(7)	174.8(2)
N(6)-N(7)	1.409(6)	O(9)-Cu(3)-N(9)	103.8(2)
O(1)-Cu(1)-O(3)	99.7(2)	N(7)-Cu(3)-N(9)	81.2(2)

Crystal structure of $[Cu_3(p2oap\text{-}H)_2(H_2O)_2](ClO_4)_4 \cdot 2H_2O$ (3)

The x-ray structure of the trinuclear copper(II) cation in **3** is shown in Figure 2-4. and selected bond distances and angles are given in Table 2-3. There are two ligands coordinating to three copper(II) ions in the trinuclear copper(II) cation. The neighboring copper-copper separations are 4.790(8) Å (Cu1-Cu2) and 4.672(7) Å (Cu2-Cu3) and all copper centers are bridged only by single N-N diazine groups in almost *trans* configurations (Cu(1)-N(2)-N(3)-Cu(2) 176.3° and Cu(2)-N(8)-N(7)-Cu(3) 169.0°). The central copper Cu(2) is bonded to two N_2O coordinating pockets from two ligands to produce an unusual distorted tetragonal CuN_4O_2 coordination environment. The copper equatorial plane is defined by N(8), N(10), N(3) and O(2) (Cu-donor distance <2.06 Å), while the longer Cu(2)-O(1) and Cu(2)-N(4) bonds provide axial coordination sites. In order to complete the trinuclear structure, the second coordination pockets from each ligand bind another copper and result in six coordinating sites by each ligand. Cu(3) has also a tetragonally distorted six-coordinate coordination environment with long contacts to perchlorate oxygens (Cu(3)-O(12) 2.51(2) Å, Cu(3)-O(16) 2.51 (2) Å), while Cu(1) is square-pyramidal with a long contact to perchlorate oxygen O(8) (Cu(1)-O(8) 2.61(2) Å). The twist of the two N-N fragments about the N(8)-Cu(2)-N(3) axis (N(2)-N(3)-N(8)-N(7) torsional angle 75°) leads to a non-linear trinuclear copper(II) structure (Cu(1)-Cu(2)-Cu(3) angle of 142.1°). The alkoxide oxygens of similar N-N diazine ligands are normally deprotonated when they coordinate to metal ions, but the short C-O bonding distances (C(6)-O(1) 1.23(1) Å, C(23)-O(2) 1.24(1) Å) in this structure show significant C=O double bond character and that the site of deprotonation might exist elsewhere in the

O-C-N-N framework of the ligand. There are no very short Cu-N distances, and intermediate bond distances within the immediate ligand backbone suggest a significant charge redistribution within the ligand itself.

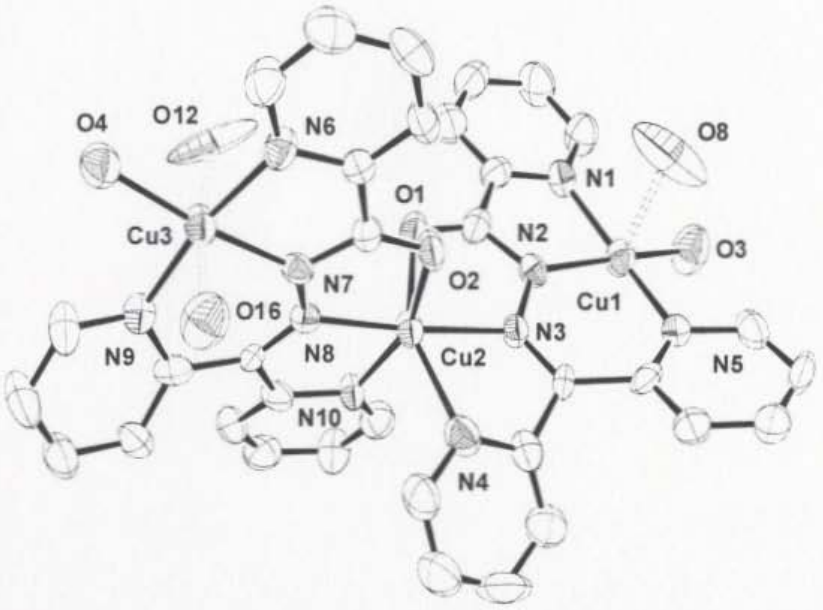

Figure 2-4. Structural representation of the cation in **3.**

Table 2-3. Selected Bond Distances (Å) and Angles (°) for **3.**

Cu(1)-O(3)	1.95(1)	O(3)-Cu(1)-N(1)	92.2(4)
Cu(1)-N(1)	2.00(1)	O(3)-Cu(1)-N(2)	167.0(5)
Cu(1)-N(2)	1.933(9)	O(3)-Cu(1)-N(5)	95.9(4)
Cu(1)-N(5)	1.97(1)	N(1)-Cu(1)-N(2)	81.5(5)
Cu(1)-O(8)	2.61(1)	N(1)-Cu(1)-N(5)	169.8(5)
Cu(2)-O(1)	2.259(9)	N(1)-Cu(1)-N(3)	91.8(4)
Cu(2)-O(2)	2.057(8)	O(1)-Cu(2)-O(2)	87.0(4)

Table 2-3. Selected Bond Distances (Å) and Angles (°) for **3**. (Continued.)

Cu(2)-N(3)	2.05(1)	O(1)-Cu(2)-N(3)	75.3(4)
Cu(2)-N(4)	2.24(1)	O(1)-Cu(2)-N(4)	151.3(4)
Cu(2)-N(8)	1.95(5)	O(1)-Cu(2)-N(8)	100.5(4)
Cu(2)-N(10)	2.01(1)	O(1)-Cu(2)-N(10)	93.4(4)
Cu(3)-O(4)	1.984(4)	O(2)-Cu(2)-N(3)	97.4(4)
Cu(3)-N(6)	2.03(1)	O(2)-Cu(2)-N(4)	99.7(4)
Cu(3)-N(7)	1.912(9)	O(2)-Cu(2)-N(8)	79.7(4)
Cu(3)-N(9)	2.03(1)	O(2)-Cu(2)-N(10)	158.8(4)
Cu(3)-O(12)	2.51(1)	N(3)-Cu(2)-N(4)	76.1(4)
Cu(3)-O(16)	2.51(1)	N(3)-Cu(2)-N(8)	175.1(4)
N(2)-N(3)	1.35(1)	N(3)-Cu(2)-N(10)	103.2(4)
N(7)-N(8)	1.35(1)	N(4)-Cu(2)-N(8)	108.2(4)
Cu(1)-Cu(2)	4.790(8)	N(4)-Cu(2)-N(10)	90.1(4)
Cu(2)-Cu(3)	4.672(7)	N(8)-Cu(2)-N(10)	79.4(4)
O(4)-Cu(3)-N(6)	95.3(4)	N(6)-Cu(3)-N(7)	81.1(4)
O(4)-Cu(3)-N(7)	172.9(4)	N(6)-Cu(3)-N(9)	169.5(4)
O(4)-Cu(3)-N(9)	94.1(4)	N(7)-Cu(3)-N(9)	90.1(4)

2.3.2. Magnetism

The magnetic exchange model for a linear trinuclear complex is represented in Figure 2-5.

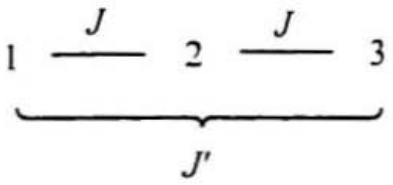

Figure 2-5. Magnetic exchange model for linear trinuclear complexes.

The isotropic exchange properties of a symmetrical system with a linear arrangement of three copper centers (S = ½) can be described by the following exchange Hamiltonian (eqn. 2-1) (Figure 2-5).

$$H = -2J[S1 \cdot S2 + S2 \cdot S3] - 2J'[S1 \cdot S3] \qquad (2\text{-}1)$$

In all three complexes (**1-3**), since the distance between external coppers (Cu1 and Cu3) is so large, J' is assumed to be zero, and eqn. 2-2 can be deduced from eqn. 2-1 (χ_M is the molar susceptibility, ρ is the fraction of paramagnetic impurity, TIP ($N\alpha$) is the temperature independent paramagnetism, θ is a Weiss-like temperature correction; all other terms have their usual significance).

$$\chi_M = \frac{Ng^2\beta^2}{3k(T-\theta)}\left[\frac{1+\exp(-2x)+10\exp(x)}{1+\exp(-2x)+2\exp(x)}\right](1-\rho)+\left(\frac{3Ng^2\beta^2}{4kT}\right)\rho + N\alpha \qquad (2\text{-}2)$$

$(x = -J/kT)$

Variable temperature magnetic susceptibility measurements were carried out on powdered samples of complexes **1-3** in the temperature range 2-300 K (4.5-300 K for **1**)

and at field strengths of 0.1T (**2** and **3**) or 1.0T (**1**). The magnetic moment per mole for complex **1** drops from 2.92 μB at 300 K to 1.85 μB at 4.5 K (Figure 2-6), which indicates strong antiferromagnetic coupling between copper(II) centers in the trinuclear fragment. The value at low temperature is the result of the residual paramagnetism associated with the odd number of copper(II) centers. The variable temperature magnetic data of **1** were fitted to eqn. 2-2 and gave excellent results with g = 2.19(1), J = -75.5(2) cm^{-1}, θ = -0.2K, ρ = 0.015, TIP = 0.000180 $emu \cdot mol^{-1}$, $10^2R = 0.6$ ($R = [\Sigma(\chi_{obs.} - \chi_{calc.})^2/\Sigma\chi_{obs}^2]^{1/2}$). The circles in Figure 2-6 represent the experimental data for **1**, while the solid line was calculated using these parameters. The very small θ correction is associated with intertrinuclear interactions and indicates that the chain structure of **1** (Figure 2-2) does not influence the magnetic properties to any significant degree, in keeping with the strictly orthogonal connections between the terminal coppers of the trinuclear subunits, and so the linear trinuclear exchange model is an accurate one.

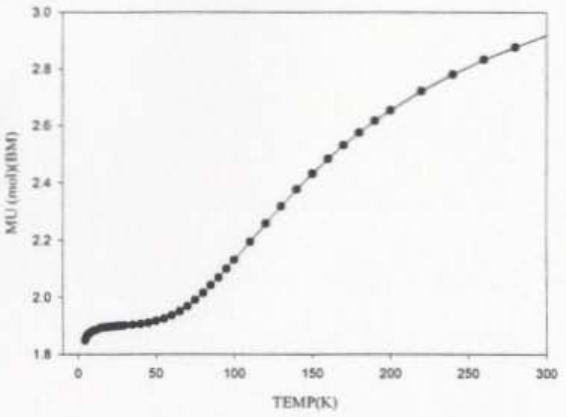

Figure 2-6. Variable temperature magnetic data for **1**.

Variable temperature magnetic data for **2** and **3** show similar profiles of magnetic moment versus temperature. Fitting of the data to eqn. 2-2 also gave excellent agreement in both cases with g = 2.24(1), J = -78.4(2) cm^{-1}, θ = -0.1 K, ρ = 0.029, TIP = 0.00022 $emu \cdot mol^{-1}$, 10^2R = 0.61 (**2**), and g = 2.12(1), J = -134.6(2) cm^{-1}, θ = -0.05 K, ρ = 0.008, TIP = 0.00020 $emu \cdot mol^{-1}$, 10^2R = 0.24 (**3**). Figure 2-7 shows the experimental and theoretical data for **3** calculated with these parameters.

The main reason for the antiferromagnetic properties of these trinuclear complexes is the single N-N bond, which is the only bridge between two adjacent copper(II) centers in the trinuclear units. Previous studies on dinuclear N-N bridged copper(II) complexes have shown clearly that exchange coupling can occur through a single N-N bond bridge and that the extent of exchange coupling is linearly dependent upon the rotational angle of the copper magnetic planes relative to the single bond itself. At large angles (a *trans* conformation) strong antiferromagnetic coupling is observed, while at smaller angles the magnetic coupling becomes weaker with a change-over to ferromagnetic coupling behavior at acute angles around 80°.[47-49] All these three trinuclear compounds have large torsional angles Cu-N-N-Cu (168.4° and 160.7° for **1**, 164.6° and 164.5° for **2**, and 176.3° and 169.0° for **3**), indicating that the central copper(II) and outer copper(II) are bridged by two almost *trans* diazine (N-N) single bonds. Compound **1** and **2** have the same ligand and similar Cu-N-N-Cu torsional angles, which lead to almost equivalent exchange integrals and compound **3** has a different ligand, but similar magnetic structural elements and larger Cu-N-N-Cu torsional angles resulting in a larger magnetic exchange integral.

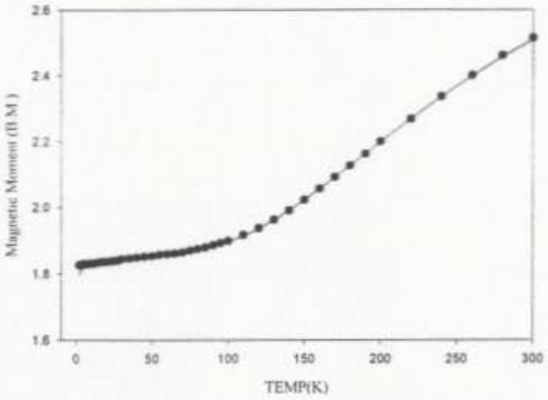

Figure 2-7. Variable temperature magnetic data for **3**.

2.4. Conclusion

Three new trinuclear complexes bridged by only N-N single bonds between the copper(II) centers are synthesized and structurally characterized. The compounds exhibit moderate to strong antiferromagnetic coupling as a result of superexchange via the N-N linkages. The magnetic properties are explained on the basis of large rotational angles of the copper magnetic planes about the diazine bridges, in agreement with previous studies on dinuclear copper(II) complexes of N-N diazine ligands.

Chapter 3. [2×2] M_4 Grids [#]

3.1 Introduction

Self-assembly processes involving carefully designed multidentate ligands can lead to sophisticated polynuclear complexes such as helicates, rings, boxes and grids. [29] At least three types of supramolecular [2×2] grids have been reported so far. One is the square grid bridged by bifunctional nitrogen donor ligands such as 4,4'-bypyridine, [93] 2,6-diazanthracene, [94] 2,6-diazanthracene-9,10-dione, [95] *cis*- or *trans*-meso-dipyridyl porphyrins [96] and the uracil monoanion, [97] where the metal ions are nonmagnetic heavy transition metals (Pd and Pt). The second type is the [2×2] grids bridged by linear polytopic cyclic N-N diazine ligands, polypyridine ligands, e.g. $Cu(II)_4$ [31], $Cu(I)_4$ from 3,6-bis(2'-pyridyl)pyridazine [98], $Co(II)_4$ from 4,6-bis(2',2''-bipyrid-6'-yl)-2-phenylpyrimidine [99, 100], $Cu(II)_4$ from 6-(3-pyrazolyl)-2,2'-bipyridine, [101] square $Ni(II)_4$ [102] and $Zn(II)_4$ [96, 103] from 3,6-bis(2-pyridyl)1,2,4,5-tetrazine. The third type is [2×2] grids bridged by only oxygens or sulfurs from the ligands, e.g., a very weak antiferromagnetically coupled phenoxo-bridged $Cu(II)_4$ grid [31], a [2×2] $Mn(II)_4$ grid bridged by non-conjugated alkoxide-type oxygen atoms [104], and a square $Co(II)_4$ grid bridged by sulfur atoms from the ligand tetra(2-pyridyl)-thiocarbazone [105] (Figure 3-1).

Recently the ligand **poap** (Figure 1-9) [50] was synthesized, which incorporates two different dinucleating fragments, alkoxo and N-N diazine, which are both well known to bridge metals and propagate spin coupling. $Cu(II)_4$, $Ni(II)_4$ and $Co(II)_4$ [2×2]

[#] Some have been published in *Inorg. Chem.*, 1999, 38, 5266 and *J. Solid State Chem.*, 2001(in press).

grids self-assembled from the reaction of this ligand and metal salts have been observed.[50, 81] In order to extend these studies, **pzoap**, **pzoapz** and **po2p** (Scheme 3-1) were prepared. In general, square $M_4(\mu\text{-}O)_4$ clusters (M = Cu(II), Ni(II), Co(II)) are self assembled from these ligands, but in one unique case (**7**, $Mn(II)_4(\mu\text{-}O)_2(N\text{-}N)_2$) a rectangular cluster results, with alternating Mn-O-Mn and Mn-N-N-Mn bridges.

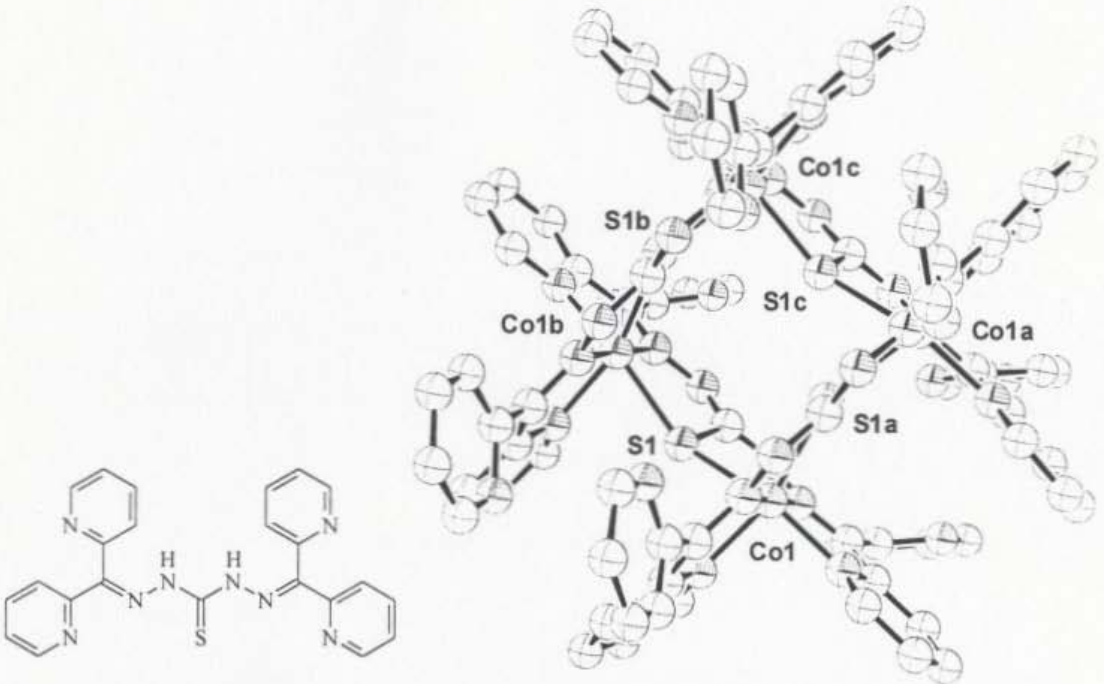

Figure 3-1. Structure of a square [2×2] Co_4 grid (b) and its ligand (a).

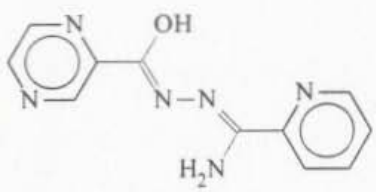

pzoap

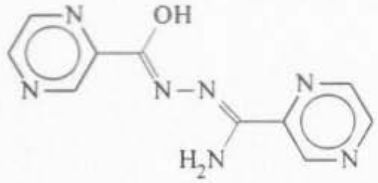

pzoapz

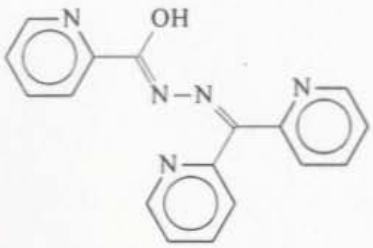

po2p

Scheme 3-1. Ligands for [2×2] clusters.

3.2 Experimental

3.2.1 Synthesis of Ligands

Pzoap, pzoapz were synthesized from the reaction of 2-pyrazine carboxylic acid hydrazide with methyl imino-picolinic acid and methyl imino 2-pyrazinecarboxylic acid respectively according to the general procedure described in Chapter 2. The synthesis of **po2p** was described in Chapter 2.

Pzoap: Yield 74%, Pale yellow powder (mp 258-9 °C). ^{1}H NMR (300 MHz, DMSO-d_6, 25 °C): 10.70 (s, 1H, OH), 9.21 (s, 1H, Ar), 8.89 (d, 1H, Ar), 8.78 (d, 1H, Ar), 8.63 (d, 1H, Ar), 8.20 (d, 1H, Ar), 7.94 (m, 1H, Ar), 7.52 (m, 1H, Ar), 7.11 (s, 2H, NH_2). Mass spectrum (major mass peaks, *m/z*): 242 (M), 225, 224 (M - NH_3 and M - H_2O, respectively), 163, 107, 79. IR (Nujol mull, cm^{-1}): 3400, 3306 (υ NH_2, OH); 1664 (s) (υ C=O); 1620 (m) (υ C=N). Anal. Calcd for $C_{11}H_{10}N_6O$: C, 54.54; H, 4.16; N, 34.69. Found: C, 54.39; H, 4.08; N, 34.88.

Pzoapz was prepared by reaction of 2-pyrazine carboxylic acid hydrazide with the methyl ester of iminopyrazine-2-carboxylic acid to give a yellow crystalline solid. Yield 86%. M.P. 268-69 °C. ^{1}HNMR (300 MHz, DMSO-d6): 10.84 (s, 1H, OH), 9.35 (s, 1H, pyz), 9.22 (s, 1H, pyz), 8.70-8.90 (m, 4H, pyz), 7.21 (s, 2H, NH_2). Mass spectrum (major mass peaks, m/z): 243(M), 226, 225, 196, 164, 138, 108, 106, 79. IR (Nujol mull, cm^{-1}): 3365, 3267, 3198 (υ NH_2, OH); 1698 (υ C=O); 1657, 1613 (υ C=N). Anal. Calcd for $C_{10}H_9N_7O$: C, 49.38; N, 3.73; N, 40.31. Found: C, 49.21; H, 3.75; N, 40.92.

3.2.2 Synthesis of Complexes

$[Cu_4(pzoap\text{-}H)_4](NO_3)_4 \cdot 3H_2O$ (4)

Pzoap (0.24g, 1.0 mmol) was added to a hot solution of $Cu(NO_3)_2 \cdot 3H_2O$ (0.98g, 4.0 mmol) in 10 mL H_2O. The resulting mixture was filtered and crystals suitable for X-ray diffraction formed from the filtrate after standing for 1-2 weeks at room temperature. Dark green crystals. Yield: 0.22g, 57%. IR (Nujol mull, cm^{-1}): 3600 (w) (υ H_2O); 3400 (w), 3350 (w) (υ NH_2); 1668 (s) (υ C=N); 1050 (m) (υ py). Vis (Nujol mull): (nm) 630 (sh), 685. Anal. Calcd for $[Cu_4(C_{11}H_9N_6O)_4](NO_3)_4 \cdot 3H_2O$: C, 34.78; H, 2.79; N, 25.83. Found: C, 34.53; H, 2.53; N, 25.79.

$[Ni_4(pzoap\text{-}H)_4(H_2O)_4](ClO_4)_4 \cdot 5H_2O$ (5)

Pzoap (0.24g, 1.0 mmol) was added to the hot solution of $Ni(ClO_4)_2 \cdot 6H_2O$ (1.46g, 4.0 mmol) in a mixture of 10 mL H_2O and 10 mL MeOH. The resulting mixture was filtered and brown crystals suitable for X-ray diffraction formed from the filtrate after

standing for 1-2 weeks at room temperature. Yield: 0.31g, 70%. IR(Nujol mull, cm^{-1}): 3445 (m) (υ H_2O), 3345 (m) (υ NH_2), 1658 (υ C=N), 1094 (υ ClO_4^-). UV-Vis (Nujol mull): (nm) 994, 650 (sh). Anal. Calcd for $[Ni_4(C_{11}H_9N_6O)_4(H_2O)_4]$ $(ClO_4)_4 \cdot 5H_2O$: C, 30.04; H, 3.07; N, 19.11. Found: C, 30.05; H, 2.94; N, 19.29.

$[Co_4(pzoapz\text{-}H)_4(H_2O)_4](ClO_4)_4 \cdot 3H_2O$ (6)

Pzoapz (0.24g, 1.0 mmol) was added to a hot solution of $Co(ClO_4)_2 \cdot 6H_2O$ (1.46g, 4.0 mmol) in a mixture of 10 mL H_2O and 5 mL MeOH. The resulting mixture was filtered and dark, almost black crystals suitable for X-ray diffraction were obtained from the mother liquor after standing for 1-2 weeks at room temperature. Yield: 0.21g, 50%. IR(Nujol mull, cm^{-1}): 1650 (υ C=N), 1039 (υ ClO_4^-). Anal. Calcd for $[Co_4(C_{10}H_8N_7O)_4 \cdot (H_2O)_4](ClO_4)_4 \cdot 3H_2O$: C, 27.81; H, 2.69; N, 22.72. Found: C, 27.75; H, 2.58; N, 22.81. UV-Vis(nm, Nujol mull): 929, 927.

$[Mn_4(po2p\text{-}H)_4(H_2O)_2](ClO_4)_4 \cdot 18H_2O$ (7)

Po2p (0.15 g, 0.5 mmol) was added to a solution of $Mn(ClO_4)_2 \cdot 6H_2O$ (1.1 g, 3.0 mmol) in MeCN/ H_2O/ MeOH mixture (10/5/5 mL) and the mixture heated to give a red-orange colored solution. Slow evaporation at room temperature gave red crystals. Yield: 0.28g, 52%. Anal. Calcd for $[Mn_4(C_{17}H_{12}N_5O)_4]$ $(ClO_4)_4 \cdot 18H_2O$: C, 37.97; H, 3.94; N, 13.02. Found: C, 37.35; H, 2.98; N, 12.93. IR (Nujol mull, cm^{-1}): 3383 (m) (υ H_2O/ NH_2), 1730 (υ C=O), 1656, 1597 (υ C=N), 1080, 1048 (υ ClO_4^-).

3.2.3 Crystallography

Data collections for **4**, **5** and **7** were made using graphite-monochromated Mo Kα X-radiation with a Siemens SMART CCD detector diffractometer equipped with a Cryostream N_2 flow cooling device.[90] Cell parameters were determined and refined with SMART [91a] using the centroid values of approximately 500 selected reflections with 2θ values between 20 and 45°. Raw frame data were integrated using the SAINT program.[91b] The structures were solved using direct methods and refined by full-matrix least squares on F^2.[92]

Diffraction data were obtained for **6** with a Rigaku AFC6S diffractometer with graphite monochromated Mo Kα radiation. The structure was solved by direct methods [84] and expanded using Fourier techniques. [85] All calculations were performed using the teXsan crystallographic software package of Molecular Structure Corporation.[89]

Non-hydrogen atoms were refined for **7** with anisotropic atomic displacement parameters (adps). Hydrogen atoms were placed in geometrically calculated positions with isotropic adps 1.2 times that of the parent atoms. Disorder problems encountered during the refinement of the structure of **7** prevent reporting full structural details at this time. Cell constants for **7**: Space group monoclinic, C2/c, a = 22.501(3) Å, b = 15.811(2) Å, c = 26.083(4) Å, β = 105.417(2)°, Z = 4.

Abbreviated crystal data for **4-6** is given in Table 2-1.

3.3 Results and Discussion

3.3.1. X-ray Structures

$[Cu_4(pzoap\text{-}H)_4](NO_3)_4 \cdot 3H_2O$ (4)

The structure of the cation of this tetranuclear grid is illustrated in Figure 3-2 and the structural square core in Figure 3-3, and important bond distances and angles are listed in Table 3-2. The four ligands are self-assembled in two parallel pairs, above and below the four copper centers, to produce a square [2×2] grid. Only the alkoxide groups link the coppers together. Copper-copper separations are close to 4 Å (Cu(1)-Cu(2') 4.0457(4) Å, Cu(1)-Cu(2) 4.0575(4) Å), with alkoxide bridge angles close to 140° (Cu(1)-O(1)-Cu(2) 140.58(7)°, Cu(1)-O(2)-Cu(2') 140.55(7)°). The Cu(1) centers have square pyramidal coordination environments, but the Cu(2) centers are six-coordinate pseudo-octahedral with a long significant contact between Cu(2) and O(5) (2.461(2) Å). The ligands are oriented with the pyrazine ends bonded individually to each copper center. The copper-oxygen bonds within the ring alternate with long and short contacts (Cu(1)-O(1) 2.015(1) Å, Cu(2)-O(1) 2.294(2) Å, Cu(2)-O(2) 2.0362(2) Å, Cu(1)-O(2) 2.261(1) Å), such that the coppers are linked alternately by the oxygen bridges with axial and equatorial contacts, leading to the strict orthogonality of magnetic orbitals of copper(II) centers.

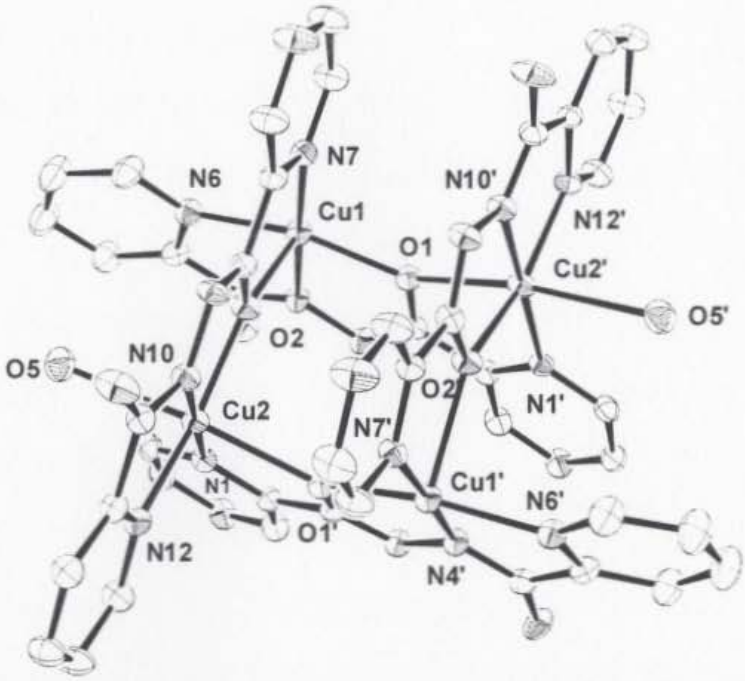

Figure 3-2. Structural representation of the cation in $[Cu_4(\mathbf{pzoap}\text{-}H)_4](NO_3)_4 \cdot 3H_2O$ (**4**) (50% probability thermal ellipsoids).

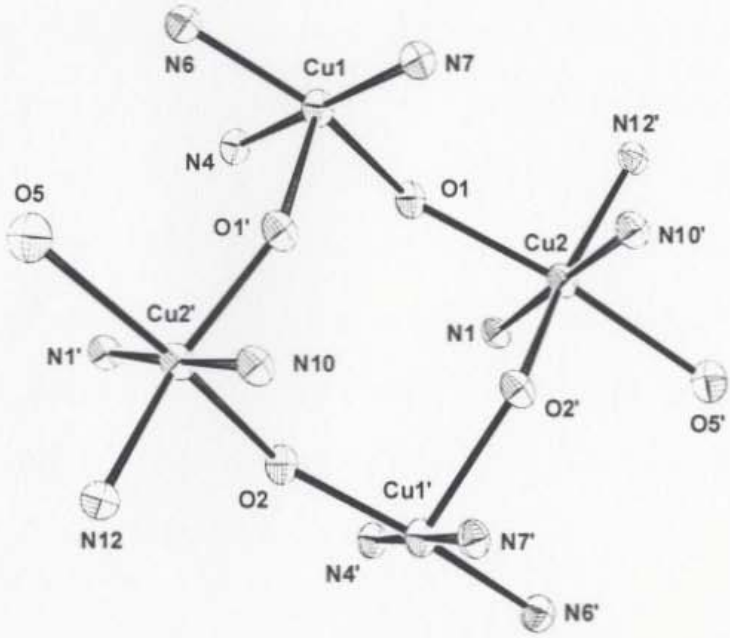

Figure 3-3. Structural representation of the tetranuclear core in **4**.

$[Ni_4(pzoap\text{-}H)_4(H_2O)_4](ClO_4)_4 \cdot 5H_2O$ (5)

The structure of the tetranuclear cation of **5** is shown in Figure 3-4, and the square structural core with just the immediate donor atoms in Figure 3-5. The important bond distances and angles are listed in Table 3-3. All the nickel centers adopt six-coordinate pseudo-octahedral coordination environments, with the pyrazine ends of the ligands bonded to the nickel centers having the coordinated water molecules, and are bridged by four alkoxide oxygens from the four deprotonated ligands. This asymmetric ligand arrangement contrasts with that in **4** where the **pzoap** ligands are arranged in an eclipsed fashion about the cluster. The four nickel centers require that 24 coordination sites be filled, which is provided by four ligands (20 coordination sites) and four water molecules, one coordinating to Ni(1), two to Ni(2) and one to Ni(1'). This leads to the situation with three different nickel centers in the cluster, *mer*-NiN_3O_3 (Ni1), *trans*-NiN_2O_4 (Ni2) and *cis*-NiN_4O_2 (Ni3). Nickel-nickel separations (Ni(1)-Ni(2) 3.967(2) Å, Ni(1)-Ni(3) 3.969(2) Å), and Ni-O-Ni angles (Ni(1)-O(1)-Ni(2) 139.08(10), Ni(1)-O(2)-Ni(3) 138.37(10)) are comparable with those in $[Ni_4(\mathbf{poap}\text{-}H)_4(H_2O)_4](NO_3)_4 \cdot 8H_2O$.[50] Nickel-oxygen (alkoxide) bond distances show an asymmetric, alternating long-short bridging arrangement within the Ni_4 square, in which Ni(2) has two short contacts to O(1) and O(1') (both 2.070 Å), Ni(3) has two long contacts to O(2) and O(2') (both 2.164 Å), while Ni(1) and Ni(1') have long and short contacts to O(1), O(2) and O(1') and O(2') (both 2.160 Å and 2.073 Å respectively).

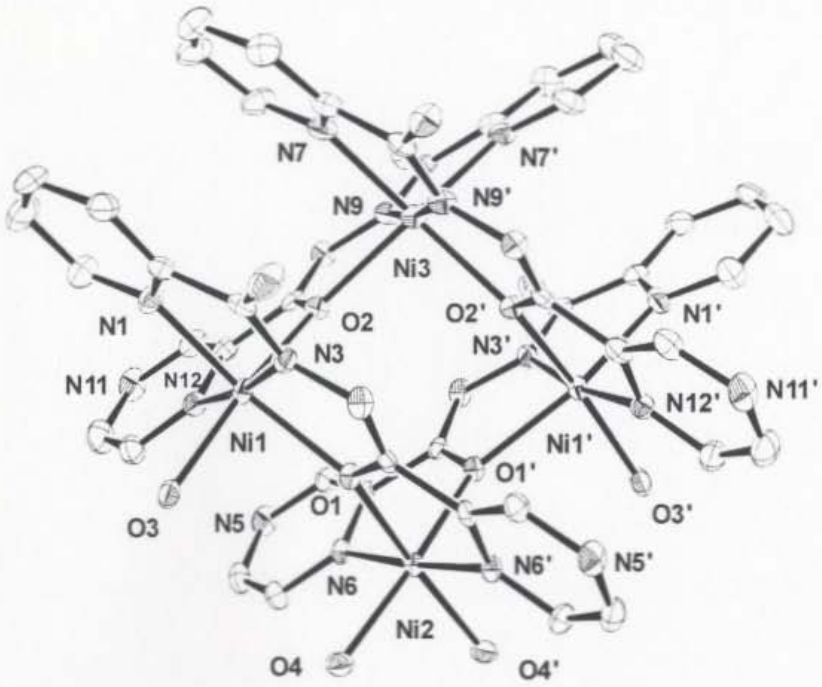

Figure 3-4. Structural representation of the square cation in **5.**

(50% probability thermal ellipsoids)

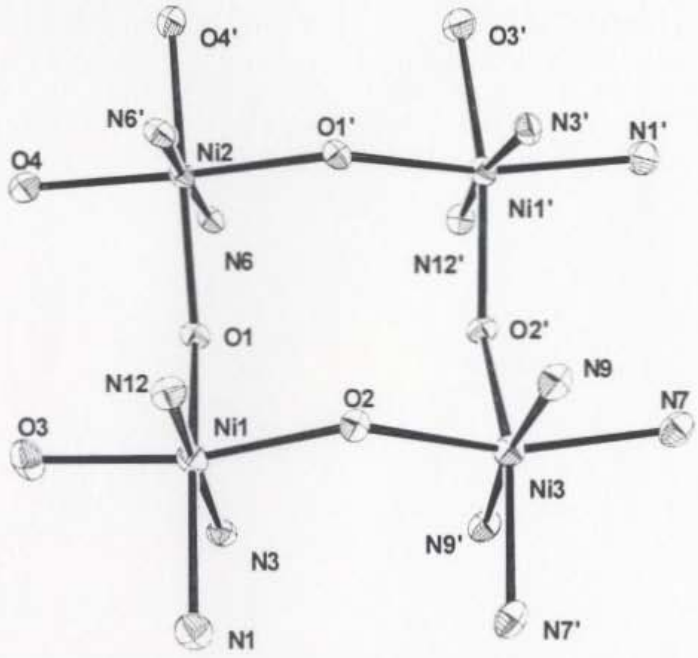

Figure 3-5. Structural representation of the tetranuclear core in **5.**

$[Co_4(pzoapz\text{-}H)_4(H_2O)_4](ClO_4)_4 \cdot 3H_2O$ (6)

A structural representation of the cation in **6** is shown in Figure 3-6, and the structural core in Figure 3-7. Selected distances and angles are listed in Table 3-4. The overall structure is a pseudo-square grid with the four cobalt centers bridged only by the alkoxide oxygens. Four pseudo-octahedral cobalt(II) centers are bound to four ligands arranged in two parallel pairs above and below the Co_4 pseudo plane. The ligands are in an opposed arrangement with NH_2 ends pointing in opposite directions. Each ligand is tetradentate, but fills five metal ion sites due to the alkoxide bridges, and four water molecules act as extra ligands, with two waters bound to Co(2) and Co(4). Co-N and Co-O distances fall in the ranges 1.99-2.19 Å and 2.01-2.18 Å, typical of six-coordinate Co(II) centers. Co-Co separations are in the range 3.88-3.95 Å, and Co-O-Co angles in the range 133.5-136.0°.

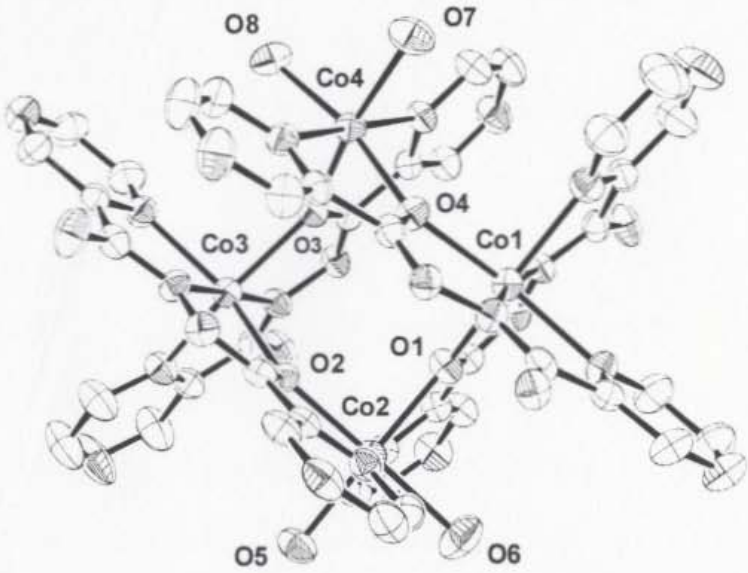

Figure 3-6. Structural representation of the tetranuclear cation in **6.**

(50% probability thermal ellipsoids).

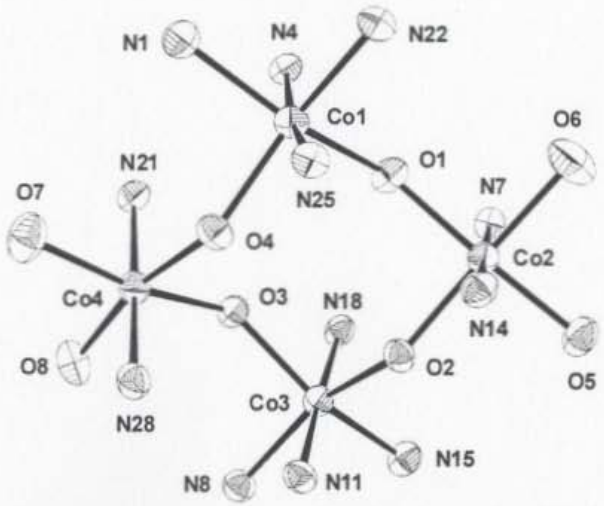

Figure 3-7. Structural representation of the tetranuclear core in **6**.

$[Mn_4(po2p\text{-}H)_4(H_2O)_2](ClO_4)_4 \cdot 18H_2O$ (7)

A structural representation of the cation in compound **7**, based on a preliminary structural determination, is shown in Figure 3-8 and the rectangular core in Figure 3-9. Four pseudo-octahedral Mn(II) centers are bound simultaneously to four depronated ligands arranged in a rectangular shape, with two ligands bridging pairs of metals with an N_2 diazine, and two providing alkoxide oxygen bridges and leaving two pyridine nitrogens uncoordinated (N30 and N30'). The ligands bridging the edges of the rectangle are tetradentate with one pyridine ring uncoordinated, while those bridging along the sides are pentadentate. Since the bridging alkoxide fills two metal coordination sites two extra ligands (water) are required to complete the six-coordination at each metal center. The manganese centers comprise two different types: MnN_5O (Mn(2)) and *mer*-MnN_3O_3 (Mn(1)). The rectangle is defined by Mn(1)-Mn(2) dimensions of 5.290 Å and 3.930 Å, with a Mn(1)-O(1)-Mn(2) angle of 127.0°, and a Mn-N-N-Mn torsional angle of 170.3°,

indicating a *trans* arrangement of the two metal centers about the N-N bridge. Mn-N and Mn-O distances fall in the ranges 2.17-2.31 Å, and 2.15-2.23 Å respectively.

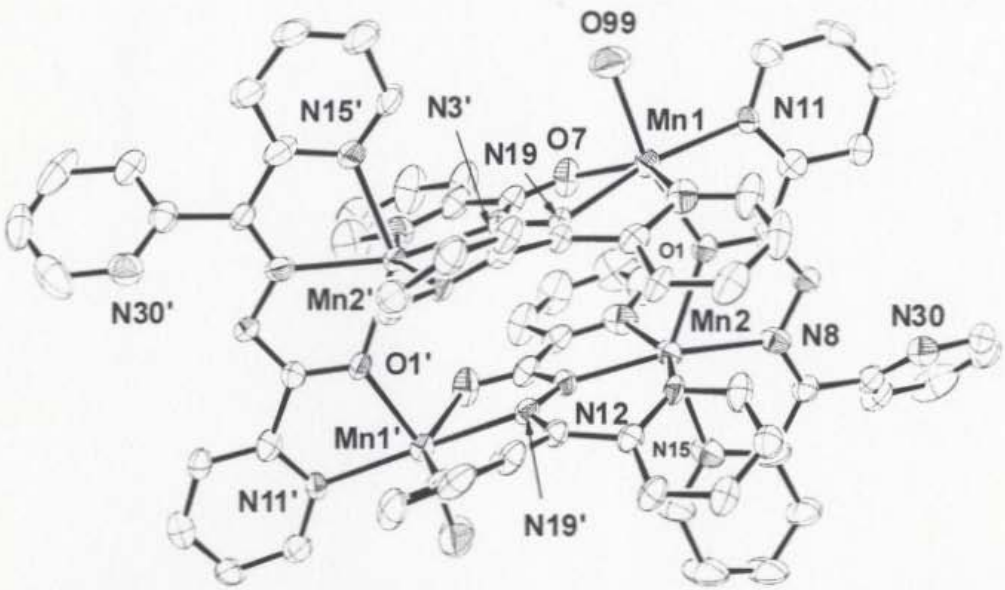

Figure 3-8. Structural representation of the tetranuclear core in **7.**

(50% probability thermal ellipsoids).

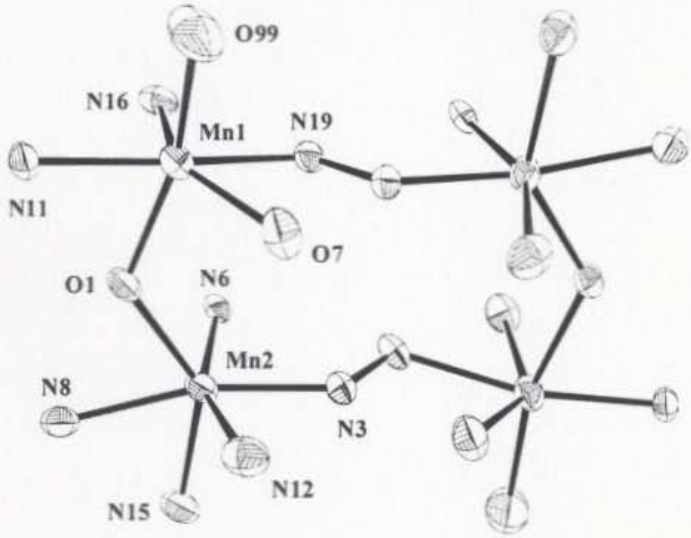

Figure 3-9. Rectangular core structure $Mn_4(N\text{-}N)_2O_2$ in **7**.

Table 3-1. Summary of Crystallographic Data for **4**. **5**. and **6**.

compd	**4**	**5**	**6**
Empirical formula	$C_{22}H_{2}$-$O_{12.5}N_{14}Cu_4$	$C_{44}H_{54}O_{28}N_{24}Cl_4Ni_4$	$C_{40}H_4$-$Cl_4Co_4N_{28}O_{2}$-
Formula Weight	814.66	1743.75	1737.53
Crystal System	Monoclinic	Orthorhombic	Monoclinic
Space group	*P2 n* (No.13)	*Pbcn* (No.60)	$P2_1$ *a* (No.14)
a (Å)	14.3573(3)	14.368(4)	23.24(1)
b (Å)	10.8910(6)	25.469(7)	13.681(3)
c (Å)	20.536(1)	18.479(5)	23.37(2)
α(deg)	90	90	90
β(deg)	96.975(4)	90	118.17(4)
γ(deg)	90	90	90
V (Å^3)	3187.4(3)	6762(3)	6550(6)
ρ_{calcd} (g cm^{-3})	1.698	1.713	1.762
Z	4	4	4
μ(mm^{-1})	1.419	1.355	1.263
λ(Å)	0.71073	0.71073	0.71069
T (K)	150(2)	100(2)	299(2)
R_1 (R)	0.0431	0.0449	0.056
wR_2 (R_w)	0.0784	0.1043	0.054

Table 3-2. Interatomic Distances (Å) and Angles (°) Relevant to the Copper Coordination Spheres in **4**.

Cu(1)-N(4)	1.9080(17)	Cu(2)-O(2')	2.0363(15)
Cu(1)-O(1)	2.0153(15)	Cu(2)-N(12')	2.0538(18)
Cu(1)-N(7)	2.0194(17)	O(2)-Cu(2')	2.0363(15)
Cu(1)-N(6)	2.0618(18)	N(10)-Cu(2')	1.9146(17)
Cu(1)-O(2)	2.2608(14)	N(12)-Cu(2')	2.0538(18)
O(1)-Cu(2)	2.2936(15)	Cu(1)-Cu(2')	4.0457(4)
N(1)-Cu(2)	2.0181(17)	Cu(1)-Cu(2)	4.0575(4)
N(4)-Cu(1)-O(1)	79.16(7)	N(10')-Cu(2)-N(1)	178.23(8)
N(4)-Cu(1)-N(7)	177.57(8)	N(10')-Cu(2)-O(2')	78.67(7)
O(1)-Cu(1)-N(7)	99.86(7)	N(1)-Cu(2)-O(2')	99.65(6)
N(4)-Cu(1)-N(6)	79.48(7)	N(10')-Cu(2)-N(12')	79.59(7)
O(1)-Cu(1)-N(6)	158.62(7)	N(1)-Cu(2)-N(12')	102.07(7)
N(7)-Cu(1)-N(6)	101.45(7)	O(2')-Cu(2)-N(12')	158.26(6)
N(4)-Cu(1)-O(2)	104.46(7)	N(10')-Cu(2)-O(1)	103.28(7)
O(1)-Cu(1)-O(2)	96.21(6)	N(1)-Cu(2)-O(1)	77.30(6)
N(7)-Cu(1)-O(2)	77.82(6)	O(2')-Cu(2)-O(1)	92.64(6)
N(6)-Cu(1)-O(2)	89.95(7)	N(12')-Cu(2)-O(1)	93.01(6)
Cu(1)-O(1)-Cu(2)	140.58(7)	Cu(2')-O(2)-Cu(1)	140.55(7)

Table 3-3. Interatomic Distances (Å) and Angles (°) Relevant to the Nickel Coordination Spheres in **5**.

Ni(1)-O(1)	2.162(2)	Ni(2)-N(6)	2.038(3)
Ni(1)-O(2)	2.077(2)	Ni(3)-O(2)	2.169(2)
Ni(1)-O(3)	2.055(2)	Ni(3)-N(7)	2.114(3)
Ni(1)-N(1)	2.127(3)	Ni(3)-N(9)	1.970(3)
Ni(1)-N(3)	1.966(3)	N(3)-N(4)	1.400(3)
Ni(1)-N(12)	2.069(3)	Ni(1)-Ni(3)	3.969(2)
Ni(2)-O(1)	2.072(2)	Ni(1)-Ni(2)	3.967(2)
Ni(2)-O(4)	2.083(2)		
O(1)-Ni(1)-O(2)	91.12(8)	O(2')-Ni(3)-N(9)	109.42(9)
O(1')-Ni(2)-N(6')	80.73(9)	N(1)-Ni(1)-N(3)	77.74(10)
O(1)-Ni(1)-O(3)	85.44(8)	N(7')-Ni(3)-N(9)	97.50(11)
O(4')-Ni(2)-N(6')	91.57(9)	N(1)-Ni(1)-N(12)	95.10(10)
O(1)-Ni(1)-N(1)	153.78(9)	N(9)-Ni(3)-N(9')	172.47(11)
O(2)-Ni(3)-N(7)	153.00(9)	N(3)-Ni(1)-N(12)	171.97(10)
O(1)-Ni(1)-N(3)	76.34(9)	O(2')-Ni(3)-N(7')	153.00(9)
O(2)-Ni(3)-N(9)	75.91(9)	O(1)-Ni(2)-O(4)	91.33(8)
O(1)-Ni(1)-N(12)	111.01(9)	O(2')-Ni(3)-N(9')	75.91(9)
O(2)-Ni(3)-O(2')	94.82(8)	O(1)-Ni(2)-N(6)	80.73(9)
O(2)-Ni(1)-O(3)	167.05(9)	N(7)-Ni(3)-N(9)	77.52(10)

Table 3-3. Interatomic Distances (Å) and Angles (°) Relevant to the Nickel Coordination Spheres in **5**. (Continued)

O(2)-Ni(3)-N(7')	89.50(9)	O(1)-Ni(2)-O(1')	90.48(8)
O(2)-Ni(1)-N(1)	95.99(9)	O(1)-Ni(2)-O(4')	172.19(8)
O(2)-Ni(3)-N(9')	109.42(9)	O(1)-Ni(2)-N(6')	96.22(9)
O(2)-Ni(1)-N(3)	97.20(9)	O(4)-Ni(2)-N(6)	91.57(9)
O(2)-Ni(1)-N(12)	79.77(9)	O(1')-Ni(2)-O(4)	172.19(8)
O(2')-Ni(3)-N(7)	89.50(9)	O(4)-Ni(2)-O(4')	87.89(8)
O(3)-Ni(1)-N(1)	92.54(10)	O(1')-Ni(2)-N(6)	96.22(9)
N(7)-Ni(3)-N(7')	98.63(10)	O(4')-Ni(2)-N(6)	91.52(9)
O(3)-Ni(1)-N(3)	94.12(10)	N(6)-Ni(2)-N(6')	175.70(11)
N(7)-Ni(3)-N(9')	97.50(10)	O(1')-Ni(2)-O(4')	91.33(8)
O(3)-Ni(1)-N(12)	89.80(10)	Ni(1)-O(1)-Ni(2)	139.08(10)
N(7')-Ni(3)-N(9')	77.52(10)	Ni(1)-O(2)-Ni(3)	138.37(10)

Table 3-4. Interatomic Distances (Å) and Angles (°) Relevant to the Cobalt Coordination Spheres in **6**.

Co(1)-N(1)	2.177(3)	Co(4)-O(3)	2.105(3)
Co(1)-O(4)	2.130(3)	Co(4)-O(4)	2.076(4)
Co(1)-N(1)	2.187(4)	Co(4)-O(7)	2.157(4)
Co(1)-N(4)	1.993(4)	Co(4)-O(8)	2.037(4)
Co(1)-N(22)	2.201(4)	Co(4)-N(21)	2.138(4)
Co(1)-N(25)	2.014(4)	Co(4)-N(28)	2.152(4)
Co(2)-O(1)	2.073(3)	Co(1)-Co(2)	3.941(2)
Co(2)-O(2)	2.100(3)	Co(2)-Co(3)	3.947(2)
Co(2)-O(5)	2.074(4)	Co(3)-Co(4)	3.880(2)
Co(2)-O(6)	2.130(4)	Co(1)-Co(4)	3.870(2)
Co(2)-N(7)	2.135(4)	O(1)-Co(1)-O(4)	99.0(1)
Co(2)-N(14)	2.154(4)	O(5)-Co(2)-N(14)	90.5(1)
Co(3)-O(2)	2.168(4)	O(1)-Co(1)-N(1)	150.6(1)
Co(3)-O(3)	2.119(3)	O(6)-Co(2)-N(7)	86.8(2)
Co(3)-N(8)	2.160(4)	O(1)-Co(1)-N(4)	75.4(1)
Co(3)-N(11)	2.007(3)	O(6)-Co(2)-N(14)	89.7(2)
Co(3)-N(15)	2.162(4)	O(1)-Co(1)-N(22)	92.8(1)
Co(3)-N(18)	1.997(3)	N(7)-Co(2)-N(14)	176.4(1)

Table 3-4. Interatomic Distances (Å) and Angles (°) in **6**. (Continued)

O(1)-Co(1)-N(25)	106.3(1)	N(22)-Co(1)-N(25)	73.9(1)
O(2)-Co(3)-O(3)	97.0(1)	N(8)-Co(3)-N(15)	87.3(2)
O(4)-Co(1)-N(1)	91.8(1)	O(1)-Co(2)-O(2)	90.7(1)
O(2)-Co(3)-N(8)	150.8(1)	N(8)-Co(3)-N(18)	106.4(2)
O(4)-Co(1)-N(4)	116.4(2)	O(1)-Co(2)-O(5)	168.5(1)
O(2)-Co(3)-N(11)	75.1(1)	N(11)-Co(3)-N(15)	103.1(1)
O(4)-Co(1)-N(22)	148.7(1)	O(1)-Co(2)-O(6)	91.6(1)
O(2)-Co(3)-N(15)	95.7(2)	N(11)-Co(3)-N(18)	177.5(2)
O(4)-Co(1)-N(25)	75.0(1)	O(1)-Co(2)-N(7)	78.2(1)
O(2)-Co(3)-N(18)	102.5(1)	N(15)-Co(3)-N(18)	76.2(1)
N(1)-Co(1)-N(4)	75.3(1)	O(1)-Co(2)-N(14)	101.0(1)
O(3)-Co(3)-N(8)	94.1(1)	O(3)-Co(4)-O(4)	88.2(1)
N(1)-Co(1)-N(22)	92.0(2)	O(2)-Co(2)-O(5)	92.2(1)
O(3)-Co(3)-N(11)	105.5(1)	N(1)-Co(1)-N(25)	102.9(2)
N(1)-Co(1)-N(25)	102.9(2)	O(3)-Co(4)-O(7)	168.9(1)
O(3)-Co(3)-N(15)	150.9(1)	O(2)-Co(2)-O(6)	167.3(1)
N(4)-Co(1)-N(22)	94.7(2)	O(3)-Co(4)-O(8)	87.3(1)
O(3)-Co(3)-N(18)	75.6(1)	O(2)-Co(2)-N(7)	105.9(1)
N(4)-Co(1)-N(25)	168.4(2)	O(3)-Co(4)-N(21)	77.0(1)
N(8)-Co(3)-N(11)	75.9(2)	O(2)-Co(2)-N(14)	77.6(1)

Table 3-4. Interatomic Distances (Å) and Angles (°) in **6**. (Continued)

O(3)-Co(4)-N(28)	106.8(1)	O(7)-Co(4)-N(28)	83.6(1)
O(5)-Co(2)-O(6)	88.0(2)	O(8)-Co(4)-N(21)	93.2(2)
O(4)-Co(4)-O(7)	90.2(1)	O(8)-Co(4)-N(28)	91.2(1)
O(5)-Co(2)-N(7)	90.3(1)	N(21)-Co(4)-N(28)	174.4(1)
O(4)-Co(4)-O(8)	166.4(1)	Co(1)-O(4)-Co(4)	133.9(1)
O(4)-Co(4)-N(21)	98.3(1)	Co(1)-O(1)-Co(2)	136.0(1)
O(4)-Co(4)-N(28)	77.8(1)	Co(2)-O(2)-Co(3)	135.2(1)
O(7)-Co(4)-O(8)	96.6(2)	Co(3)-O(3)-Co(4)	133.5(1)
O(8)-Co(4)-N(21)	92.4(1)		

3.3.2 Self Assembly

These ditopic ligands, for example **pzoap** (Scheme 3-1), generally form square and rectangular tetranuclear grids when they react with metal ions in their deprotonated forms. The current group of ligands produce square $M_4(\mu\text{-}O)_4$ alkoxide bridged grids with Cu(II), Ni(II), Co(II) salts, and a rectangular mixed bridge grid, $Mn_4(\mu\text{-}O)_2(\mu\text{-}N\text{-}N)_2$. A mechanism for self-assembly in the process of forming these clusters is hard to pinpoint, but the bridging of the deprotonated alkoxide oxygens and the contiguous coordination pockets capable of producing five-membered chelate rings on bonding to transition metal centers are believed to play the key roles. The self-assembly process may involve pre-coordination of a metal ion on one side of the ligand in a NO or N_2O pocket, with extra coordination sites occupied by solvent molecules (usually water

molecules), which would produce a viable building block. The sequential docking of such subunits would then proceed to construct the grid in a square or rectangular arrangement based on the matching of the positions of the pockets, and the octahedrally based bond angles around the metal centers themselves. The ultimate subtle differences in resulting grid conformations may rest with subtle differences in the ligands themselves.

3.3.3 Magnetic Properties

The magnetic exchange model for the square grid complexes is represented in Figure 3-10a (For simplicity the model assumes that all exchange integrals between adjacent pairs of metal centers are the same.) and is described by the exchange Hamiltonian given in eqn. 3-1.

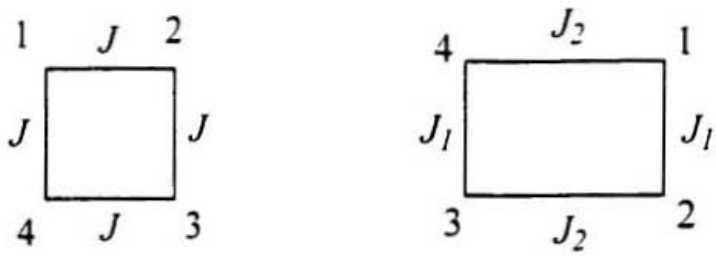

a. b.

Figure 3-10. Exchange model for square (a) and rectangle (b) [2×2] grids.

$$H = -2J(S_1 \cdot S_2 + S_2 \cdot S_3 + S_3 \cdot S_4 + S_1 \cdot S_4) \qquad (3\text{-}1)$$

$$\chi_{M'} = \frac{Ng^2\beta^2}{3k(T-\theta)} \frac{\sum S_T(S_T+1)(2S_T+1)e^{-E(S_T)/kT}}{\sum S_T(2S_T+1)e^{-E(S_T)/kT}} \qquad (3\text{-}2)$$

$$\chi_M = \chi_{M'}(1-\rho) + \frac{2N\beta^2 g^2 \rho}{3kT} + TIP \qquad (3\text{-}3)$$

The normal procedure for generating the exchange equation requires the calculation of the total spin state combinations, using a spin vector coupling approach, and their associated energies, followed by substitution into the Van Vleck equation (eqn. 3-2). This is a very tedious procedure for large grids and clusters, and to simplify this process all the calculations have been combined in a software package (MAGMUN), [106] which generates the exchange equation internally, and allows the non-linear regression fittings of the experimental susceptibility data as a function of temperature. The exchange Hamiltonian information is transferred to the file OW01.ini [106a] (Figure 3-11) as spin number, coupling patterns, and arbitrary coupling strength (The value of -1 cm^{-1} is simply factored in the non-linear regression process to generate the best fit 'J' value.), and the S' values and their energies are calculated using OW01.exe. The resulting .spk file is read by MAGMUN.exe to create the exchange equation and allow data fitting. Eqn. 3-2 and 3-3 allows for inclusion of paramagnetic impurity fraction (ρ), TIP (temperature independent paramagnetism) and Weiss intermolecular exchange effects (θ). Other terms have their usual meaning.

Spins: 2 2 2 2

Couplings: 12 23 34 41

Strengths: -1 -1 -1 -1

Eigenvectors: no

Output:Ni4

Figure 3-11. Example of OW01.ini file for square $Ni(II)_4$ grid.

The magnetic exchange model for the rectangular grid complexes is represented in Figure 3-10b and the Hamiltonian equation (eqn. 3-4) can be used to describe it. Data fitting can be done by simply fixing one J as a fraction of the other, i.e. J_1 and αJ_1 using MAGMUN [106] as described above.

$$H = -2J_1[S_1.S_2+S_3.S_4] -2J_2 [S_2.S_3+S_1.S_4] \qquad (3\text{-}4)$$

Variable temperature magnetic susceptibility measurements were carried out on powdered samples of complexes **4**-**7** in the temperature range 2-300 K (**5**, **7**) (5-300K for **4**, **6**) and at field strengths of 0.1T (**7**) or 0.2T (**4**, **6**) or 1.0T (**5**). Magnetic data for complexes **4**-**7** are summarized in Table 3-5.

Magnetic moment (per mole) versus temperature (K) data for **4** are shown in Figure 3-12. The magnetic moment at room temperature for **4** is higher than normal values for uncoupled copper(II) complexes, and suggests either the absence of exchange or the possible presence of ferromagnetic exchange. Compound **4** shows an approximately constant value of 4.0 μ_B in the range of 300-100 K, followed by a sharp increase to 5.0 μ_B at 5 K. This behavior is typical of a cluster exhibiting intramolecular ferromagnetic coupling. The variable temperature magnetic data were fitted to an exchange expression (eqn 3-3) for a square arrangement of four S = ½ metal centers. The solid circles in Figure 3-12 represent the experimental data and the solid line represents the best fit of the data with g = 2.221(5), J = 8.2(4) cm^{-1}, = 0.0004, TIP = 242 $\times 10^{-6}$ emu·mol^{-1}, θ = -0.4 K, 10^2R = 1.1 ($R = [\Sigma (\chi_{obs} - \chi_{calc})^2 / \Sigma \chi_{obs}^2]^{1/2}$). The positive J value confirms the intramolecular ferromagnetic coupling, which can be expected from its peculiar Cu_4O_4 structure. The structure shows that all the copper(II) centers are linked

by axial/equatorial (orthogonal) contacts through the alkoxide bridges, which nominally indicates a lack of antiferromagnetic coupling, as observed. The dominant strong ferromagnetism may be due to the close proximity of the four copper centers within the square arrangement.

The variable temperature magnetic data of **5** (magnetic susceptibility *vesus* temperature) are shown in Figure 3-13, which indicates completely different behavior, compared to the square Cu_4O_4 (**4**). Compound **5** has a room-temperature magnetic moment of 2.01 μ_B (per mole) and shows a maximum at 26 K in the χ_M versus temperature profile (Figure 3-13), indicating intramolecular antiferromagnetic coupling. An excellent fit of the data to eqn 3-3 (S = 1) was obtained with g = 2.205(4), J = -3.2(2) cm^{-1}, ρ = 0.005, θ = 0 K, $TIP = 800 \times 10^{-6}$ emu·mol^{-1}, 10^2R = 0.35 ($R = [\Sigma(\chi_{obs} - \chi_{calc})^2/\Sigma\chi_{obs}^2]^{1/2}$). The solid line in Figure 3-13 was calculated with these parameters. The presence of antiferromagnetic exchange in **5** is entirely consistent with its structure, in which the four octahedral Ni(II) centers are bridged only by the alkoxide groups with Ni-O-Ni angles of 138.53° and 139.00°. However, the calculated J value for **5** is smaller than anticipated, based on the magnitude of the Ni-O-Ni angles,[107] and this may be due to the alternating short-long contact arrangement within the Ni_4O_4 square.

Compound **6** (Figure 3-14) has a molar magnetic moment of 11.2 μ_B at room temperature (300 K), and drops steadily to 1.5 μ_B at 5 K, which is clearly indicating the presence of significant intramolecular antiferromagnetic exchange. The data for **6** were fitted to an isotropic exchange expression (eqn. 3, S = 3/2) for a square tetranuclear complex, and gave good fitting parameters of g = 2.42(1), J = -6.95(4) cm^{-1}, ρ = 0.004,

TIP = 0.000120 emu·mol^{-1}, θ = 0 K, 10^2R = 1.20 (R = $[\Sigma(\chi_{obs} - \chi_{calc})^2/\Sigma\chi_{obs}^2]^{1/2}$). The solid line in Figure 3-14 was calculated with these parameters. The negative J value confirms the antiferromagnetic exchange, which is consistent with its alkoxide bridged square structure, and large Co-O-Co angles.

The variable temperature magnetic data for **7** are shown in Figure 3-15. Magnetic moments (per mole) versus temperature of **7** show a similar profile to compound **6** from 2-300 K, indicative of intramolecular antiferromagnetic exchange. The susceptibility data were fitted to an appropriate exchange expression derived as described above from a spin Hamiltonian (eqn. 3-4) appropriate to a rectangle of four S = 5/2 centers. A very good data fit was obtained with g = 2.00, J_1 = -1.9(2) cm^{-1}, J_2 = -0.1(1) cm^{-1}, ρ = 0.037, TIP = 0 emu.mol^{-1}, 10^2R = 0.60 (R = $[\Sigma(\chi_{obs} - \chi_{calc})^2/\Sigma\chi_{obs}^2]^{1/2}$). The solid line in Figure 3-15 was calculated with these values. Two negative J values are consistent with the structure, which shows a Mn-O-Mn angle 127.0°, and a Mn-N-N-Mn torsional angle of 170.3°. J_1 is tentatively assigned to the Mn-O-Mn bridging interaction, and J_2 to the *trans* N-N bridge arrangement. Both bridges would be expected to produce antiferromagnetic coupling due to their large angles. [48]

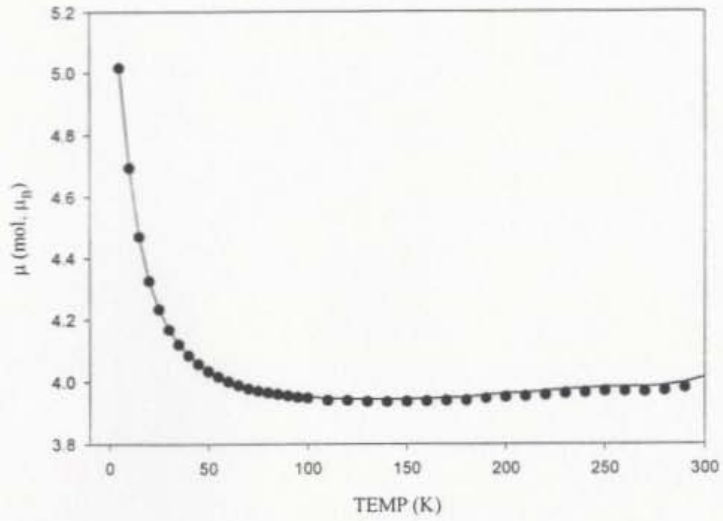

Figure 3-12. Variable temperature magnetic data for **4**.

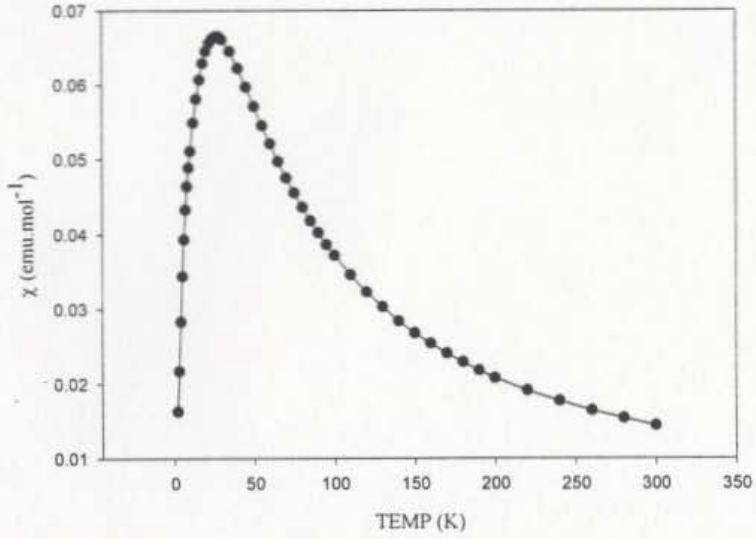

Figure 3-13. Variable temperature magnetic data for **5**.

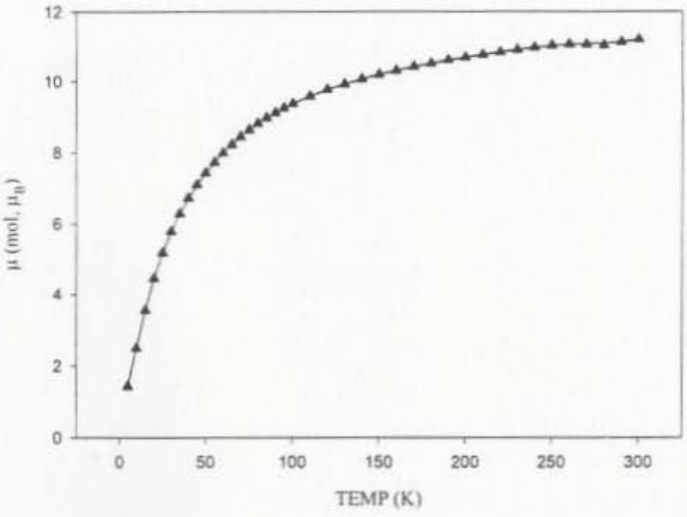

Figure 3-14. Variable temperature magnetic data for **6**.

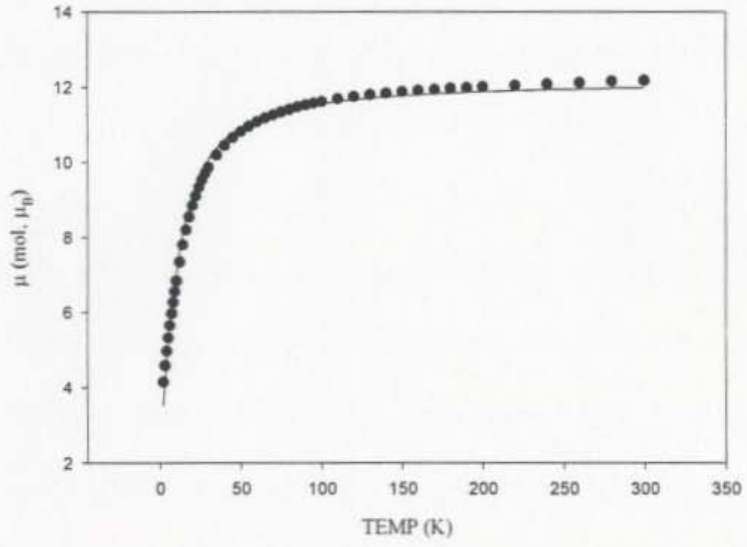

Figure 3-15. Variable temperature magnetic data for **7**.

Table 3-5. Magnetic Data for M_4 Grid Compounds.

Compd.	g	J (cm^{-1})	ρ	TIP ($\times 10^{-6}$ $emu.mol^{-1}$)	θ (K)	10^2R
4	2.221(5)	8.2(4)	0.0004	242	-0.4	1.1
5	2.205(4)	-13.2(2)	0.005	800	0	0.35
6	2.42(1)	-6.95(4)	0.004	120	0	1.20
7	2.00	J_1 -1.9(2)	0.037	0	0	0.60
		J_2 -0.1(1)				

3.4 Conclusion

A series of polynucleating ligands with dual bridging functionality has been successfully used to generate predominantly square $M_4(\mu\text{-}O)_4$ (M = Cu(II), Ni(II) and Co(II)) complexes and a rectangular $Mn_4(N\text{-}N)_2O_2$ grid complex. These examples arise through a self-assembly process, which is controlled in the sense that a predetermined structural arrangement is logically based on the strategic positions of the donor groups within the ligand backbone. The square copper cluster exhibits intramolecular ferromagnetic spin exchange, associated with the orthogonal alkoxide bridging arrangement and the close proximity of the copper centers. Both the $Ni_4(\mu\text{-}O)_4$ and $Co_4(\mu\text{-}O)_4$ clusters are antiferromagnetically coupled due to the large M-O-M angles and for the rectangular Mn_4 the exchange is dominated by antiferromagnetic coupling via both the alkoxide and the N-N bridges.

Chapter 4. From [2×2] Square Grid to a Metallacyclic Ni_8 Cluster

4.1 Introduction

Self-assembly reactions producing high nuclearity spin-coupled metallamacrocycles have been achieved in the past decade. Using alkoxides or carboxylates as bridging ligands, Fe_6 [108, 109], Fe_8 [6], Fe_{10} [6], Fe_{12} [110] rings, a Fe_{18} wheel [10], and a $Cr(III)_8$ ring [111] have been synthesized and structurally characterized. In all the cases, the metal-metal interactions are antiferromagnetic, yielding ground states S = 0. A square-antiprismatic ring cluster $[La_8L_8]$ (L = 4-(1,3,5-benzenecarbonyl)-tris(3-methyl-1-phenyl-2-pyrazolin-5-one)) [112] has also been reported recently. Winpenny, et al. reported a Ni_{12} wheel featuring acetate and 6-chloro-2-pyridonate ligands which shows ferromagnetic exchange between the metal centers, and a resulting S=12 spin ground state. [113] More recently, they synthesized a cyclic Ni_{24} cage $[Ni_{24}(OH)_8(mpo)_{16}(O_2CMe)_{24}\cdot(\mathbf{Hmpo})_{16}]$ (Figure 4-1) from the heterocyclic ligand, 3-methyl-3-pyrazolin-5-one (**Hmpo**).[114] These metallamacrocycles involve combinations of bridges, including exogenous bridging groups (e.g. acetate, methanol, etc.) in addition to the primary ligand. The bridging ligand *N*-acetylsalicylhydrazide reacts with Mn(II) acetate in air by a self-assembly process to produce a [18]metallacrown-6, a hexanuclear Mn(III) metallamacrocycle, with no exogenous ligand bridge but a $[M\text{-}N\text{-}N]_n$ repeating unit.[60, 115] More recently, a decanuclear Mn_{10} metallamacrocycle, [30]metallacrown-10, in which the manganese atoms are bridged by only the N-N diazine single bonds, self-assembled from a similar ligand *N*-phenylsalicylhydrazidate (H_3bzshz) was also

reported.[61] Variable temperature magnetism studies show that antiferromagnetic exchange interactions between manganese centers is dominant in this Mn_{10} ring.

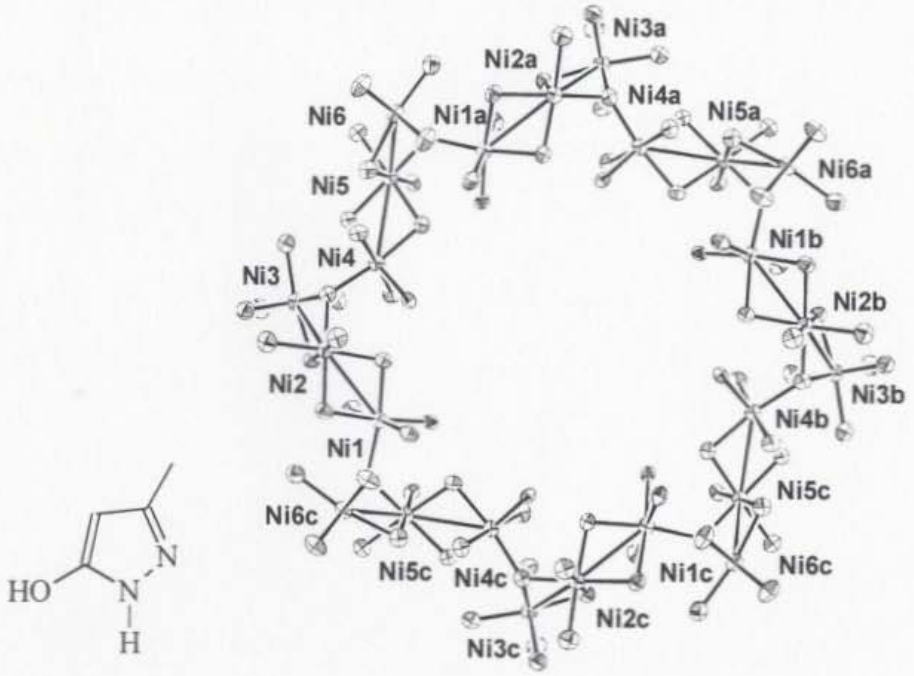

Figure 4-1. Core structure of the Ni_{24} wheel (b) and its ligand (a).

Self assembly processes with single bridging ligands can lead to predetermined cluster architectures similar to those described in Chapter 3, if certain critical structural elements are incorporated into the ligand backbone. The ligand **paoh**, built on a central oxalic dihydrazide fragment, has two widely separated tridentate (N_2O) terminal coordination pockets (Scheme 4-1). Reaction of this ligand with $Fe(II)(ClO_4)_2$ produces a square homoleptic [2×2] $Fe(II)_4$ grid (**8**). Replacement of the NH_2 groups with 2-pyridyl residues to give **dpkoh** now presents the same terminal coordinating elements,

but with the additional coordination capacity of an exo-N_4 coordination pocket, and creates a repeating element that now involves three metal ions. Reaction of **dpkoh** with $NiX_2 \cdot 6H_2O$ (X = ClO_4, BF_4) produces the octanuclear metallacyclic cluster complexes $[Ni_8(\mathbf{dpkoh}\text{-}2H)_4(H_2O)_8](ClO_4)_8 \cdot 4H_2O$ (**9**) and $[Ni_8(\mathbf{dpkoh}\text{-}2H)_4(H_2O)_8](BF_4)_8 \cdot 4H_2O$ [116] in high yield by an equivalent self-assembly process.

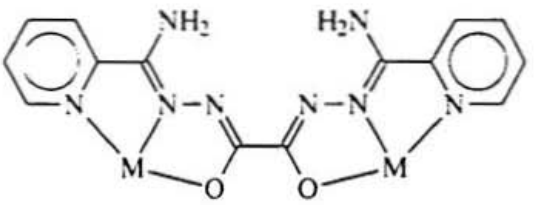

paoh

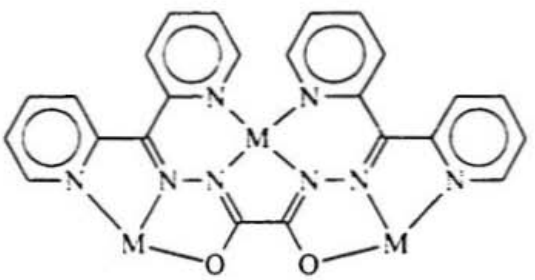

dpkoh

Scheme 4-1. Coordinating modes for the ligands **poah** and **dpkoh**.

4.2 Experimental

4.2.1 Synthesis of Ligands

Paoh The methyl ester of imino-picolinic acid was prepared in situ by reaction of 2-cyanopyridine (2.2 g, 22 mmol) with sodium methoxide solution, produced by dissolving sodium metal (0.050 g, 2.2 mmol) in dry methanol (50 mL). Oxalic

dihydrazide (22 mmol) (prepared from the reaction of ethyl oxalate with hydrazine hydrate in methanol) was added to the above solution and the mixture refluxed for 24 h. A yellow powder was obtained, which was filtered off, washed with methanol, and then diethyl ether and dried under vacuum. Yield: 5.4g, 83%. M.P. > 360 °C. Mass spectrum (major mass peaks, m/z): 243(M), 226, 225, 196, 164, 138, 108, 106, 79. IR (Nujol mull, cm^{-1}): 3405 (υ NH), 3257 (υ OH); 1613, 1595, 1584 (υ C=N); 997 (Py). Anal. Calcd for $C_{14}H_{14}N_8O_2 \cdot H_2O$: C, 48.83; H, 4.68; N, 32.54. Found: C, 48.09; H, 4.22; N, 33.57.

Dpkoh Oxalic dihydrazide (1.18 g, 10.0 mmol) was added to di-2-pyridyl ketone (3.68 g, 20.0 mmol) in methanol (100 mL), then the mixture was refluxed for 10 hr. A pale yellow solid was obtained, which was filtered off, washed with methanol and dried under vacuum. Yield: 3.38g, 75 %. M.P. > 270 °C. IR (Nujol mull, cm^{-1}): 3405 (υ NH), 1692, 1580, 1564 (υ C=N); 997 (Py). Mass Spectrum (M/z): 451(M+H), 226, 225, 197, 169, 105, 78. Anal. Calcd for $C_{24}H_{18}N_8O_2$: C, 63.98; N, 4.03; N, 24.89. Found: C, 63.69; H, 3.96; N, 24.97.

4.2.2 Synthesis of Complexes

$[Fe_4(paoh)_4](ClO_4)_8$ (8)

Paoh (0.33 g, 1.0mmol) was added to a hot solution of $Fe(ClO_4)_2 \cdot 6H_2O$ (1.4 g, 4.0 mmol) in MeCN / H_2O (5/10 mL). The mixture was stirred for 30 min., then filtered and the filtrate was left at room temperature. Black crystals were obtained from the dark orange solution after a few days. Yield: 0.47g, 81%. Anal. Calc. for $[Fe_4(C_{14}H_{14}N_8O_2)_4] \cdot$

$(ClO_4)_8 \cdot 0.5CH_3OH$: C. 29.00: H. 2.50: N. 19.15. Found: C. 29.83: H. 2.65: N. 19.79. IR (Nujol mull. cm^{-1}): 1691. 1643 (υ C=O. C=N): 1091 (υ ClO_4). UV-Vis (Nujol mull): (nm) 830. 641.

$[Ni_8(dpkoh)_4(H_2O)_8](ClO_4)_8(H_2O)_4$ (9)

Dpkoh (0.45 g. 1.0 mmol) was added to a solution of $Ni(ClO_4)_2 \cdot 6H_2O$ (1.46 g. 4.0 mmol) in methanol water (10:20 mL). and the mixture warmed. Dark red-brown crystals. suitable for X-ray analysis were obtained on standing from a brown solution (Yield: 0.67g. 82%). Anal. Calcd. for $[Ni_8(C_{24}H_{16}N_8O_2)_4(H_2O)_8](ClO_4)_8 \cdot H_2O$ (9): C. 35.21: H. 2.71: N. 13.69. Found: C. 35.12: H. 2.48: N. 13.77. IR (Nujol mull. cm^{-1}): 3461 (υ H_2O). 1627. 1586 (υ C=O. C=N). 1086.1018 (υ ClO_4^-).

4.2.3 Crystallography

Diffraction data for single crystals of **8** were collected using a Bruker SMART CCD diffractometer. equipped with an Oxford Cryostream N_2 cooling device.[90] with graphite monochromated Mo-Kα radiation. Cell parameters were determined and refined using the SMART software.[91a] raw frame data were integrated using the SAINT program.[91b] Cell constants for **8** (preliminary structure): Space group monoclinic. C2/c. a = 20.2844(6) Å. b = 29.8341(6) Å. c = 31.4446(7) Å. β = 91.153(2)°. Z = 4. R_1 = 0.1523 for 10888 data with Fo > 4σ (Fo) and 0.2285 for all 19580 data (1704 parameters).

Diffraction data for single crystals of **9** were collected using a Bruker P4/CCD system using graphite-monochromatized Mo-Kα X-radiation, and a rotating anode generator. SHELX97 [117] and teXsan [118] were used for the structure solution and refinement based on F^2. Cell constants for **9** (preliminary structure): Space group monoclinic, $P2_1/n$, a = 18.206(3) Å, b = 41.433(7) Å, c = 19.080(3) Å, β = 99.408(4) °, Z = 2, R_1 = 0.1522 for 10313 data with Fo > 4σ (Fo) and 0.3112 for all 29322 data (1704 parameters).

4.3 Results and Discussion

4.3.1 X-ray Structures

Structure of **$[Fe_4(paoh)_4](ClO_4)_8$ (8)**

The structural representation of the tetranuclear cation in **8**, based on a preliminary structural determination, is depicted in Figure 4-2. The basically flat tetranuclear Fe(II) cation contains four metal centers and four ligands, with each iron(II) ion bound by the remote N_2O donor pockets of the four essentially flat ligands. The tetranuclear metal grid is not rigidly square, but has one side (Fe(1)-Fe(2) significantly longer (7.25 Å) than the others (<6.95 Å). Two ligands adopt *cis* conformations and two *trans* with equivalent pairs arranged in parallel to produce a square cluster with a large internal void inside, but no anions or solvent molecules were found in the cavity. Metal ligand distances are consistent with each iron center being Fe(II). Fe-N distances and Fe-O distances fall in the ranges 2.03-2.10 Å and 1.97-2.17 Å respectively.

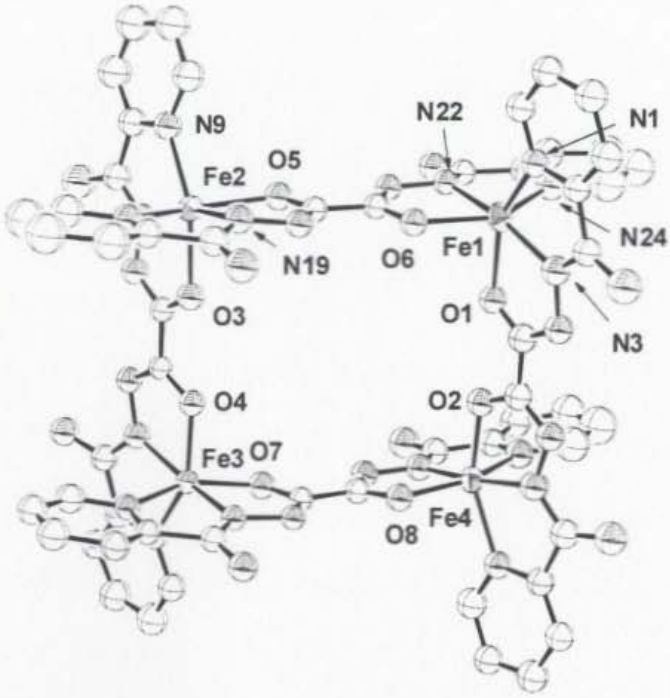

Figure 4-2. Structural representation of the tetranuclear core in **8** (50% probability thermal ellipsoids).

Structure of **$[Ni_8(dpkoh)_4(H_2O)_8](ClO_4)_8(H_2O)_4$ (9)**

The structure of the cation in **9**, based on a preliminary structural determination, is depicted in Figure 4-3 and the core structure in Figure 4-4. The core structure of the cation is a 24-membered metallamacrocycle, in which there are eight distorted octahedral Ni(II) ions. Four *cis*-NiN_4O_2 centers are roughly at the corners of a square (Ni1, Ni3, Ni5, and Ni7), and four *trans*- NiN_4O_2 centers are bound externally in a roughly tetrahedral arrangement (Ni2, Ni4, Ni6, and Ni8). Water molecules occupy the *trans* coordination positions (Ni2, Ni4, Ni6, and Ni8) and the Ni_8 ring is folded, somewhat like a saddle. The structural core shows that all the eight nickel ions are directly linked by diazine (N_2) bridges to neighboring atoms to form a ring. Longer Ni-Ni linkages also

involve O-C-N bridges. The large cavity within the Ni_8 ring appears to be devoid of any solvent molecules or anions, and the size of the cavity is measured between the opposite oxygen atoms as 7.45 Å (O(1)-O(5)), 7.42 Å (O(3)-O(7)), 7.02 Å (O(9)-O(14)), and 6.53 Å (O(12)-O(15)) respectively. Ni-O and Ni-N bond distances fall in the range of 2.09-2.17 Å and 1.96-2.14 Å respectively. Ni-Ni distances of the square nickel centers fall in the range 6.88-6.98 Å, while the external tetrahedral Ni-Ni distances fall in the range 9.02-9.22 Å. The nickel ions are linked by almost *trans* N-N bridges (Ni-N-N-Ni torsional angles 154-173°). The charge balance of the cluster molecule shows that two negative charges are associated with each ligand.

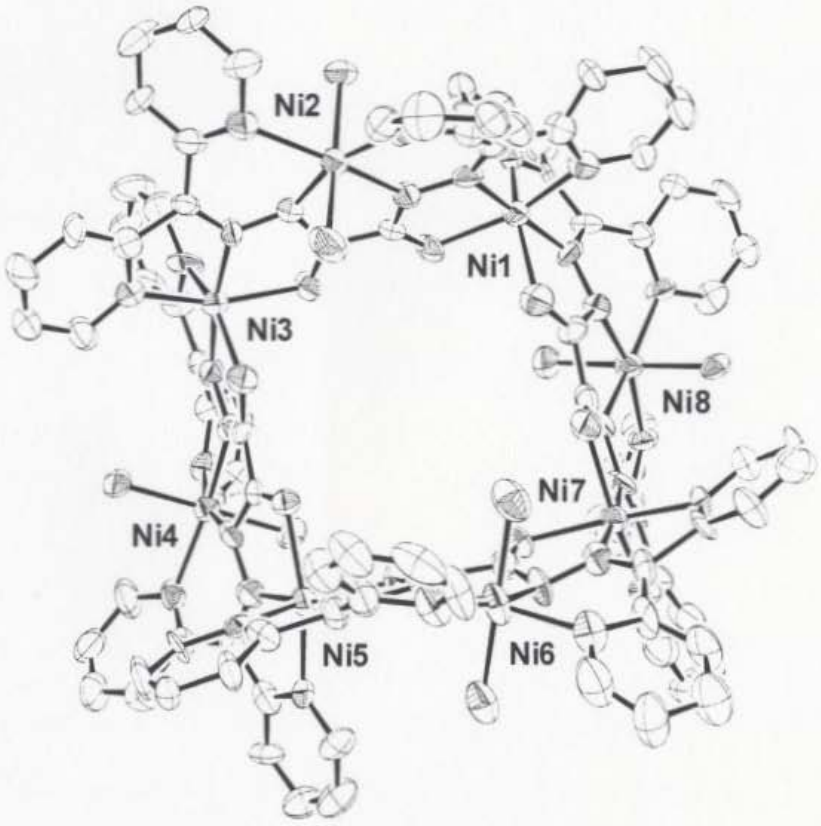

Figure 4-3. Structural representation of **9**. (50% probability thermal ellipsoids)

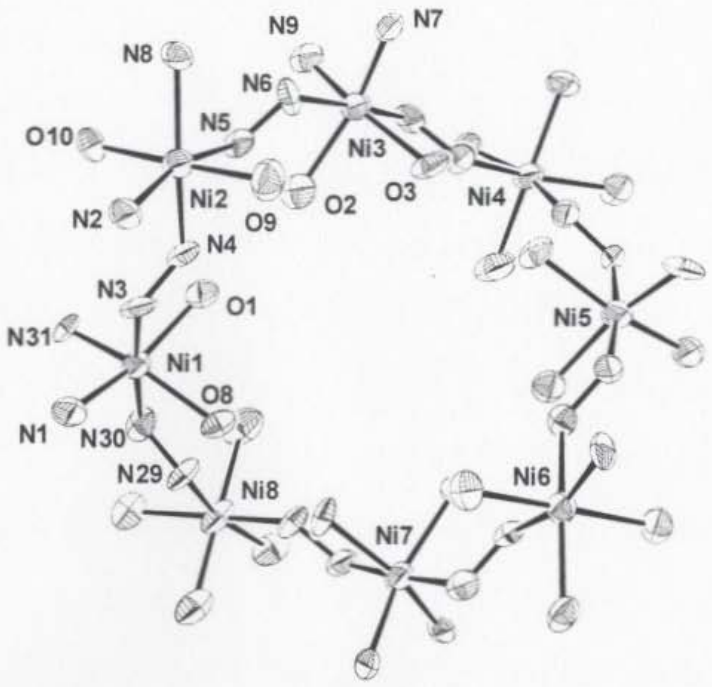

Figure 4-4. Structural representation of the octanuclear core in **9**.

4.3.2 Magnetic Properties

Variable temperature magnetic susceptibility measurements were carried out on powdered samples of complexes **8**, **9** in the temperature range 2-300 K and at field strengths of 0.1T.

$[Fe_4(paoh)_4](ClO_4)_8$ (8)

The molar magnetic susceptibility versus temperature data for **8** (χ *vs* T) are shown in Figure 4-5 and molar magnetic moment *vs* temperature in Figure 4-6. The iron(II) cluster has an essentially constant magnetic moment per mole of 11.2 μ_B from 300 to 25 K, which indicates the absence of any significant coupling between iron(II)

centers at high temperature. This corresponds to an effective magnetic moment of 5.6 μ_B per metal, consistent with the presence of Fe(II) in a d^6 high-spin electronic configuration (S = 2). There is a sharp drop of magnetic moment to 6.1 μ_B per mole at 2.0 K, which could be associated with very weak antiferromagnetic exchange. This has been confirmed by fitting these data to the square Fe(II) model (Figure 3-10, S = 2) using MAGMUN [106], giving $g = 2.35$, $J = -0.23$, TIP = 0.000300 emu·mol^{-1}, $\theta = 0$ K, $10^2R = 3.9$ ($R = [\Sigma(\chi_{obs.} - \chi_{calc.})^2/\Sigma\chi_{obs}^2]^{1/2}$). (Solid line in Figure 4-5 and Figure 4-6 were drawn from these best-fit parameters.) But this sharp drop at low temperature could partly be due to zero-field splitting. The slight discrepancy between the experimental data and the theoretical line in the plot of molar magnetic moment versus temperature may be due to small temperature errors in the data or slight errors in the cup correction. A rise in moment on decreasing the temperature might suggest ferromagnetic coupling, but this is highly unlikely given the long distance of separation of the Fe(II) centers.

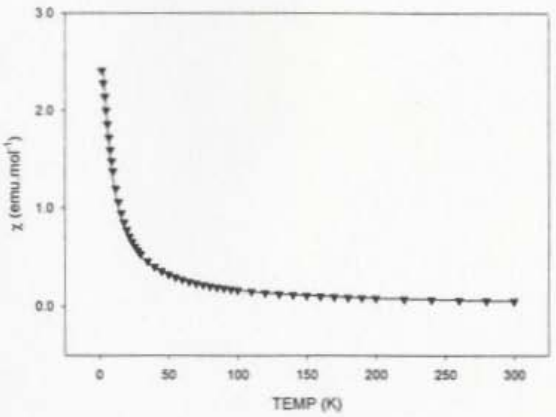

Figure 4-5. Molar susceptibility *vs* temperature data for **8**.

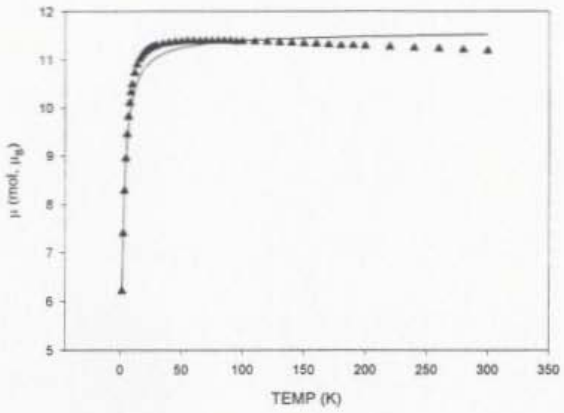

Figure 4-6. Molar magmetic moment *vs* temperature data for **8**.

$[Ni_8(dpkoh)_4(H_2O)_8](ClO_4)_8(H_2O)_4$ (9)

The magnetic exchange model for the octanuclear metal ring complex is represented in Figure 4-7. For simplicity the model assumes that just nearest neighbor exchange coupling within the ring is considered and all exchange integrals between adjacent pairs of metal centers are the same. The Hamiltonian equation (eqn. 4-1) can be used to describe it.

$$H = -J\,(S_1.S_2 + S_2.S_3 + S_3.S_4 + S_4.S_5 + S_5.S_6 + S_6.S_7 + S_7.S_8 + S_1.S_8) \qquad (4\text{-}1)$$

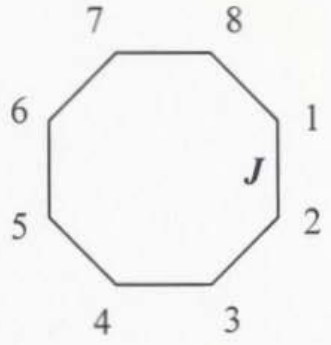

Figure 4-7. Exchange expression model for M_8 ring.

The variable temperature magnetic data for **9** are shown in Figure 4-8. Magnetic moments (per mole) for **9** drop smoothly from 8.3 μ_B at 300 K to 1.96 μ_B at 2 K, typical of a system with dominant intramolecular antiferromagnetic coupling. The data were fitted to an isotropic exchange expression based on the exchange Hamiltonian (eqn. 4-1) using MAGMUN [106]. An excellent data fit gave g = 2.235(4), J = -14.9(2) cm^{-1}, TIP = 0.00145 $emu \cdot mol^{-1}$, corrected for 5% paramagnetic impurity (solid line in Figure 4-7). The antiferromagnetic coupling within the wheel can be readily rationalized on the basis of the close to *trans* arrangement of the Ni(II) centers about N-N single bond bridges (Ni-N-N-Ni torsional angles 154-173°). This result agrees with the magnetostructural correlations in a series of dinuclear copper(II) complexes bridged just by N-N bonds, and spanning a range of torsional angles from 75-180°, which showed a systematic linear variation in exchange integral from ferromagnetic exchange < 80° to antiferromagnetic exchange > 80°, associated with p orbital orientation and overlap in the N-N bond as a function of angular rotation.[48]

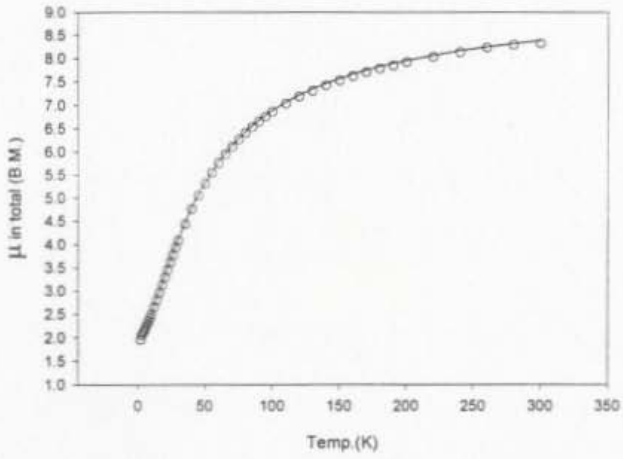

Figure 4-8. Variable temperature magnetic data for **9**.

4.4 Conclusion

The ligand **paoh**, which has two widely separated tridentate (N_2O) terminal coordination pockets, produced an essentially uncoupled square [2×2] $Fe(II)_4$ grid (**8**). Replacement of the NH_2 groups with 2-pyridyl residues gives **dpkoh** with the additional coordination capacity of an exo-N_4 coordination pocket, leading to the octanuclear metallacyclic cluster complex $[Ni_8(\mathbf{dpkoh}\text{-}2H)_4(H_2O)_8]\cdot(ClO_4)_8\cdot 4H_2O$ (**9**). Eight nickel(II) centers are bridged by only the diazine N-N single bonds. This bridge has been shown to propagate magnetic exchange between the metal centers, and in the present case substantial antiferromagnetic coupling exists between the nickel(II) ions throughout the metallacycle. This strategy may have general application for generating more complicated clusters or metallacycles.

Chapter 5. [3×3] M_9 Grids [*,]

5.1 Introduction

Although self-assembly strategies have succeeded in a few cases for the formation of relatively low nuclearity molecular clusters, for example [2×2] M_4 grids [31, 50, 81, 93-105], a [2×3] rectangle Ag_6 grid [119], higher nuclearity predetermined grids are still rare. Besides the nonmagnetic [3×3] $Ag(I)_9$,[32] Lehn etc. also reported one [4×4] $Pb(II)_{16}$ square grid with appropriate extension of the polytopic pyridazine ligands, based on NMR and ES mass spectrometry (no X-ray structure).[120] Recently [2×2] Cu_4, Ni_4, Mn_4, Co_4 tetranuclear complexes self-assembled from simple tetradentate alkoxy-diazine ligands have been synthesized (see also Chapter 3).[50] Extension of the alkoxy-diazine ditopic ligand **poap** (Scheme 5-1) to effectively double the alkoxo-bridging fragment can be achieved by using a 2,6-disubstituted pyridine central unit (Scheme 5-1), which results in the formation of two tritopic ligands **2poap** and **2poapz**. Unique nona-nuclear [3×3] ($M_9[\mu\text{-}O_{12}]$) paramagnetic grids with Mn(II) [82] and Cu(II) [83, 121] salts have been prepared by a strict self-assembly process from these ligands. The Mn_9 systems exhibit intra-molecular antiferromagnetic coupling, while for the Cu_9 complexes ferromagnetic exchange is observed with S = 7/2 ground states.

---

* 1. **L. Zhao**, C. J. Matthews, L. K. Thompson, S. L. Heath, *Chem. Commun.* 2000, 265-266.
2. **L. Zhao**., Z. Xu, L.K. Thompson, S.L. Heath, D.O. Miller, and M. Ohba, *Angew. Chem. Int. Ed.*, 2000, 39(17), 3114-3117.

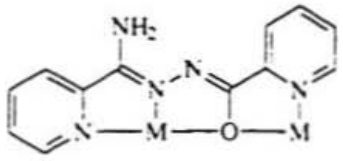

poap

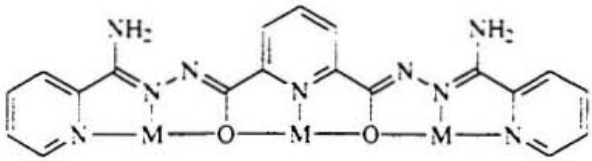

2poap

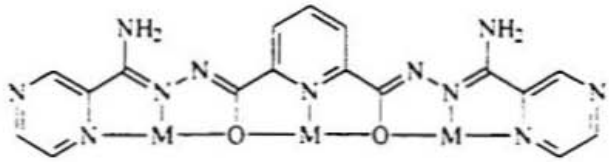

2poapz

Scheme 5-1. Coordination modes for the ligands **poap**, **2poap**, and **2poapz**.

5.2 Experimental

5.2.1 Synthesis of Ligands

Preparation of **2poap** was described in Chapter 2.

2poapz The methyl ester of iminopicolinic acid was prepared in situ by reaction of 2-cyanopyrazine (5.2 g, 50 mmol) with sodium methoxide solution, produced by dissolving sodium metal (0.12 g, 50mmol) in dry methanol (100 mL). The 2,6-pyridine dicarboxylic acid dihydrazide was added to the above solution and the mixture was refluxed for 24 h. A yellow powder was obtained, which was filtered off, washed with water, methanol, and then diethyl ether and dried under vacuum. Yield, 6.3 g, 79 %. M.P. 259°C (Dec.). Found: C, 49.19; H, 3.66; N, 37.06. Calcd. for $C_{17}H_{15}N_{11}O_2 \cdot 0.5H_2O$ = 414.4: C, 49.27; H, 3.89; N, 37.18%. IR (cm^{-1}): 3413, 3317, 3156 (υ NH_2/ H_2O); 1685,

1632, 1611 (υ C=O/C=N). ^{1}H NMR (ppm, d_6-DMSO): 11.090 (s, 2H, OH), 8.653 (d, 2H, py), 8.235 (m, 5H, py), 7.955 (m, 2H, py), 7.544 (m, 2H, py), 7.069 (s, 4H, NH_2). MS: 403 (M^+), 386, 367 (M-2H_2O), 338, 310, 261, 223, 194, 169, 107, 78.

5.2.2 Synthesis of Complexes

[Mn_9(2poap)$_6$](ClO_4)$_6$·18H_2O (10):

2poap (0.403 g, 1.0 mmol) was added to a hot solution of $Mn(ClO_4)_2$·6H_2O (1.45 g, 4.0 mmol) in water (5 mL). MeCN (15 mL) was then added and the mixture left at room temperature. Red crystals formed after several days. Yield: 0.46g, 72%. Found (vacuum dried sample): C, 35.77; H, 2.63; N, 19.61. Calcd. for $Mn_9(C_{16}H_{15}N_9O_2)_6(ClO_4)_6$·18$H_2O$: C, 35.81; H, 3.29; N, 19.78%. IR (Nujol mull, cm^{-1}): 3450, 3339, 3247 (υ NH/H_2O); 1689, 1654(υ CO/CN); 1095 (υ ClO_4^-). UV-vis (Nujol mull): 546 nm (sh); (MeCN) 1027 nm (19.6 $dm^3 \cdot mol^{-1} \cdot cm^{-1}$). μ_{RT} = 16.9 BM (per mol)

[Mn_9(2poapz-2H)$_6$](NO_3)$_6$·12H_2O (11):

2poapz (0.403 g, 1.0 mmol) was added to a hot solution of $Mn(NO_3)_2$·3H_2O (0.716 g, 4.0 mmol) in water (5 mL) and MeCN (15 mL) and the resulting red solution was left at room temperature. Red crystals formed after several days. Yield: 0.49g, 84%. Calcd. for $Mn_9(C_{17}H_{13}N_{11}O_2)_6 \cdot (NO_3)_6 \cdot 12H_2O$: C, 34.97; H, 2.94; N, 28.79%. Found (vacuum dried sample): C, 34.47; H, 2.62; N, 28.85. IR (Nujol mull, cm^{-1}): 3409, 3315 (υ NH/H_2O); 1650, 1605 (υ CO/CN).

$[Cu_9(2poap\text{-}H)_6](NO_3)_{12}\cdot 9H_2O$ (12):

2poap (0.40 g. 1.0 mmol) was added to a hot solution of $Cu(NO_3)_2\cdot 3H_2O$ (1.44 g. 6.00 mmol) in water (15 mL) and the mixture was stirred for 30 min. filtered. and the yellowish solution allowed to stand at room temperature for several days. during which time brown crystals suitable for X-ray structural determination were deposited. Yield: 0.65g. 71%. Elemental analysis. Calcd. for $[Cu_9(C_{19}H_{16}N_6O_2)_6](NO_3)_{12}\cdot 9H_2O$ (%): C 35.21. H 2.96. N 23.76: found (vacuum dried sample): C 35.33. H 3.05. N 23.31. IR (Nujol mull. cm^{-1}): 3450. 3293 (υ NH_2 /H_2O): 1670 (υ C=N): UV/Vis (Nujol mull): 810 nm: $\mu_{RT} = 6.3\ \mu_B$ (per mol).

5.2.3 Crystallography

Diffraction data for single crystals of **10. 12** were collected with a Bruker SMART CCD diffractometer. equipped with an Oxford Cryostream N_2 cooling device. [90] with graphite monochromated Mo-Kα radiation. SHELXTL [92] was used for the structure solution and the refinement based on F^2.

The diffraction intensities of an orange-red prismatic crystal of **11** were collected with graphite-monochromatized Mo-Kα X-radiation (rotating anode generator) using a Bruker P4/CCD diffractometer. The data was corrected for Lorentz and polarization effects. The structure was solved by direct methods.[84. 85] All atoms except hydrogens were refined anisotropically. Hydrogen atoms were placed in calculated positions. Neutral atoms scattering factors[86] and anomalous-dispersion terms[87. 88] were taken from

the usual sources. All other calculations were performed with the teXsan[89] crystallographic software package using a PC computer.

5.3 Results and Discussion

5.3.1 X-ray Structures

Structure of **$[Mn_9(2poap\text{-}2H)_6](ClO_4)_6 \cdot 18H_2O$ (10):**

The structure of the cation of **10** is illustrated in Figure 5-1 and the grid core in Figure 5-2. Important bond distances and angles are listed in Table 5-2. The structure of **10** is unique with a [3×3] grid of nine pseudo-octahedral, alkoxo-bridged Mn(II) centers coordinated by two groups of three roughly parallel dianionic ligands arranged above and below the metal pseudo-plane. The Mn centers comprise three different types: *trans*-MnN_2O_4 (central), *cis*-MnN_4O_2 (corners) and *mer*-MnN_3O_3 (sides). The [3×3] square grid can be visualized as a fusion of four individual $Mn_4[\mu\text{-}O]_4$ square grids, and then each square resembles a similar Mn_4 [2×2] grid of the ligand **poapz** reported recently.[81] Within each subunit a puckered boat-like bridging arrangement exists involving an alternation of oxygens above and below the Mn_4 pseudo-plane. This then translates symmetrically throughout the fused arrangement that comprises the whole grid. The metal ion geometries are controlled to some extent by the way in which the six ligands assemble, and this depends on the 'bite' of each ligand. The contiguous, linear arrangement of five membered chelate rings associated with the three coordination pockets creates strain within the grid such that each Mn(II) ion has very long Mn-N contacts (Mn-N 2.292-2.501 Å) to the terminal pyridine groups, which fall in the plane of

the nine metal ions. All other Mn-ligand bonds in **10** are less than 2.2 Å. All the Mn-O-Mn angles fall in the range 126.6-130.0°.

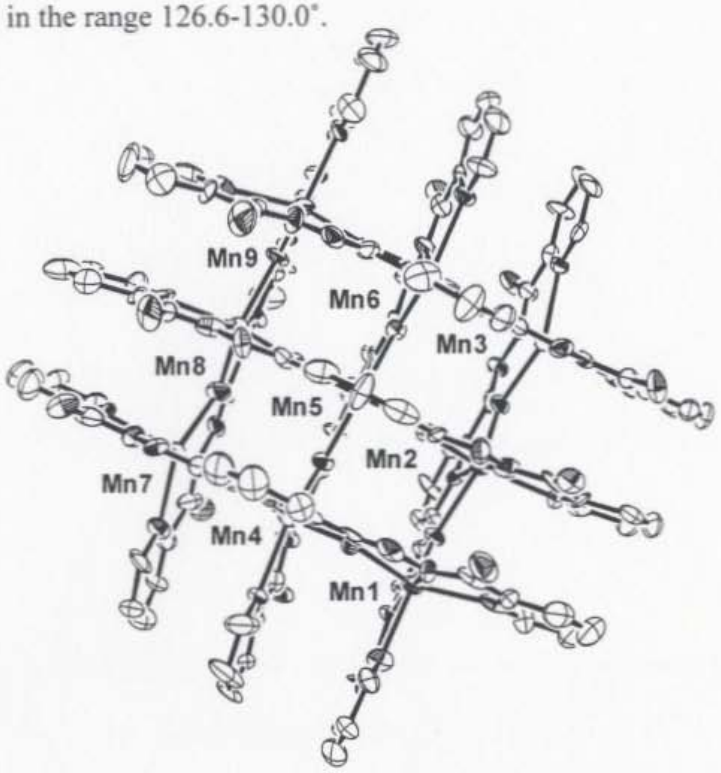

Figure 5-1 Structural representation of the cation $[Mn_9(\mathbf{2poap}\text{-}2H)_6]^{6+}$ (**10**) (50% probability thermal ellipsoids).

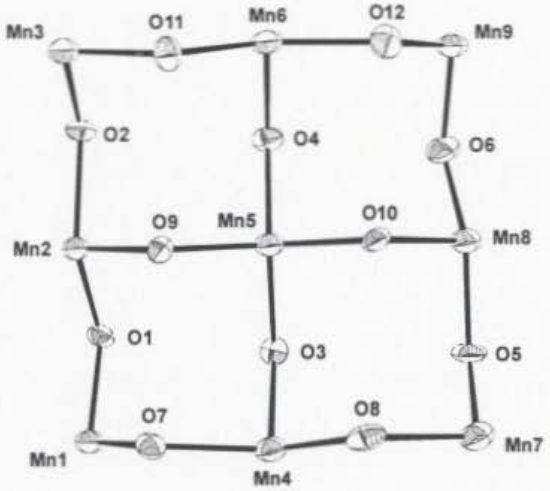

Figure 5-2 Structural representation of the nonanuclear core in **10**.

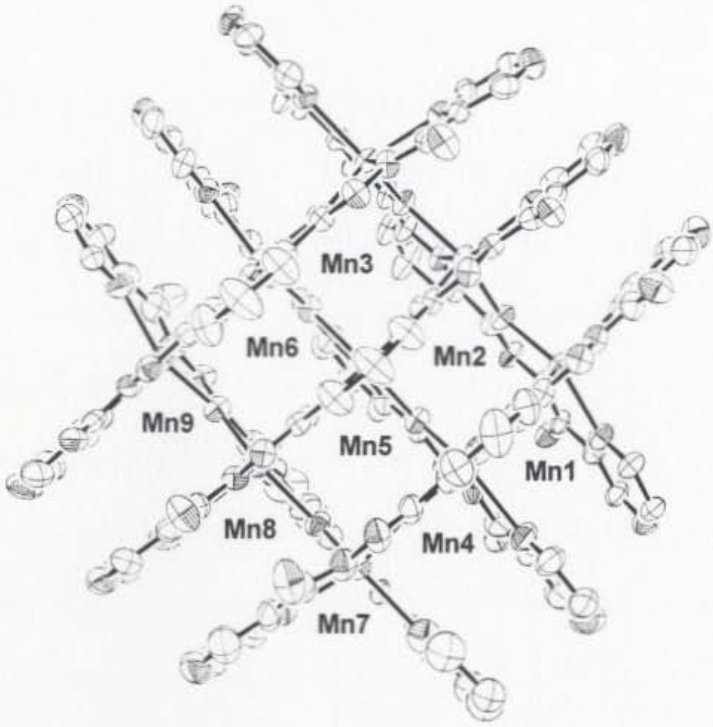

Figure 5-3. Structural representation of the cation $[Mn_9(\mathbf{2poapz}\text{-}2H)_6]^{6+}$ (**11**). (40% probability thermal ellipsoids).

Structure of $\mathbf{[Mn_9(2poapz\text{-}2H)_6](NO_3)_6 \cdot 12H_2O}$ (**11**):

The structure of the cation in **11** is illustrated in Figure 5-3, and important bond lengths and angles are listed in Table 5-3. The structure resembles closely that for $[Mn_9(\mathbf{2poap}\text{-}2H)_6]$ $(ClO_4)_6 \cdot 18H_2O$ (**10**). Mn-Mn separations fall in the range 3.900-3.935 Å, and Mn-O-Mn angles fall in the range 126.9-128.4°. The aromatic rings of each ligand are almost eclipsed with their neighboring counterparts, with separations (~ 3.9 Å based on the Mn-Mn distances) that suggests some interaction between aromatic π electron clouds. The alkoxide bridged Mn_9 core is similar to that of **10** in Figure 5-2.

Structure of **$[Cu_9(2poap\text{-}H)_6](NO_3)_{12}\cdot 9\ H_2O$ (12)**:

The structure of the cation of **12** is illustrated in Figure 5-4 and the structure of the nona-nuclear copper(II) core in Figure 5-5, and important bond distances and angles are listed in Table 5-4. The structure of **12** involves a [3×3] grid of nine pseudo-octahedral Cu^{II} centers coordinated by two groups of three roughly parallel ligands arranged above and below the metal pseudo-plane, with the metals bridged just by alkoxide oxygen atoms, which is similar to that in **11**. The ligands are roughly eclipsed, but have a slight stagger. Three different pseudo-octahedral copper(II) centers are found: the central Cu atom has a *trans*-N_2O_4 donor arrangement, the corner Cu centers have *cis*-N_4O_2 donor arrangements, and the side Cu centers have *mer*-N_3O_3 donor arrangements.

The Cu_9O_{12} core (Figure 5-5) consists of four fused Cu_4O_4 square subunits. Each subunit has a similar structure to known square, tetranuclear copper(II) complexes of **poap** [50]. Adjacent copper-copper separations fall in the range 4.032-4.227 Å, which generates a roughly square grid with overall core dimensions of 8.2×8.3 Å. Cu-O-Cu angles fall in the range 136.5-143.6° and Cu-O and Cu-N distances fall in the ranges 2.061-2.314 Å and 1.858-2.231 Å, respectively. The formation of the homoleptic grid structure in **12** is a clear consequence of the exact matching of the nine coordination pockets to the coordination requirements of the nine metal centers. However, the formation of a complex with nine pseudo-octahedral copper(II) centers is rather unusual, since copper(II) generally prefers to adopt square or square-pyramidal geometries. This leads to a complicated situation with regard to the magnetic ground states of each copper center. The central copper atom (Cu5) has a compressed tetragonal geometry (d_z^2 ground

state), with four long equatorial Cu-O contacts to O3, O4, O9, and O10 (2.163-2.210 Å), and two short Cu-N bonds to N14 and N41 (1.941(10) and 1.912(11) Å, respectively). Cu3 and Cu7 have similar distorted geometries, while the other copper centers are best described as elongated tetragonal ($d_{x^2-y^2}$ ground state). However in all cases connections between copper centers through the alkoxide bridges appear to be orthogonal, based on the ground-state assessment (vide infra).

5.3.2 Magnetic properties

Variable temperature magnetic susceptibility measurements were carried out on powdered samples of complexes **10-12** in the temperature range 2-300 K (4.5-300 K for **12**) and at a field strength of 0.1T.

$[Mn_9(2poap\text{-}2H)_6](ClO_4)_6 \cdot 18H_2O$ (10):

A plot of μ_{mol} *versus* temperature for **10** is illustrated in Figure 5-6. The magnetic moment drops smoothly from 16.9 μ_B at 300 K to 6.9 μ_B at 5 K, and then there is a very slight rise below this temperature. The room temperature value is consistent with the presence of nine high spin Mn(II) centers, and the drop to 6.9 μ_B at 5 K is associated with the presence of intramolecular antiferro-magnetic exchange with the equivalent of one residual Mn(II) center in the spin coupled (S = 5/2) ground state. This situation is an exact parallel to that occurring in the penta-nuclear manganese(II) cluster of **poap**.[121] The slight rise in μ_B at temperatures <4 K may be due to a very weak ferromagnetic component.

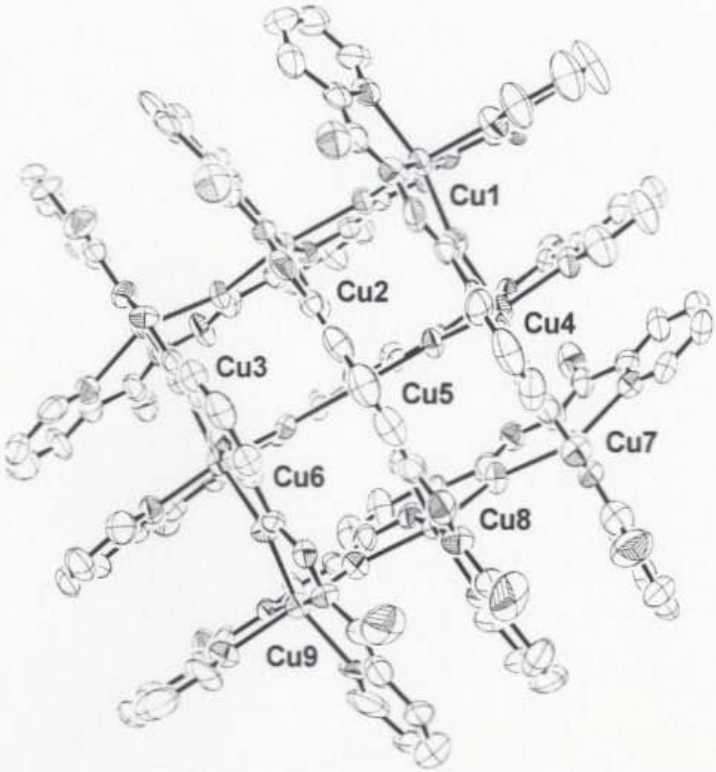

Figure 5-4. Structural representation of the cation $[Cu_9(\mathbf{2poap}\text{-}H)_6]^{12+}$ in **12**.

(50% probability thermal ellipsoids)

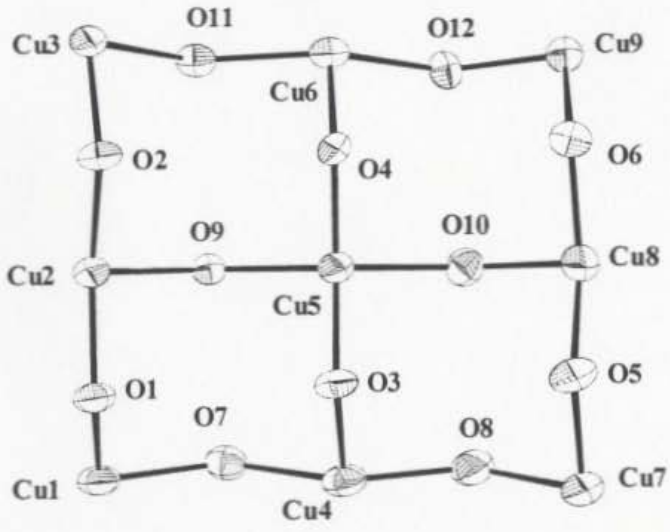

Figure 5-5. Structural representation of the pseudo-square Cu_9O_{12} core in **12**.

Table 5-1. Summary of Crystallographic Data for **10**. **11**. **12**.

compd.	**10**	**11**
Empirical formula	$C_{121.14}H_{122.71}N_{57.57}O_{47}Cl_4Mn_9$	$C_{102}H_{78}N_{70}O_{55}Mn_9$
Formula Weight	3844.3	3658.6
Crystal System	Monoclinic	Triclinic
Space group	C2/c	P $\bar{1}$
A (Å)	26.0641(16)	18.1578(12)
B (Å)	26.0910(16)	18.2887(12)
C (Å)	53.291(3)	27.7641(15)
α(deg.)	90	105.7880(10)
β(deg.)	102.473(1)	101.547(2)
γ(deg.)	90	91.1250(9)
V ($Å^3$)	35385(4)	8353.6(9)
ρ_{calcd} (g cm^{-3})	1.448	1.445
Z	1	1
μ(mm^{-1})	0.81	0.754
λ(Å)	0.71073	0.71073
T (K)	150(2)	293
R_1	0.1419	0.1394
wR_2	0.3936	0.4087

Table 5-1. Summary of Crystallographic Data for **10. 11. 12**. (Continued)

compd.	**12**
Empirical formula	$C_{114}H_{134}Cu_9N_{60}O_{52}$
Formula Weight	3748.67
Crystal System	Triclinic
Space group	P $\bar{1}$
A (Å)	18.698(10)
B (Å)	18.920(5)
C (Å)	27.602(8)
α(deg.)	95.89(2)
β(deg.)	102.41(3)
γ(deg.)	117.62(2)
V ($Å^3$)	8208(6)
ρ_{calcd} (g cm^{-3})	1.541
Z	2
μ(mm^{-1})	1.240
λ(Å)	0.71073
T (K)	150
R_1	0.1043
wR_2	0.2903

Table 5-2. Selected Bond Distances (Å) and Angles (°) for **10**.

Mn1-O1	2.164(8)	Mn4-N10	2.287(8)
Mn1-O7	2.213(8)	Mn4-N12	2.143(9)
Mn1-N1	2.337(11)	Mn4-N32	2.171(9)
Mn1-N3	2.148(11)	Mn5-O3	2.217(8)
Mn1-N28	2.312(11)	Mn5-O4	2.194(8)
Mn1-N30	2.137(11)	Mn5-O9	2.196(8)
Mn2-O1	2.209(8)	Mn5-O10	2.182(8)
Mn2-O2	2.197(8)	Mn5-N14	2.171(8)
Mn2-O9	2.164(8)	Mn5-N41	2.160(8)
Mn2-N5	2.189(11)	Mn6-O4	2.155(8)
Mn2-N37	2.326(11)	Mn6-O11	2.254(8)
Mn2-N39	2.151(11)	Mn6-O12	2.152(8)
Mn3-O2	2.168(8)	Mn6-N16	2.136(9)
Mn3-O11	2.175(8)	Mn6-N18	2.287(10)
Mn3-N7	2.131(11)	Mn6-N50	2.188(10)
Mn3-N9	2.276(10)	Mn7-O5	2.175(8)
Mn3-N46	2.297(11)	Mn7- O8	2.203(7)
Mn3-N48	2.156(11)	Mn7-N19	2.292(8)
Mn4-O3	2.169(8)	Mn7-N21	2.133(8)
Mn4-O7	2.152(8)	Mn7-N34	2.163(9)
Mn4-O8	2.277(8)	Mn7-N36	2.286(8)

Table 5-2. Selected Bond Distances (Å) and Angles (°) for **10**. (Continued)

Mn8-O5	2.148(8)	Mn1-O1-Mn2	129.4(4)
Mn8-O6	2.328(8)	Mn1-O7-Mn4	130.0(4)
Mn8 O10	2.165(8)	Mn2-O2-Mn3	127.1(4)
Mn8 N23	2.222(8)	Mn2-O9-Mn5	127.9(4)
Mn8-N43	2.112(9)	Mn3-O11-Mn6	126.5(4)
Mn8-N45	2.315(11)	Mn4-O3-Mn5	127.1(3)
Mn9-O6	2.218(8)	Mn4-O8-Mn7	126.8(3)
Mn9-O12	2.180(8)	Mn5-O4-Mn6	127.6(4)
Mn9-N25	2.199(9)	Mn5-O10-Mn8	128.5(3)
Mn9-N27	2.262(8)	Mn6-O12-Mn9	125.86()
Mn9-N52	2.146(10)	Mn7-O5-Mn8	128.1(3)
Mn9-N54	2.288(11)	Mn8-O6-Mn9	124.8(3)

Table 5-3. Selected Bond Distances (Å) and Angles (°) for **11**.

Mn1-O9	2.152(9)	Mn4-N12	2.411(14)
Mn1-O18	2.139(9)	Mn4-N15	2.147(13)
Mn1-N1	2.320(12)	Mn4-N39	2.167(11)
Mn1-N4	2.159(10)	Mn5-O10	2.203(9)
Mn1-N34	2.356(12)	Mn5-O11	2.208(10)
Mn1-N37	2.1243(11)	Mn5-O16	2.189(8)
Mn2-O8	2.210(9)	Mn5-O17	2.230(8)
Mn2-O9	2.197(9)	Mn5-N50	2.169(8)
Mn2-O16	2.157(8)	Mn5-O10	2.141(9)
Mn2-N6	2.175(8)	Mn6-O14	2.199(8)
Mn2-N45	2.376(12)	Mn6-O15	2.212(9)
Mn2-N48	2.127(10)	Mn6-N19	2.151(10)
Mn3-O8	2.151(9)	Mn6-N22	2.173(6)
Mn3-O14	2.161(8)	Mn6-N61	2.160(10)
Mn3-N8	2.163(10)	Mn7-O13	2.162(10)
Mn3-N11	2.364(12)	Mn7- O19	2.163(10)
Mn3-N56	2.290(11)	Mn7-N23	2.42(2)
Mn3-N59	2.127(10)	Mn7-N26	2.137(17)
Mn4-O11	2.134(9)	Mn7-N41	2.095(13)
Mn4-O18	2.209(9)	Mn7-N44	2.347(16)
Mn4-O19	2.190(10)	Mn8-O12	2.207(9)

Table 5-3. Selected Bond Distances (Å) and Angles (°) for **11**. (Continued)

Mn8-O13	2.219(10)	Mn1-O9-Mn2	127.6(4)
Mn8-O17	2.139(8)	Mn1-O18-Mn4	128.8(4)
Mn8-N28	2.183(13)	Mn2-O8-Mn3	127.4(4)
Mn8-N52	2.142(10)	Mn2-O16-Mn5	128.7(4)
Mn8-N55	2.381(11)	Mn3-O14-Mn6	127.0(4)
Mn9-O12	2.165(10)	Mn4-O11-Mn5	128.3(4)
Mn9-O15	2.158(9)	Mn4-O19-Mn7	128.1(5)
Mn9-N30	2.161(18)	Mn5-O10-Mn6	128.0(4)
Mn9-N33	2.313(13)	Mn5-O17-Mn8	128.3(4)
Mn9-N63	2.109(13)	Mn6-O15-Mn9	128.5(4)
Mn9-N66	2.371(13)	Mn7-O13-Mn8	128.5(5)
		Mn8-O12-Mn9	126.3(4)

Table 5-4. Selected Bond Distances (Å) and Angles (°) for **12**.

Cu1-O1	2.115(8)	Cu4-N10	2.094(11)
Cu1-O7	2.250(9)	Cu4-N12	1.901(9)
Cu1-N1	2.104(12)	Cu4-N32	2.015(11)
Cu1-N3	1.927(12)	Cu5-O3	2.163(7)
Cu1-N28	2.199(14)	Cu5-O9	2.210(10)
Cu1-N30	1.992(12)	Cu9-O10	2.199(9)
Cu2-O1	2.288(7)	Cu5-O4	2.197(7)
Cu2-O2	2.305(9)	Cu5-N14	1.941(10)
Cu2-O9	2.090(9)	Cu5-N41	1.912(11)
Cu2-N5	1.996(11)	Cu6-O4	2.081(8)
Cu2-N37	2.129(14)	Cu6-O11	2.268(10)
Cu2-N39	1.887(12)	Cu6-O12	2.276(9)
Cu3-O2	2.183(9)	Cu6-N16	1.888(12)
Cu3-O11	2.190(8)	Cu6-N18	2.115(10)
Cu3-N7	1.937(13)	Cu6-N50	2.010(12)
Cu3-N9	2.187(12)	Cu7-O5	2.187(9)
Cu3-N46	2.181(14)	Cu7-O8	2.222(13)
Cu3-N48	1.969(12)	Cu7- N19	2.158(13)
Cu4-O3	2.084(7)	Cu7-N21	1.945(11)
Cu4-O7	2.290(11)	Cu7-N34	1.947(14)
Cu4-O8	2.211(12)	Cu7-N36	2.19(2)

Table 5-4. Selected Bond Distances (Å) and Angles (°) for **12**. (Continued)

Cu8-O5	2.230(10)	Cu1-O1-Cu2	140.7(4)
Cu8-O6	2.256(11)	Cu1-O7-Cu4	137.3(4)
Cu8-O10	2.081(11)	Cu2-O2-Cu3	138.5(5)
Cu8-N23	1.987(13)	Cu2-O9-Cu5	142.2(5)
Cu8-N43	1.858(14)	Cu3-O11-Cu6	138.4(5)
Cu8-N45	2.079(19)	Cu4-O3-Cu5	143.3(4)
Cu9-O6	2.266(11)	Cu4-O8-Cu7	136.6(5)
Cu9-O12	2.103(10)	Cu5-O4-Cu6	142.0(4)
Cu9-N25	1.996(13)	Cu5-O10-Cu8	143.6(4)
Cu9-N27	2.227(14)	Cu6-O12-Cu9	137.7(5)
Cu9-N52	1.921(13)	Cu7-O5-Cu8	136.5(5)
Cu9-N54	2.112(19)	Cu8-O6-Cu9	137.8(5)

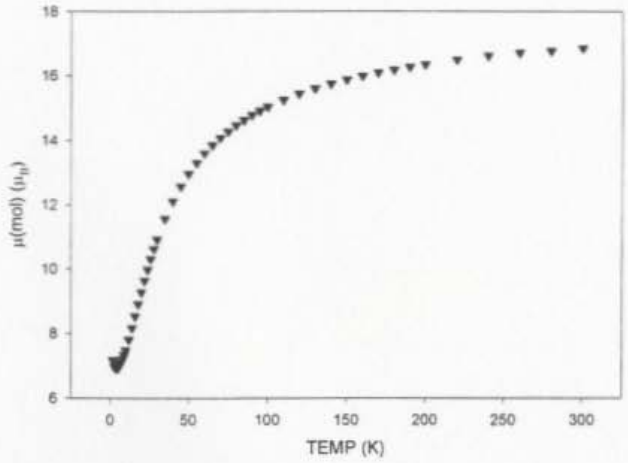

Figure 5-6. Variable-temperature magnetism data for **10**.

$[Mn_9(2poapz\text{-}2H)_6](NO_3)_6 \cdot 12H_2O$ (11):

A plot of μ_{mol} *versus* temperature for **11** is illustrated in Figure 5-7. The magnetic properties of **11** are very similar to that of **10.** The moment drops from 15.3 μ_B to 6.3 μ_B at 4 K, followed by a slight rise at lower temperature. This behavior is consistent with the presence of significant antiferromagnetic coupling within the grid, with the low temperature moment that is equivalent to one 'uncoupled' Mn(II) center. The slight rise in magnetic moment below 4 K is possibly due to a small intra-molecular ferromagnetic interaction.

$[Cu_9(2poap\text{-}H)_6](NO_3)_{12} \cdot 9\ H_2O$ (12):

The magnetic exchange model for a [3×3] grid complex of nine paramagnetic spin centers is represented in Figure 5-8, in which the Hamiltonian expression (eqn. 5-1) with two exchange integrals for the grids accounts for an equivalent exchange interaction

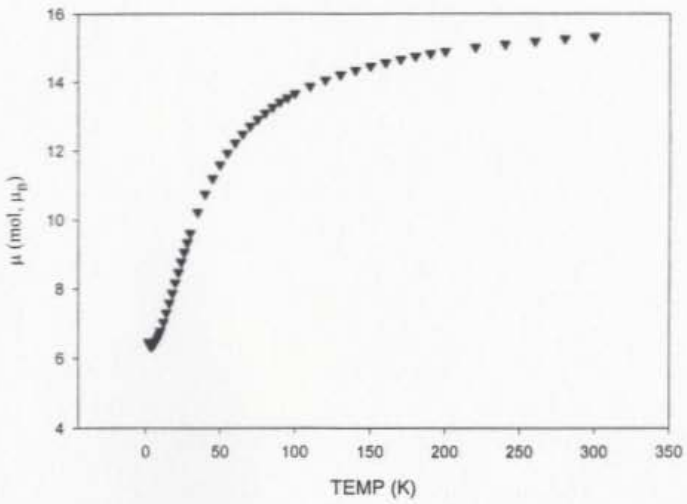

Figure 5-7. Variable-temperature magnetism data for **11**.

between each adjacent pairs of copper(II) centers in an eight-membered ring, and a second exchange integral (J_1) between the central copper Cu(9) and its immediate neighbors. The exchange expression can be derived from the appropriate Hamiltonian equation (eqn. 5-1) and eqn. 5-2 can be used to describe the exchange if we take the fraction of paramagnetic impurity and the temperature independent paramagnetism into account. (χ_M is the molar susceptibility, ρ is the fraction of paramagnetic impurity, *TIP* is the temperature independent paramagnetism, θ is a Weiss-like temperature correction; all other terms have their usual significance). Data fitting was done using MAGMUN [106] described in Chapter3.

$$H = -2J_2 (S_1.S_2 + S_2.S_3 + S_3.S_6 + S_6.S_9 + S_9.S_8 + S_8.S_7 + S_7.S_4 + S_1.S_4)$$
$$-2J_1 (S_5.S_2 + S_5.S_4 + S_5.S_8 + S_5.S_6) \quad (5\text{-}1)$$

$$\chi_M = \chi_{M'}(1-\rho) + \frac{2N\beta^2 g^2 \rho}{3kT} + TIP \quad (5\text{-}2)$$

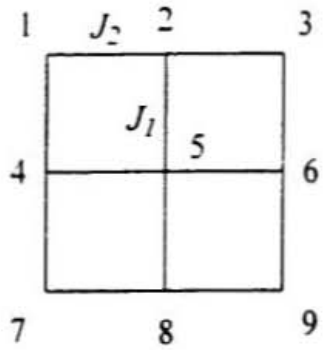

Figure 5-8. Exchange model for [3×3] M_9 grids.

A plot of molar magnetic moment versus temperature of **12** is shown in Figure 5-9. The magnetic moment drops slightly from 5.9 μ_B at 300 K to 5.5 $_B$ at 30 K, followed by a rise below this temperature to a value of 6.2 μ_B at 4.5 K. The room-temperature value is consistent with the presence of nine Cu(II) centers, and the small drop towards 30 K suggests the presence of an antiferromagnetic exchange interaction within the cluster. The rise in μ_B at temperatures below 30 K is associated with a ferromagnetic component, which appears to be dominating the exchange process at low temperatures.

Magnetic data for **12** have been successfully fitted to the above exchange model. A reasonable data fit was obtained for g = 2.30, J_2 = 0.52 cm^{-1}, J_1 = -24.3 cm^{-1}, TIP = 0.000540 emu·mol^{-1}, θ = -0.5 K, 10^2R = 5.0 ($R = [\Sigma(\chi_{obs} - \chi_{calc})^2/\Sigma\chi_{obs}^2]^{1/2}$) (Solid line in Figure 5-9). Cu(5) is therefore antiferromagnetically coupled with its immediate neighbors, which leads to a situation where within the central group of five copper(II) centers an S = 3/2 ground state exists, while the copper(II) centers in the exterior ring are all ferromagnetically coupled ($|J_1/J_2| >> 1$). All of these lead to an overall ground state

of S = 7/2 for the $Cu(II)_9$ grid.[122] This can be rationalized in terms of strict magnetic orbital orthogonality in the external ring of eight copper(II) centers, corroborated by structure evidence, and a peculiar state of ground state fluxionality (dynamic Jahn-Teller distortion) at the central copper ion. The ferromagnetic behavior in the external ring exactly matches the properties of a series of square tetranuclear copper(II) complexes with the ligands **poap** and **poapz**.[50] which have structures involving strict orthogonality between the copper centers, and are exactly analogous to the square subunits within the [3×3] Cu_9 grid system.

A magnetization study at 2.0 K for **12** (Figure 5-10) was also carried out in the range of 0-5.0 T in an attempt to establish the magnetic ground state of the complex ion. The system is almost saturated at 5.0 T, and a comparison with the Brillouin function calculated at 2.0 K for g = 2.23 shows that the Cu_9 cluster approaches the theoretical value for spin system with an S = 7/2 ground state. While the fit is not perfect it shows that a sensible interpretation of the magnetic structure of the grid accounts for one averaged exchange pathway that is antiferromagnetic. This is reasonably associated with the unusual ground state for Cu(5), and a fluxional ground state behavior in an interaction with all four adjacent copper(II) centers. At 30 K a magnetization versus field profile (0-5.0 T) is a straight line, with a constant magnetic moment of 5.5 μ_B. This clearly corresponds to a curie-like situation but may reflect the small intramolecular antiferromagnetic exchange component.

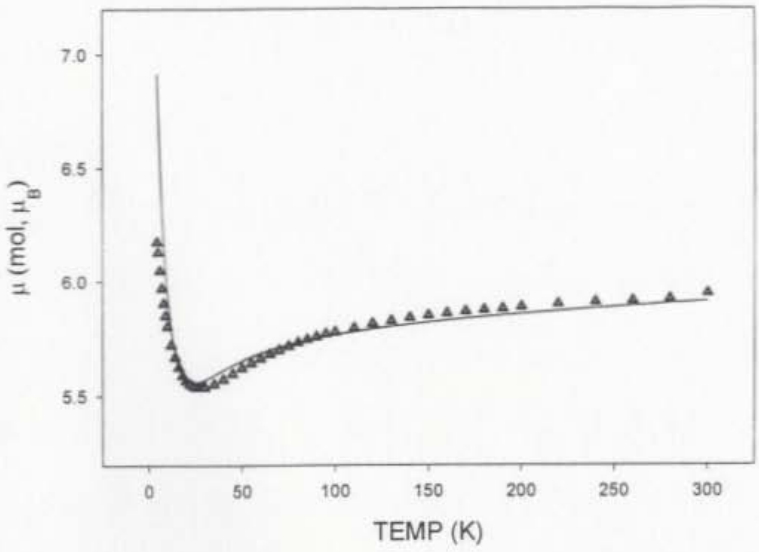

Figure 5-9. Variable-temperature magnetism data for **12**.

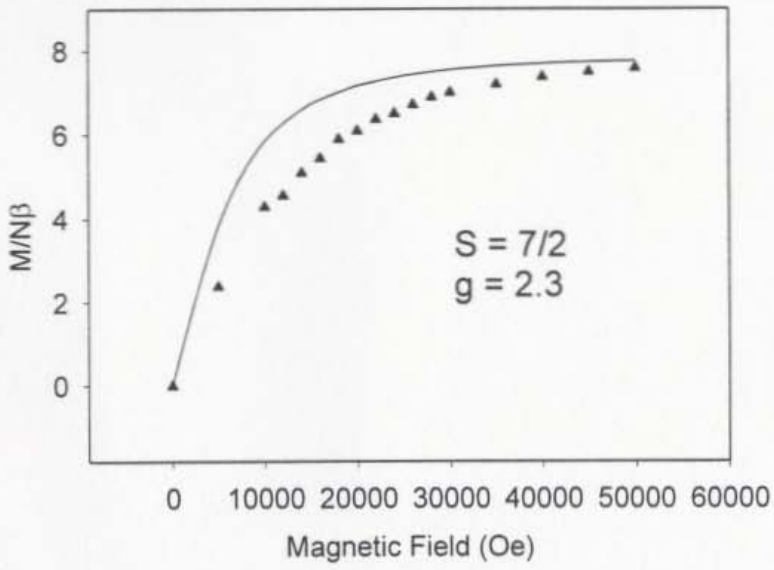

Figure 5-10. Plot of magnetization *vs.* magnetic field for **12**.

5.4 Conclusion

The aggregation of nine octahedral Mn(II), Cu(II) centers (fifty four coordination positions) into alkoxo-bridged, portcullis-like 3 × 3 grids by six heptadentate **2poap** ligands (fifty four donor positions) is a unique example of a self assembly process in which the coordination algorithm of the nine metal assembly is exactly matched by the aligned arrangement of the two sets of parallel ligands arranged above and below the metal grid pseudo-plane. This strategy has general application and a simple extension of this type of ligand with additional five-membered chelate ring compartments can be envisaged to produce [4×4] and [5×5] grids, and even higher homologues.

Chapter 6. General Conclusion and Future Work

6.1 General Conclusion

This thesis described the synthesis, X-ray structural and magnetic properties of the first two magnetic [3×3] $Mn(II)_9$ and $Cu(II)_9$ grids formed by strict self-assembly. The $Cu(II)_9$ complex exhibits intramolecular ferromagnetic coupling, while intramolecular anti-ferromagnetic exchange is observed in the $Mn(II)_9$ grid. The first antiferromagnetic $Ni(II)_8$ ring cluster bridged by only N-N single bonds was also structurally characterized. Moreover, X-ray structures and magnetic properties of three M_4 [2×2] square grids (M = Cu(II), Ni(II), Co(II)), one [2×2] rectangle grid $Mn(II)_4$ cluster and three trinuclear complexes were also reported here. For the $Cu(II)_4$ square grid, ferromagnetic coupling exists, while in all the other cases antiferromagnetic coupling is observed. Their magnetic properties were also successfully explained according to their X-ray structures.

6.1.1 Synthesis of Ligands

The syntheses of polytopic pyridazine ligands used for self-assembly of [3×3] [32] and [4×4] [120] grids were carried out by Lehn's group. The ligands are usually difficult to purify and the yields are low. However, the ligands described in this thesis are much easier to prepare and purify, and moreover their yields are usually high. These synthetic routes have general applications in the design of new polytopic ligands and actually

provide model ligands for magnetism studies of cluster complexes as components of new molecular magnetic materials.

6.1.2 Synthesis of Complexes

Most of the complexes mentioned in this thesis are stable in the air and aqueous solution at room temperature. Usually they can be prepared by simply mixing the warm mixed aqueous organic solutions of metal salts with the ligands. Ligands are in general insoluble in water, methanol or acetonitrile. However, they will react with the metal salts and dissolve gradually in the metal salt solution since the complexes they form are normally extremely soluble in the mixed aqueous/organic solution. So these self-assembled complexes are easy to purify by recrystallization and to grow single crystals for single crystal X-ray structure determination.

6.1.3 Magneto-structural Correlations for Grids and Clusters

The studies on magneto-structural correlations for grids and polynuclear complexes described in this thesis agree with the linear relationship described for dinuclear copper(II) complexes reported by our group, which indicated the correlation between the rotational angle of the metal magnetic planes about the N-N bond (M-N-N-M) and the coupling constant, with ferromagnetic coupling at angles < 80° and antiferromagnetic coupling > 80°. The rotational angles of most of the clusters reported here are usually large and antiferromagnetic coupling resulted with only N-N single bond bridges. When there is anther type of bridge, e.g., carbonyl oxygen in the primary

ligands, with large bridging angles (M-O-M) this also leads to antiferromagnetic coupling, since they usually have the same effect on the magnetic orbital interactions in the complexes.

However, if strict orthogonality of the magnetic orbitals between the copper centers exists (for grids $Cu(II)_4$ (**4**) and $Cu(II)_9$ (**12**)), intramolecular ferromagnetic coupling dominates. If the distance between metal centers is long enough (i.e. $Fe(II)_4$ grid (**8**)), no coupling is observed.

6.2 Future Work

6.2.1 Iron(III) Complexes of 2poap and 2poapz

A nona-nuclear iron(III) complex of the ligand **2poap** (Scheme 2-1) was recently prepared and characterized by IR, UV-vis, elemental analysis, etc. The following details describe its preparation and characterization.

$[Fe_9(2poap)_6](NO_3)_{15}\cdot 18H_2O$ (13): **2poap** (0.403 g, 1.0 mmol) was added to a hot solution of $Fe(NO_3)_3\cdot 6H_2O$ (1.45 g, 4.0 mmol) in water (10 mL). The black solution formed was left at room temperature. Black crystals formed after a couple of weeks. Yield: 0.58g, 84%. Found (vacuum dried sample): C, 32.84; H, 2.66; N, 23.08. Calcd. for $Fe_9(C_{19}H_{15}N_9O_2)_6(NO_3)_{15}\cdot 18H_2O$: C, 32.85; H, 3.05; N, 23.20%. IR (Nujol mull, cm^{-1}): 1680, 1655(υ CO/CN). UV-vis (Nujol mull): 916 nm. $\mu_{RT} = 5.8\ \mu_B$ (per iron)

Although X-ray structure determination of the single crystals of this complex failed, the above characterization clearly shows that it is an iron(III) nona-nuclear cluster. The variable magnetism study confirms this conclusion. Moreover, the preliminary

magnetization study shows that it has a 27/2 ground state, which is peculiar and extremely high for this type of cluster. More studies on this interesting cluster are needed in order to explain why it has such peculiar magnetic properties.

6.2.2 New Polytopic Ligands and Their Complexes

In order to construct more complicated clusters for new magnetic materials, a few new ligands were designed. Figure 6-1 shows three such examples.

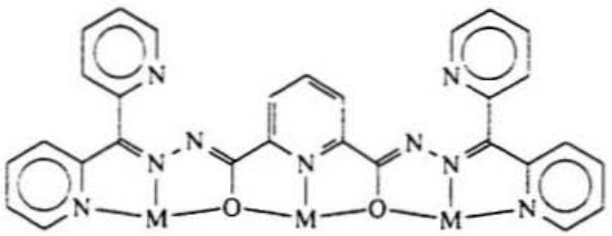

A.

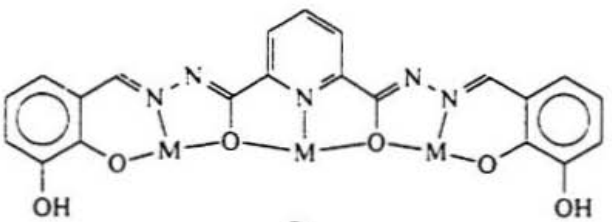

B.

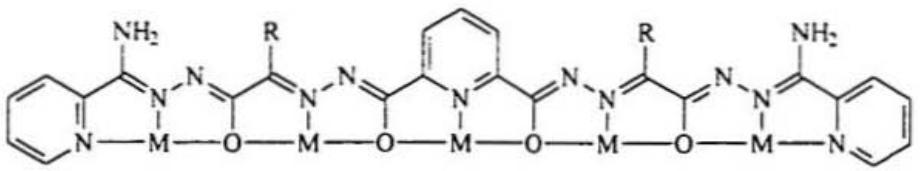

C. R = -CH_3, -Ph, etc

Figure 6-1. Coordination modes of future ligands for more complicated clusters.

Ligand **A** in Figure 6-1 has two more pyridyl groups besides the tritopic component compared with ligand **2poap** (Scheme 2-1), which might coordinate to more metal ions to link the trinuclear complexes together or produce more complicated clusters. It also can be visualized as a double of ligand **po2p** (Scheme 2-1), but its coordinating mode seems to be impossible to just double that of **po2p**, since the tritopic coordinating pockets in these ligands are excellent traps for metal ions considering our present results of both trinuclar and nona-nuclear complexes. This ligand has been synthesized and some of its complexes examined. Detailed studies will be reported elsewhere.

Ligand **B** in Figure 6-1 has two more hydroxyl groups besides the tritopic component, which might coordinate to more metal ions to link the trinuclear complexes together or produce more complicated clusters. This ligand also might be transformed to a paramagnetic ligand with catechol-based radicals. The radical ligand could then react with metal salts to produce metal complexes of coordinated radicals, in which direct magnetic exchange coupling between metal and ligand spins is possible.[123] Ligand **B** and a trinuclear copper(II) complex have been prepared. More detailed results will be reported elsewhere and form the basis for future studies.

Ligand **C** is the most interesting one, though it is challenging to synthesize it. It has fifteen coordinating sites (deprotonated carbonyl oxygen providing two coordinating sites as a bridge) and five coordinating pockets. The coordinating sites provided by ten

ligands are 150 (15×10), which is the exact number of required coordinating sites by 25 six-coordinated metal ions (6×25). This ligand resembles **poap** and **2poap** (Scheme 2-1), therefore it may assemble 25 metal ions together to produce a [5×5] 25-nuclear grid (Figure 6-2) which has not been reported so far.

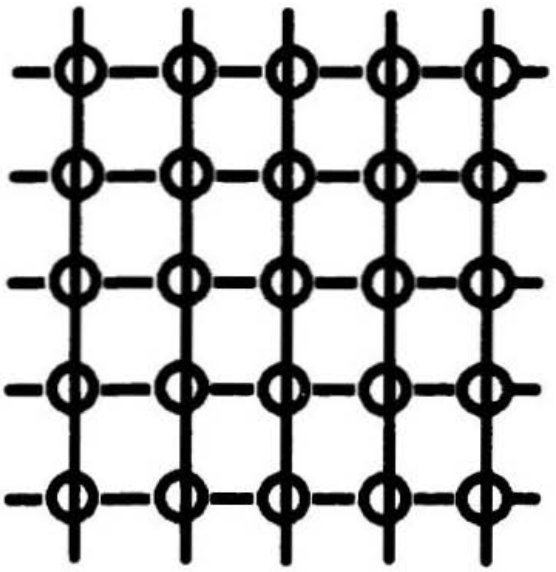

Figure 6-2. Illustration of an expected [5×5] 25-nuclear grid.

References

1. S. J. Lippard. *Principle of Bioinorganic Chemistry*. University Science Books. Mill Valley. CA. 1994.

2. M. K. Chan. J. Kim. and D.C. Rees. *Science*. 1993. **260**.792.

3. K. L. Taft. G. C. Papaefthymiou. and S. J. Lippard. *Science*. 1993. **259**. 1302.

4. a) W. Micklitz. S. J. Lippard. *Inorg. Chem.*. 1988. **27**. 3067.

   b) C. J. Harding. A. K. Powell. *Angew. Chem. Int. Ed.*. 1993. **32**. 570.

5. a) K. Wieghardt. K. Pohl. G. Huttner. *Angew. Chem. Int. Ed.*. 1984. **23**. 77.

   b) C. D. Delfs. D. Gatteschi. L. Pardi. R. Sessoli. K. Wieghardt. D. Hanke. *Inorg Chem.*. 1993. **32**. 3099.

6. a) K. L. Taft and S. J. Lippard. *J. Am. Chem. Soc.*. 1990. **112**. 9629.

   b) K. L. Taft. C. D. Delfs. G. C. Papaefthymiou. S. Foner. D. Gatteschi. and S. J. Lippard. *J. Am. Chem. Soc.*. 1994. **116**. 823.

7. S. M. Gorun. G. C. Papaefthymiou. R. B. Frankel. and S. J. Lippard. *J. Am. Chem. Soc.*. 1987. **109**. 3337.

8. A. Caneschi. A. Cornia. A. C. Fabretti. and D. Gatteschi. *Angew. Chem. Int. Ed.*. 1999. **38**. 1295.

9. S. L. Heath and A. K. Powell. *Angew. Chem. Int. Ed.*. 1992. **31**. 191.

10. a) S. P. Watton. P. Fuhrmann. L. E. Pence. A. Caneschi. A. Cornia. G. L. Abbati. S. J. Lippard. *Angew. Chem. Int. Ed.*. 1997. **36**. 2774.

    b) L. Marshall. K. Parris. J. Rebek. Jr.. S. V. Luis. M. I. Burguete. *J. Am. Chem. Soc.*. 1988. **110**. 5192.

11. P. D. W. Boyd, Q. Li, J. B. Vincent, K. Folting, H.-R. Chang, W.E Streib, J. C. Huffman, G. Christou, and D. N. Hendrickson, *J. Am. Chem. Soc.*, 1988, **110**,8537.

12. A. Caneschi, D. Gatteschi,, R. Sessoli, A.-L. Barra, L.C. Brunel and M. Guillot, *J. Am. Chem. Soc.*, 1991, **113**, 5873.

13. a) R. Sessoli, D. Gatteschi, A. Caneschi and M. A. Novak, *Nature (London)*, 1993, **365**, 141.

b) S. M. Holmes and G. S. Girolami, *J. Am. Chem. Soc.*, 1999, **121**, 5593 and references therein.

14. J. Yoo, E. K. Brechin, A. Yamaguchi, M. Nakano, J. C. Huffman, A. L. Maniero, L.-C. Brunel, K. Awaga, H. Ishimoto, G. Christou and D. N. Hendrickson, *Inorg. Chem.*, 2000, **39**, 3615.

15. H. J. Eppley, H.-L. Tsai, A. R. Schake, S. Wang, J. B. Vincent, K. Folting, G. Christou, and D. N. Hendrichson, *J. Am. Chem. Soc.*, 1995, **117**, 301.

16. D. Ruiz, Z. Sun, B. Albela, K. Folting, J. Ribas, G. Christou, and D. N. Hendrickson, *Angew. Chem. Int. Ed.*, 1998, **37**, 300.

17. M. A. Bolcar, S. M. Aubin, K. Folting, D. N. Hendrickson, and G. Christou, *Chem. Comm.*, 1997, 1485

18. E. K. Brechin, J. Yoo, M. Nakano, J. C. Huffman, D. N. Hendrickson, and G. Christou, *Chem. Comm.*, 1999, 783.

19. S. L. Castro, Z. M. Sun, C. M. Grant, J. C. Bollinger, D. N. Hendrickson, and G. Christou, *J. Am. Chem. Soc.*, 1998, **120**, 2365.

20. S. Ferlay, T. Mallah, R. Ouahes, P. Veillet, and M. Verdaguer, *Inorg. Chem.*, 1999, **38**, 229.

21. T. Mallah, C. Auberger, M. Verdaguer, and P. Veillet, *J. Chem. Soc. Chem. Comm.*, 1995, 61.

22. S. Parsons, A. A. Smith, and R. E. P. Winpenny, *Chem. Comm.*, 2000, 579.

23. A. K. Powell, S.L. Heath, D. Gatteschi, L. Pardi, R. Sessoli, G. Spina, F. Del Giallo, and F. Pieralli, *J. Am. Chem. Soc.*, 1995, **117**, 2491.

24. A. L. Barra, P. Debrunner, D. Gatteschi, C. E. Schulz, and R. Sessoli, *Europhys. Lett.*, 1996, **35**, 133.

25. A. L. Barra, A. Caneschi, A. Ccornia, F. Fabrizi de Biani, D. Gatteschi, C. Sangregorio, R. Sessoli, and L. Sorace, *J. Am. Chem. Soc.*, 1999, **121**, 5302.

26. F. Cramer, *Chaos and Order. The Complex Structure of Living Systems*, VCH, Weinheim, 1993.

27. G. Nicolis, I. Prigogine, *Self-organization in Non-equilibrium Systems*, Wiley, New York, 1977.

28. J.-M. Lehn, *Supramolecular Chemistry. Concepts and Persceptives*, VCH, 1995.

29. G. F. Swiegers and T. J. Malefetse, *Chem. Rev.*, 2000, **100**(9), 3483-538.

30. A. M. Garcia, F. J. Romero-Salguero, D. M. Bassani, J.-M. Lehn, G. Baum, and D. Fenske, *Chem. Eur. J.*, 1999, **5**(6), 1803.

31. J. Rojo, J.-M. Lehn, G. Baum, D. Fenske, O. Waldmann, P. Müller, *Eur. J. Inorg. Chem.* 1999, 517.

32. P. N. W. Baxter, J.-M. Lehn, J. Fischer, M.-T. Youinou, *Angew. Chem. Int. Ed.*, 1994, **33**, 2284.

33. L. K. Thompson, S. S. Tandon, M. E. Manuel, *Inorg. Chem.*, 1995, **34**, 2356.

34. C. J. O'Connor, R. J. Romananch, D. M. Robertson, E. E. Eduok and F. R. Fronczek, *Inorg. Chem.*, 1983, **22**, 449.

35. T. C. Woon, L. K. Thompson and P. Robichaud, *Inorg. Chim. Acta*, 1984, **90**, 201.

36. P. Souza, A. I. Matesanz and V. Fernández, *J. Chem. Soc. Dalton Trans.*, 1996, 011.

37. J. García-Jojal, J. Garcia-Jaca, R. Cortés, T. Rojo, M. K. Urtiaga and M. I. Arriortua, *Inorg. Chim. Acta*, 1996, **249**, 25.

38. A. Mangia, C. Pelizzi and G. Pelizzi, *Acta Crystallogr., Sect. B*, 1974, **30**, 2146.

39. A. Bonardi, S. Ianelli, C. Pelizzi and G. Pelizzi, *Inorg. Chim. Acta*, 1991, **187**, 167.

40. A. Bacchi, A. Bonini, M. Carcelli, F. Ferraro, E. Leporati, C. Pelizzi and G. Pelizzi, *J. Chem. Soc., Dalton Trans.*, 1996, 2699.

41. A. E. Koziol, R. C. Palenik and G. J. Palenik, *J. Chem. Soc., Chem. Commun.*, 1989, 650.

42. M. Lagrenée, S. Sueur and J. P. Wignacourt, *Acta Crystallogr., Sect. C*, 1991, **47**, 1158.

43. A. Bacchi, L. P. Battaglia, M. Carcelli, C. Pelizzi, G. Pelizzi, C. Solinas and M. A. Zoroddu, *J. Chem. Soc., Dalton Trans.*, 1993, 775.

44. E. W. Ainscough, A. M. Brodie, J. D. Ranford and J. M. Waters, *Inorg. Chim. Acta*, 1995, **236**, 83.

45. X. Chen, S. Zhan, C. Hu, Q. Meng and Y. Liu, *J. Chem. Soc., Dalton Trans.*, 1997, 245.

46. P. J. van Koningsbruggen, E. Muller, J. G. Haasnoot and J. Reedijk, *Inorg. Chim. Acta*, 1993, **208**, 37.

47. Z. Xu, L. K. Thompson and D. O. Miller, *Inorg. Chem.*, 1997, **36**, 3985.

48. L. K. Thompson, Z. Xu, A. E. Goeta, J. A. K. Howard, H. J. Clase and D. O Miller, *Inorg. Chem.*, 1998, **37**, 3217.

49. Z. Xu, L. K. Thompson, C. J. Matthews, D. O. Miller, A. E. Goeta, C. Wilson, J. A. K. Howard, M. Ohba and H. kawa, *J. Chem. Soc., Dalton Trans*, 2000, 69.

50. C. J. Matthews, K. Avery, Z. Xu, L. K. Thompson, L. Zhao, D. O. Miller, K. Biradha, K. Poirier, M. J. Zaworotko, C. Wilson, A. E. Goeta and J. A. K. Howard, *Inorg. Chem.*, 1999, **38**, 5266.

51. V. L. Pecoraro, A.J. Stemmler, B.R. Gibney, J.J. Bodwin, H. Wang, J.W. Kampf, A. Baewinski, *Progress in Inorganic Chemistry*, Vol. 45, pp. 83-177, 1997. (Ed. K.D. Karlin), Wiley, New York.

52. M. S. Lah, V. L. Pecoraro, *Comments Inorg. Chem.* 1990, **11**, 59.

53. B. R.Gibney, A. J. Stemmler, S. Pilotek, J. W. Kampf, V. L. Pecoraro, *Inorg. Chem.* 1993, **32**, 6008.

54. M. S. Lah, V. L. Pecoraro, *J. Am. Chem. Soc.* 1989, **111**, 7258.

55. A. J. Stemmler, J. W. Kampf, V. L. Pecoraro, *Inorg. Chem.* 1995, **34**, 2271.

56. B. Kurzak, E. Farkas, T. Glowiak, H. Kozlowski, *J. Chem. Soc. Dalton Trans.* 1991, 163.

57. B. R. Gibney, D. P. Kessissoglou, J. W. Kampf, V. L. Pecoraro, *Inorg. Chem.* 1994, **33**, 4840.

58. J. A. Halfen, J. J. Bodwin, V. L. Pecoraro, *Inorg. Chem.* 1998, **37**, 5416.

59. A. J. Stemmler, A. Barwinski, M. J. Baldwin, V. Young, V. L. Pecoraro, *J. Am. Chem. Soc.* 1996, **118**, 11 962.

60. B. Kwak, H. Rhee, S. Park, M. S. Lah, *Inorg. Chem.* 1998, **37**, 3599.

61. S.-X. Liu, S. Lin, B. Z. Lin, C.-C. Lin, and J. Q. Huang, *Angew. Chem. Int. Ed.*, 2001, **40**(6), 1084.

62. Semenov, J. P. Spatz, M. Möller, J.-M. Lehn, B. Sell, D. Schubert, C. H. Weidl, and U. S. Schubert, *Angew. Chem. Int. Ed.*, 1999, **38**(17), 2547.

63. D. S. Brown, V. H. Crawford, J. W. Hall and W. E. Hatfield, *J. Phys. Chem.*, 1977, 81, 1303.

64. Ed. K. D. Karlin and Z. Tyeklar, *Bioinorgaic Chemistry of Copper*, Chapman and Hall, 1993, NewYork.

65. Z. Tyeklar and K. D. Karlin, *Acc. Chem. Res.*, 1989, **22**, 241.

66. E. Bouwmann, W. L. Driessen, and J. Reedijk, *Coord. Chem. Rev.*, 1990, **104**, 143.

67. P. A. Vigato, S. Tamburini, and D. E. Fenton, *Coord. Chem. Rev.*, 1990, **106**, 25.

68. T. N. Sorrell, *Tetrahedron*, 1989, **45**, 3.

69. M. Inoue and M. Kubo, *Coord. Chem. Rev.*, 1976, **21**, 1.

70. W. E. Hatfield, *Comments Inorg. Chem.*, 1981, **1**,105.

71. M. Melnik, *Coord. Chem. Rev.*, 1982, **42**, 259.

72. O. Kahn, *Molecular Magnetism*, VCH, 1993.

73. L.K. Thompsor. and S.S. Tandon. *Comments Inorg. Chem.*, 1996, **18**(3), 125.

74. P. Arrizabalaga, P. Castan, and F. Dahan, *Inorg. Chem.*, 1983, **22**, 2245.

75. H. Knuutila, *Inorg. Chim. Acta*, 1983, **72**, 11.

76. R. Veit, J.J. Girerd, O. Kahn, F. Robert, Y. Jeannin, *Inorg. Chem.*, 1986, **25**, 4175.

77. H. Ökawa, M. Kaikawa, S. Kida, D. Luneau, H. Oshio, *J. Chem. Soc., Dalton Trans.*, 1990, 469.

78. D. Luneau, H. Oshio, H. Ökawa, S. Kida, *J. Chem. Soc., Dalton Trans.*, 1990, 2283.

79. R. Sillanpaa, J. Valkonen, *Acta Chem. Scand.*, 1992, **46**, 1072.

80. R. Costa, A. Garcia, and J. Ribas, *Inorg. Chem.*, 1993, **32**, 3733.

81. L. K. Thompson, C. J. Matthews, L. Zhao, Z. Xu, D. O. Miller, C. Wilson, M. A. Leech, K. Poirier, J. A. K. Howard, S. L. Heath, A. G. Whittaker, and R. E. P. Winpenny, *J. Solid State Chem.*, 2001 (in press).

82. L. Zhao, C. J. Matthews, L. K. Thompson and S. L. Heath, *Chem. Commun.*, 2000,265.

83. L. Zhao, Z. Xu, L. K. Thompson and S. L. Heath, D. O. Miller, and M. Ohba, *Angew. Chem. Int. Ed.*, 2000, **39**, 3114.

84. SIR92: A. Altomare, M. Cascarano, C. Giacovazzo and A.Guagliardi, *J. Appl. Cryst.*, 1993, **26**, 343.

85. DIRDIF94: P. T. Beurskens, G. Admiraal, G. Beurskens, W. P. Bosman, R. de Gelder, R.Israel and J. M. M. Smits, *The DIRDIF-94 program system, Technical Report of the Crystallography Laboratory*, University of Nijmegen, The Netherlands.

86. D. T.Cromer and J. T. Waber : "*International Tables for X-ray Crystallography*", Vol. IV. The Kynoch Press. Birmingham. England. Table 2.2 A (1974).

87. J. A. Ibers and W. C. Hamilton. *Acta Crystallogr.*, 1964.**17**. 781.

88. D. C. Creagh and W. J. McAuley; "*International Tables for Crystallography*". Vol C. (A.J.C. Wilson. ed.). Kluwer Academic Publishers. Boston. Table 4.2.6.8. pages 219-222 (1992).

89. teXsan for Windows: *Crystal Structure Analysis Package*. Molecular Structure Corporation (1997).

90. J. Cosier and A. M. Glazer. *J. App. Crystallogr.*, 1986. **19**. 105.

91. a) Siemenns. SMART Data Collection Software. Version 4.050. Siemenns Analytical X-ray Instruments Inc.. Madison. WI. 1996.

b) Siemenns. SAINT Data Reduction Software. Version 4.050. Siemenns Analytical X-ray Instruments Inc.. Madison. WI. 1996.

92. G. M. Shedrick. SHELXTL 5.04/VMS. A integrated system for solving. refining and displaying crystal structures from diffraction data. Siemens Analytical X-ray Instruments Inc.. Madison. WI. 1995.

93. M. Fujita. Y. J. Kwon. S. Washizu. and K. Ogura. *J. Am. Chem. Soc.*, 1994. **116**. 1151.

94. P. J. Stang a.d B. Olenyuk. *Angew. Chem. Int. Ed.*, 1995. **35**. 372.

95. C. M. Drain and J.-M. Lehn. *J. Chem. Soc., Chem. Comm.*, 1994. 2313.

96. R. Holger. E. C. Hillgeris. A. Erxleben. and B. Lippert. *J. Am. Chem. Soc.*, 1994. **116**. 2616.

97. P.J. Stang and K. Chen. *J. Am. Chem. Soc.*, 1995, **117**, 1667.

98. M.-T. Youinou, N. Rahmouni, J. Fischer, J. A. Osborn, *Angew. Chem. Int. Ed.*, 1992, **31**, 733.

99. J. Rojo, F. J. Romero-Salguero, J.-M. Lehn, G. Baum, D. Fenske, *Eur. J. Inorg. Chem.* 1999, 1421.

100. G. S. Hanan; D. Volkmer; S. S. Ulrich, J.-M. Lehn, G. Baum, D. Fenske, *Angew. Chem., Int. Ed.* 1997, **36**, 1842.

101. K. L. V. Mann, E. Psillakis, J. C. Jeffery, L. H. Rees, N. M. Harden, J. A. McCleverty, M. D. Ward, D. Gatteschi, F. Totti, F. E. Mabbs, E. J. L. McInnes, P. C. Riedi, and G. M. Smith, *J. Chem. Soc., Dalton Trans.*, 1999, 339.

102. C. S. Campos-Fernández, R. Clérac, K. R. Dunbar, *Angew. Chem. Int. Ed.*, 1999, **38**(23), 3477.

103. X.-H. Bu , H. Morishita , K. Tanaka , K. Biradha , S. Furusho and M. Shionoya, *Chem. Comm.*, 2000, 971.

104. A. Gelasco, A. Askenas, and V. L. Pecoraro, *Inorg. Chem.*, 1996, **35**, 1419.

105. C.-Y. Duan, Z.-H. Liu, X.-Z. You, F. Xue, and T. C. W. Mak, *Chem. Comm.*, 1997, 381.

106. a) Program ow01.exe, Version 19.6.00, by Oliver Waldmann, 2000.

b) MAGMUN, Version 2.0, by Z.-Q. Xu, 2001. (http://www.ucs.mun.ca/~lthomp)

107. K. K. Nanda, L. K. Thompson, J. N. Bridson, and K. Nag, *J. Chem. Soc., Chem. Comm.*, 1994, 1337.

108. R. W. Saalfrank, I. Bernt, E. Uller, and F. Hampel, *Angew. Chem. Int. Ed.*, 1997, **36**, 2482.

109. A. Caneschi, A. Cornia, and S. J. Lippard, *Angew. Chem. Int. Ed.*, 1995, **34**, 467.

110. K. L. Taft, G. C. Papaefthymiou, and S. J. Lippard, *Inorg. Chem.*, 1994, **33**, 1510.

111. I. M. Atkinson, C. Benelli, M. Murrie, S. Parsons, and R. E. P. Winpenny, *Chem. Comm.*, 1999, 285.

112. J. Xu and K. N. Raymond, *Angew. Chem. Int. Ed.*, 2000, **39**, 2745.

113. A. J. Blake, C. M Grant, S. Parsons, J. M. Rawson, and R. E. P. Winppenny, *J. Chem. Soc., Chem. Comm.*, 1994, 2363.

114. A. L. Dearden, S. Parsons, and R. E. P. Winppenny, *Angew. Chem. Int. Ed.*, 2001, **40**, 151.

115. M. Moon, I. Kim, and M. S. Lah, *Inorg. Chem.*, 2000, **39**, 2710.

116. V. A. Milway, L. Zhao, L. K. Thompson, unpublished result.

117. G. M. Shedrick, SHELX97, A integrated system for solving, refining and displaying crystal structures from diffraction data, Siemens Analytical X-ray Instruments Inc., Madison, WI, 1997.

118. teXsan for Windows version 1.06: *Crystal Structure Analysis Package*, Molecular Structure Corporation (1997-9).

119. P. N. W. Baxter, J.-M. Lehn, B. O. Kneisel, D. Fenske, *Angew. Chem. Int. Ed.*, 1997, **36**, 1978.

120. A. M. Garcia, F. J. Romero-Salguero, D. M. Bassani, J.-M. Lehn, G. Baum, and D. Fenske, *Chem. Eur. J.*, 1999, **5**(6), 1803.

121. C. J. Matthews, Z. Xu, S. K. Mandal, L. K. Thompson, K. Biradha, K. Poirier, and M. J. Zawarotko, *Chem. Comm.*, 1999, 347.

122. O. Waldmann, R. Koch, S. Schromm, P. Muller, L. Zhao, L. K. Thompson, *Chem. Phys. Lett.*, 2000, **332**, 73.

123. T. M. Barclay, R. G. Hicks, M. T. Lemarie, and L. K. Thompson, *Chem. Comm.*, 2000, 2142 and references therein.